Novel view of the flavor-singlet spectrum from multi-flavor QCD on the lattice

Yasumichi Aoki,[1] Tatsumi Aoyama,[2] Ed Bennett,[3] Toshihide Maskawa,[4,*] Kohtaroh Miura,[5] Hiroshi Ohki,[6] Enrico Rinaldi,[7] Akihiro Shibata,[8] Koichi Yamawaki,[4] and Takeshi Yamazaki[9,10]

(LatKMI Collaboration)

[1]*RIKEN Center for Computational Science, Kobe 650-0047, Japan*
[2]*Institute for Solid State Physics, University of Tokyo, Kashiwa 277-8581, Japan*
[3]*Swansea Academy of Advanced Computing, Swansea University, Bay Campus, Swansea, SA1 8EN, United Kingdom*
[4]*Kobayashi-Maskawa Institute for the Origin of Particles and the Universe, Nagoya University, Nagoya 464-8602, Japan*
[5]*Institute of Particle and Nuclear Studies, High Energy Accelerator Research Organization (KEK), Tsukuba 305-0801, Japan*
[6]*Department of Physics, Nara Women's University, Nara 630-8506, Japan*
[7]*Interdisciplinary Theoretical and Mathematical Science (iTHEMS) Program, RIKEN, Wako, Saitama 351-0198, Japan*
[8]*Computing Research Center, High Energy Accelerator Research Organization (KEK), Tsukuba 305-0801, Japan*
[9]*Institute of Pure and Applied Sciences, University of Tsukuba, Tsukuba, Ibaraki 305-8571, Japan*
[10]*Center for Computational Sciences, University of Tsukuba, Tsukuba, Ibaraki 305-8577, Japan*

(Received 15 May 2025; accepted 6 October 2025; published 3 December 2025)

SU(3) gauge theories with an increasing number of light fermions are the templates of strongly interacting sectors and studying their low-energy dynamics and spectrum is important, both for understanding the strong dynamics of QCD itself, and for discovering viable UV completions of beyond the Standard Model physics. In order to contrast many-flavor strongly interacting theories with QCD on a quantitative footing, we use lattice field theory simulations. We focus on the study of the flavor-singlet spectrum in the scalar and pseudoscalar channels: This is an interesting probe of the dynamics of the strongly interacting sector, as reminded by the QCD case with the $f_0(500)$ (σ) and η' mesons. The hierarchy of the spectrum of a strongly coupled new gauge sector of the Standard Model defines the potential reach of future colliders for new physics discoveries. In addition to a novel hierarchy with light scalars, introducing many light flavors at fixed number of colors can influence the dynamics of the lightest flavor-singlet pseudoscalar. We present a complete lattice study of both of these flavor-singlet channels on high-statistics gauge ensembles generated by the LatKMI Collaboration with 4, 8, and 12 copies of light mass-degenerate fermions. We also present other hadron masses on the lightest ensemble for $N_f = 8$ generated by the LatKMI Collaboration and discuss the chiral extrapolation of the spectrum in this particular theory. We contrast the results to $N_f = 4$ simulations and previous results of $N_f = 12$ simulations.

DOI: 10.1103/vnml-g6nx

I. INTRODUCTION

Since the discovery in 2012 of the Higgs boson [1,2], the Standard Model (SM) has been so successful that there has been little hint of new physics beyond the SM. However, the origin of mass remains a central mystery of the SM in the form of the naturalness problem (see Ref. [3] for a recent review), which is suggestive that there should be

[*]Deceased.

some underlying theory to account for it. Walking technicolor [4,5] is a candidate for such a theory; it is characterized by a chiral condensate with a large anomalous dimension $\gamma_m \simeq 1$, and by an approximate scale symmetry which is broken spontaneously and explicitly (the scale anomaly) by the same chiral condensate.[1] The latter of these predicts the Higgs boson as a composite light pseudodilaton ("technidilaton"), a pseudo-Nambu-Goldstone (NG) boson of the broken scale symmetry. Such a theory would be strongly coupled with a slowly running ("walking") gauge coupling.

Such a walking gauge theory may be realized by an asymptotically free $SU(N_c)$ gauge theory with a large number of massless flavors $N_f(\gg N_c)$ [9], which we may refer to as "large-N_f QCD." It is inspired by the near scale-invariant/conformal structure around the Caswell-Banks-Zaks infrared (IR) fixed point α_* in the two-loop beta function at large N_f ($8 < N_f \leq 16$ for $N_c = 3$) [10,11].

The walking regime is anticipated to be at a value of the IR strong coupling α_* larger than a critical value $\alpha_* \gtrsim \alpha_{\rm cr}$, such that $1 \ll n_f \equiv N_f/N_c < n_f^{\rm cr}$, where $n_f = n_f^{\rm cr}$ at $\alpha_* = \alpha_{\rm cr}$. We expect a significant separation between the UV scale $\Lambda_{\rm UV}$ and the scale of the chiral condensate with dynamical mass $m_D \ll \Lambda_{\rm UV}$, where $\Lambda_{\rm UV}$ is identified with $\Lambda_{\rm QCD}$ generated by the regularization in perturbation theory. This is in contrast to QCD where $\Lambda_{\rm QCD} \approx m_D$. In the infrared region $\mu < \Lambda_{\rm IR} = O(m_D)$, the coupling α blows up with the fermion loop decoupled; i.e., the perturbative IR fixed point α_* is washed out. For $\Lambda_{\rm IR} < \mu < \Lambda_{\rm UV}$, it starts running slowly in units of $\Lambda_{\rm IR}$ as $\alpha(\mu) \searrow \alpha_{\rm cr}$ and $\gamma_m(\alpha(\mu)) \neq 0$, with $\alpha_{\rm cr}$ now being the UV fixed point; this gives rise to a nonperturbative trace anomaly of order $\mathcal{O}(m_D^4)$ in contrast to the perturbative one of order $\mathcal{O}(\Lambda_{\rm UV}^4)$.

On the other hand, the region $\alpha_* < \alpha_{\rm cr}$ ($n_f > n_f^{\rm cr}$) is the conformal window, with $m_D \equiv 0$.

While experiments provide direct access to this spectrum in the case of QCD with light flavors $N_f = 2 + 1$, the case $N_f \gg 2$ has not been observed in nature, and so it can only be studied theoretically. Analytic approaches involve making an approximation, such as the ladder approximation (see, e.g., Ref. [12] and references therein), which introduces somewhat large theoretical uncertainties in our understanding of the spectrum. Lattice simulations fill this gap, providing a nonperturbative first-principles approach relatively free of large or uncontrolled approximations, and providing us with data which can be used to benchmark phenomenological models.

Several lattice groups, including the LatKMI Collaboration, have searched for a candidate walking theory within the space of large-N_f QCD ($N_c = 3$) theories on the lattice. The cases $N_f = 8$ and 12 have drawn particular attention. The spectrum of the theory toward the chiral limit gives one avenue to probing the viability of such a theory as a candidate walking theory. Among other observables, we have particularly focused on the possible large anomalous dimension visible in the spectra of bound states, with a special focus on a flavor-singlet scalar σ, which would be a candidate for the light pseudodilaton [13–17]. In order to shed light on signals of near-conformal dynamics, we have checked the hyperscaling and otherwise compared the behavior of the σ mass from lattice simulations of $N_f = 4, 8$, and 12 QCD with simulations that have used the same lattice setup to minimize systematic differences between the results from the three theories.

Our prior lattice numerical simulations indicated that these three different values of N_f correspond to rather different types of dynamics, implying that $n_f^{\rm cr} \lesssim 4$.

(i) $N_f = 4$ shows [14,17] essentially the same features as of $N_f = 2 + 1$ QCD, specifically, spontaneous chiral-symmetry breaking, and neither hyperscaling nor a light flavor-singlet scalar state σ are observed.

(ii) The $N_f = 12$ theory appears to show [13,17] conformal dynamics, and hence lies in the conformal window, implying $m_D \equiv 0$. The two-body hadronic mass $M_{\rm H}$ shows typical universal hyperscaling of the (renormalized) fermion mass $m_f^{(R)}$, $M_{\rm H}/2 \sim m_D + m_f^{(R)} = m_f^{(R)} \sim (m_f)^{1/(1+\gamma_m(\alpha_*))}$ [18–20], with $\gamma_m(\alpha_*) \simeq 0.4 - 0.5$.[2] The ratios of various bound state mass scales remain constant toward the chiral limit. We subsequently found a light σ [15], even lighter than the pion π, an observation to which we shall return to in this work.

In the conformal window, the presence of an explicit fermion mass m_f means that all bound states are in fact nonrelativistic "unparticles" due to the conformal phase transition [22], since there are no bound states in the chiral limit. Nevertheless, σ is still a pseudo-NG boson, while π is not: Chiral symmetry is only broken explicitly by m_f, while scale symmetry is further broken spontaneously by the gluon condensate (triggered in turn by the same m_f). We will return to this discussion in Sec. II.

(iii) Most excitingly, we found [14,17,23] that $N_f = 8$ is a candidate for a walking theory. The pion mass decreases $M_\pi \to 0$ toward the chiral limit $m_f \to 0$, while other (flavor-non-singlet) bound states mass

[1]Walking technicolor has also been advocated without the notion of scale-symmetry breaking giving a dilaton or a large anomalous dimension [6–8].

[2]This result is roughly consistent with the ladder Schwinger-Dyson (SD) equation in the conformal phase, with $\gamma_m = 1 - \sqrt{1 - \alpha/\alpha_{\rm cr}} \sim 0.8$ at $\alpha = \alpha_*$. Including nonleading terms for the large mass and finite size gives $\gamma_m \sim 0.5$–0.6 when fitted by a simple hyperscaling form (with only the leading term) as in the lattice analyses in [21].

$M_{\rm H}$ do not, i.e., $M_{\rm H}/M_\pi \to \infty$. This signals that the π is a pseudo-NG boson of a spontaneously broken symmetry. At the same time, the theory shows signals of being in the near-conformal phase. Specifically, most states in the mass spectrum (including F_π and the string tension) dominated by the explicit chiral-symmetry breaking $m_f^{(R)} \gtrsim m_D$ obey the approximate hyperscaling relation with a large anomalous dimension

$$\gamma_m \simeq 1. \tag{1.1}$$

The exception to this is the pion, as we expect: Since the pion is a pseudo-NG boson, the hyperscaling form is expected to fit best near the chiral limit, while for other states, the scaling breaks in this region. The would-be anomalous dimension that we see for the pion is "γ_m" ≃0.6 in the mass region we study [17]; we refer to this as "nonuniversal" hyperscaling. This has been found to be consistent with other groups' results [24–26].[3]

Moreover, for the $N_f = 8$ theory we reported [16,17] a signal that the flavor-singlet scalar state σ may be a pseudodilaton. Specifically, it was observed to be as light as the pseudo-NG boson pion π all the way down to the vicinity of the chiral limit

$$M_\sigma \simeq M_\pi \ll M_\rho \tag{1.2}$$

and displayed "γ_m" ≈0.5 (again, as far as γ_m can be considered meaningful for a pseudo-NG boson). These observations contrast sharply with QCD with a smaller number of flavors. By implementing the proposal in Ref. [29], we also observed that the ratio of decay constants of the σ and π,[4]

$$\frac{F_\sigma}{F_\pi/\sqrt{2}} \approx 4 \gg 1, \tag{1.3}$$

which, with Eq. (1.2), suggests that σ in this theory may be identified as a candidate for the Higgs boson.

We obtained the latter result by fitting the lattice data using the mass formula [29]

$$M_\sigma^2 \equiv d_0 + d_1 \cdot M_\pi^2. \tag{1.4}$$

This relation may be derived[5] via the scale and axial Ward-Takahashi (WT) identities. Since its original derivation via these routes, there have been further developments in a variant of this mass formula based on a low-energy dilaton effective field theory description [30–39]. To preempt the results that we will present in Sec. II, we will later demonstrate that $d_1 \approx 1$ in this theory, implying $\gamma_m \approx 1$, and hence, Eq. (1.4). This allows a direct comparison among the three theories we consider here, regardless of whether they are conformal or chirally broken, which we will employ in this work. Here, $d_0 = \mathcal{O}(m_D^2)(\ll \Lambda_{\rm UV}^2)$, which is due to the nonpertubative trace anomaly, and will be nonzero even in the chiral limit.

We have also observed [16] that this coincides with both linear-sigma-model-based and holographic calculations, a result that was further confirmed by subsequent lattice computations of the scalar decay constant F_S [17,40]. The light σ has been confirmed by lattice studies by other groups [41,42]. (For more recent lattice studies, see, e.g., Refs. [43–46]). The value we obtain for F_σ is roughly consistent with more recent analyses of data from the Lattice Strong Dynamics (LSD) Collaboration, $F_\sigma/(F_\pi/\sqrt{2}) \simeq 3.4$ [33,47] (see also Refs. [34,46,48]).

We have also reported preliminary results for the flavor-singlet pseudoscalar η' [49,50], which has a mass even in the chiral limit due to the chiral anomaly in the anomalous chiral WT identity:

$$M_{\eta'}^2 = (M_{\eta'}^2)^{(\rm anomalous)} + M_\pi^2. \tag{1.5}$$

While for M_σ, d_0, and d_1 depend on N_f and N_c only implicitly via γ_m, we found [50] that when normalized by an appropriate IR scale t_0, the η' mass depends directly on these as [12]

$$8t_0 \cdot M_{\eta'}^2 \simeq 8t_0 \cdot (M_{\eta'}^2)^{(\rm anomalous)} \sim n_f^2, \tag{1.6}$$

where $n_f = N_f/N_c$. These flavor-singlet bound states have additional mass due to anomalies—the trace anomaly for σ and the chiral anomaly for η'—which gives extra symmetry breaking beyond the fermionic mass term. We will revisit this in more detail in Sec. II.

Extending our previous study of the flavor-singlet scalar σ [15–17] and also the preliminary studies of the flavor-singlet pseudoscalar η' [49,50], in this work we perform lattice field theory simulations of QCD with different N_f to study the spectrum of bound states. We highlight the differences, and similarities, between QCD theories with different numbers of light (or massless) flavors, in a quantitative way, with new data. In particular, we present an extensive study of η', as well as an updated study of the

[3]See also Refs. [27,28] for recent and different approaches that suggest that the $N_f = 8$ QCD theory exhibits a fixed point existing at a much stronger coupling region than previous studies, consistent with being near the onset of the conformal window.

[4]Decay constants of the pion and σ are defined as $\langle 0|D_\mu(0)|\sigma(q_\mu)\rangle = iF_\sigma q_\mu$, or equivalently, $\langle 0|\theta_{\mu\nu}|\sigma(q_\mu)\rangle = -F_\sigma(q_\mu q_\nu - g_{\mu\nu}q^2)/3$, $\langle 0|A_\mu^\alpha(0)|\pi^\beta(q_\mu)\rangle = i\delta^{\alpha\beta}(F_\pi/\sqrt{2})\cdot q_\mu$, where our F_π corresponds to 130 MeV for the usual QCD pion.

[5]This was first derived in Ref. [29] in the context of dilaton chiral perturbation theory, giving the same expressions for d_0 and d_1.

spectra of σ and other bound states, all of which are consistent with our previous results mentioned above.

This comparison is informed by the mass formulas above, Eqs. (1.4) and (1.5), discussed in more detail in Sec. II, which are valid independently of the chiral phase (spontaneously broken or conformal), and hence may be applied equally to all values of N_f we consider.

We also measure the gradient flow energy scale $1/\sqrt{8t_0}$ for $N_f = 4, 8, 12$, with the same systematics, including a study of the hyperscaling of t_0 for $N_f = 8, 12$.

The remainder of this paper is organized as follows: In Sec. II we motivate the use of the gradient flow scale $1/\sqrt{8t_0}$ as an infrared scale and derive mass formulas from anomalous WT identities for the scale symmetry (for σ) and for the $U(1)_A$ symmetry (for η'), which will be used to contextualize the lattice data in subsequent sections. In Sec. III, we describe our setup of the lattice measurements. We then present an update of the flavor-non-singlet spectra:

(1) We first confirm our previous results on the characteristic m_f dependence of M_ρ/M_π toward the chiral limit for $N_f = 4, 8, 12$, as deeply broken, walking, and conformal phases, respectively.
(2) We present measurements of the gradient flow energy scale $1/\sqrt{8t_0}$ for $N_f = 4, 8, 12$, which provide the basis for comparing the lattice results for different N_f. We show that it obeys hyperscaling for $N_f = 8$ and 12, while not for $N_f = 4$, reinforcing previous indications that the former theories are in a (near-) conformal phase, while the latter has a deeply spontaneously broken chiral symmetry.
(3) Then the updated results for the nonsinglet $N_f = 8$ spectra are given, which are all consistent with our previously published data [17].

Then in Sec. IV, we present the data for σ mass, giving an update to our previous data for $N_f = 8$, which are analyzed according to the formula Eq. (1.4) and found to give d_0, d_1 consistent with the previous publications [16,17]. We also present new data for $N_f = 4$, and further compare d_0, d_1 among $N_f = 4, 8$ and $N_f = 12$. We also present the σ mass and the nonsinglet masses both in units of $F_\pi/\sqrt{2}$ and in units of $1/\sqrt{8t_0}$, and highlight the characteristic features of $N_f = 4, 8, 12$.

Section V is the core part of the present paper, presenting completed results for the η' in comparison with other spectra. We show the results for the mass both in terms of the UV and IR scales; the latter indicate good agreement with the prediction of the n_f dependence in the anti-Veneziano limit Eq. (1.6), thus confirming the previous results [49,50]. Section VI is devoted to the summary.

We also include more detailed data and analyses in the Appendixes. In particular, Appendix C compares our results with those of the LSD Collaboration in units of $1/\sqrt{8t_0}$.

II. MESON MASSES IN THE ANTI-VENEZIANO LIMIT

In the following sections, we will present new lattice data for $N_f = 4, 8, 12$ QCD. In particular, we will present results for the masses of the flavor-singlet scalar σ and the pseudoscalar η', each of which has characteristic contributions from the anomaly, the scale, and the $U(1)$ axial anomaly. In order to understand and contextualize the numerical results we will present, we must have a theoretical functional form to compare them with. In this section, we will discuss the theoretical issues surrounding the characteristic $n_f(\equiv N_f/N_c)$ dependence of the anomalous parts of the two mesons we will be focusing on, in the limit

$$N_c \to \infty \quad \text{with} \quad N_c\alpha = \text{fixed}, \qquad n_f = N_f/N_c = \text{fixed} \gg 1. \tag{2.1}$$

We refer to this as the anti-Veneziano limit [12], by analogy with the related limit proposed by Witten [51] and Veneziano [52] in which n_f is fixed at a small value referred to as the Veneziano limit. The anti-Veneziano limit is of interest in our setup as in the theories we are considering, $n_f \in [\frac{4}{3}, 4]$; this range is well away from the Veneziano limit, and we may expect the upper end to be better represented by the anti-Veneziano limit than the lower end.

A. An IR scale from the gradient flow

In the discussion that follows, we will normalize the spectral quantities using an IR scale $\Lambda_{\rm IR} = \Lambda_{\rm IR}|_{N_c,N_f}$; that is, a scale where the coupling becomes strong, allowing the formation of bound states from the nonperturbative dynamics. This scale is intrinsic to the theory specified by the combination of N_c and N_f. To allow comparisons between theories with different N_f, bound state masses such as those of the η' and σ should be measured in terms of such a scale.

In the broken phase, $\Lambda_{\rm IR}$ is essentially the confinement scale and/or the spontaneous chiral breaking scale m_D (the "dynamical mass"). More properly, this can be called the "consitutent quark mass" $m_f^{(\text{constituent})}$; it is related to the mass of the ground state bound state

$$\Lambda_{\rm IR} \simeq 2m_f^{(\text{constituent})} \simeq 2m_D + 2m_f^{(R)} \simeq M_\rho, \tag{2.2}$$

where $m_f^{(R)}$ is the "current quark mass" defined as the renormalized, on-shell mass of the fermion: $m_f^{(R)} = m_f^{(R)}(\mu)\big|_{\mu=m_f^{(\text{constituent})}}$.[6]

[6]Note that another ground state mass, that of the π, is the NG boson mass in the broken phase, and so it has a different dependence on m_D and $m_f^{(R)}$.

However, defining $\Lambda_{\rm IR}$ via Eq. (2.2) is not suitable for theories in the conformal phase, where bound states exist only in the presence of a nonzero explicit fermion mass $m_f^{(R)} \neq 0$. Ordinary fermionic bound states (except for the flavor-singlet scalar σ discussed in a later subsection) are formed via the weakly coupled Coulomb force instead of the confining force. The masses of two-body hadrons then become

$$M_{\rm H} \sim 2m_f^{(R)} = 2m_f \cdot Z_m^{-1} = 2m_f \left(\frac{\Lambda_{\rm UV}}{m_f^{(R)}}\right)^{\gamma_m} = 2\Lambda_{\rm UV}\left(\frac{m_f}{\Lambda_{\rm UV}}\right)^{\frac{1}{1+\gamma_m}}, \tag{2.3}$$

where $\gamma_m = \gamma_m(\alpha(\mu))|_{\mu=m_f^{(R)}}$ and $\Lambda_{\rm UV}$ a corresponding UV scale (the intrinsic scale denoted in QCD as $\Lambda_{\rm QCD}$), which characterizes the asymptotically free running of the coupling. Specifically, for scales $\mu \gg \Lambda_{\rm UV}$, then $\gamma_m(\alpha(\mu)) \sim \alpha(\mu) \sim 1/\ln(\mu/\Lambda_{\rm UV}) \ll 1$. On the lattice, we may identify this UV scale with the inverse lattice spacing $\Lambda_{\rm UV} = 1/a$, then this is nothing but the hyperscaling relation [18–20]

$$aM_{\rm H} \sim 2am_f^{(R)} = 2(am_f)^{\frac{1}{1+\gamma_m}}. \tag{2.4}$$

This explicit fermion mass also introduces a new IR scale $\Lambda_{\rm YM}$ below which the fermions decouple, leaving a confined pure Yang-Mills theory. [Although the IR fixed point α_* is washed out, there still remains a remnant $\alpha(\mu) \simeq \alpha_*$ for $m_f^{(R)} < \mu < \Lambda_{\rm UV}$.] This is given by [18]

$$\Lambda_{\rm YM} = m_f^{(R)} \exp\left(-\frac{1}{b_0\alpha_*}\right) = \Lambda_{\rm UV}\left(\frac{m_f}{\Lambda_{\rm UV}}\right)^{\frac{1}{1+\gamma_m}} \exp\left(-\frac{1}{b_0\alpha_*}\right), \tag{2.5}$$

where $b_0 = \frac{11N_c}{6\pi}$ is the coefficient of the one-loop beta function of pure Yang-Mills theory, and α_* the IR fixed point in two-loop perturbation theory.

For the specific case of $N_c = 3$, $N_f = 12$, then $b_0 = \frac{11}{2\pi}$, $\alpha_* \simeq 0.754$, giving $\exp(-\frac{1}{b_0\alpha_*}) \simeq 0.47$. On the lattice, Eq. (2.5) then becomes

$$a\Lambda_{\rm YM} = am_f^{(R)} \exp\left(-\frac{1}{b_0\alpha_*}\right) \simeq 0.47am_f^{(R)} < am_f^{(R)}. \tag{2.6}$$

Comparing Eq. (2.3) with Eq. (2.6), we see that in the conformal phase,

$$\Lambda_{\rm YM} < M_{\rm H}. \tag{2.7}$$

When comparing theories in different phases including inside and outside the conformal window, we may choose to use for $\Lambda_{\rm IR}$ the gradient flow scale [53]

$$\Lambda_{\rm IR} = \frac{1}{\sqrt{8t_0}} \tag{2.8}$$

as an alternative to using M_ρ as in Eq. (2.2). As a gluonic operator, we expect this to be relatively independent of explicit chiral breaking effects, and allow a more robust comparison between theories in different phases. On the lattice, we may compare $\Lambda_{\rm IR}$ with a corresponding UV scale $\Lambda_{\rm UV} = 1/a$. Analogous to Eq. (2.2), we expect the scale $1/\sqrt{8t_0}$ to consist of two contributions: the chiral limit value from the dynamics of the theory $1/\sqrt{8t_0}|_{m_f=0}$, and a deformation due to the fermion mass, proportional to $m_f^{(R)}$. This leads us to anticipate the following behavior for the ratio of the two scales:

$$\frac{\Lambda_{\rm IR}}{\Lambda_{\rm UV}} = \frac{a}{\sqrt{8t_0}} \simeq 2am_D + C_{t_0}am_f^{(R)} \simeq \left.\frac{a}{\sqrt{8t_0}}\right|_{m_f=0} + C_{t_0}(am_f)^{\frac{1}{1+\gamma_m}}. \tag{2.9}$$

The first term is expected to scale with the dynamical mass m_D generated by the chiral condensate $a/\sqrt{8t_0}|_{m_f=0} \sim a \cdot 2m_D$; this then tends to zero as the conformal window is approached from below, while in the conformal window, there is no chiral condensate, and $a/\sqrt{8t_0}|_{m_f=0} \equiv 0$. We also introduce the coefficient C_{t_0}, which depends on the flow time. Since this is a gluonic operator, C_{t_0} is expected to be smaller than the coefficients associated with the two-body hadron masses in Eq. (2.3). Therefore, in the broken phase, we expect $C_{t_0} \leq 2$, while in the conformal phase, Eq. (2.6) implies $C_{t_0} < 1$.

More concretely, as we will demonstrate in Sec. III, these expectations—or even the stronger condition $C_{t_0} \leq 1$ for $N_f = 4, 8$—are typically satisfied for our chosen values of the flow time. This implies

$$\text{Broken(near-conformal)}: \quad M_\rho\sqrt{8t_0} \simeq \frac{2m_D + 2m_f^{(R)}}{2m_D + C_{t_0}m_f^{(R)}} \to \begin{cases} \gtrsim 2 & (m_f^{(R)} \gg m_D), \\ \simeq 1 & (m_f^{(R)} \ll m_D), \end{cases}$$

$$\text{Conformal}: \quad M_\rho\sqrt{8t_0}(\gtrsim M_\pi\sqrt{8t_0}) > 2. \tag{2.10}$$

B. η' mass in the anti-Veneziano limit

We will consider first the η' meson. In QCD with N_f degenerate fermions, the flavor-singlet axial-vector current

$$A_\mu^0(x) = \sum_{i=1}^{N_f} \bar{\psi}_i(x)\gamma_\mu\gamma_5\psi_i(x) \tag{2.11}$$

has divergence

$$\partial^\mu A_\mu^0(x) = 2m_f \sum_{i=1}^{N_f} \bar{\psi}_i i\gamma_5\psi_i + 2N_f \frac{\alpha}{8\pi} G^{\mu\nu}\tilde{G}_{\mu\nu}(x), \tag{2.12}$$

where the second term is the chiral anomaly. We may then define the η' decay constant via

$$\langle 0|A_\mu^0(x)|\eta'(q_\mu)\rangle = i\sqrt{2N_f}F_{\eta'}q_\mu e^{-iqx}, \tag{2.13}$$

$$\langle 0|\partial^\mu A_\mu^0(x)|\eta'(q_\mu)\rangle = \sqrt{N_f}F_\pi M_{\eta'}^2 e^{-iqx}, \tag{2.14}$$

which then gives $F_{\eta'} = F_\pi/\sqrt{2}$; this is independent of whether the theory is in the broken or conformal phase.

The relevant anomalous chiral WT identity then takes the form

$$\begin{aligned} 0 &= \lim_{q^\mu\to 0} iq^\mu \int d^4x e^{-iqx}\langle T(A_\mu^0(x)\cdot\partial^\mu A_\mu^0(0)\rangle \\ &= \langle[iQ_5^0, \partial^\mu A_\mu^0(x)]\rangle + i\mathcal{F}.\mathcal{T}.\langle T(\partial^\mu A_\mu^0(x)\cdot\partial^\mu A_\mu^0(0))\rangle|_{q_\mu\to 0}, \end{aligned} \tag{2.15}$$

$$\begin{aligned} -\langle[iQ_5^0, \partial^\mu A_\mu^0(x)]\rangle &= i\mathcal{F}.\mathcal{T}.\langle T(\partial^\mu A_\mu^0(x)\cdot\partial^\mu A_\mu^0(0))\rangle|_{q_\mu\to 0} \\ &= \frac{N_f F_\pi^2 M_{\eta'}^4}{M_{\eta'}^2 - q^2}\bigg|_{q_\mu\to 0} \end{aligned} \tag{2.16}$$

$$\begin{aligned} &= N_f F_\pi^2 M_{\eta'}^2 \\ &= N_f F_\pi^2[(M_{\eta'}^2)^{(\text{non-anomalous})} \\ &\quad + (M_{\eta'}^2)^{(\text{anomalous})}], \end{aligned} \tag{2.17}$$

where $\mathcal{F}.\mathcal{T}.$ refers to the Fourier transform of the correlator, which the anti-Veneziano (i.e., large-N_c) limit allows us to evaluate using a single pole.

The nonanomalous and anomalous contributions are then given by

$$\begin{aligned} (M_{\eta'}^2)^{(\text{non-anomalous})} &= \frac{1}{N_f F_\pi^2}\left\langle\left[-iQ_5^0, 2m_f\sum_{i=1}^{N_f}\bar{\psi}_i i\gamma_5\psi_i\right]\right\rangle, \\ &= \frac{1}{N_f F_\pi^2}\cdot 2m_f\sum_{i=1}^{N_f} -2\langle\bar{\psi}_i\psi_i\rangle = M_\pi^2 \to 0(m_f\to 0), \end{aligned} \tag{2.18}$$

$$\begin{aligned} (M_{\eta'}^2)^{(\text{anomalous})} &= M_{\eta'}^2 - M_\pi^2 = \frac{1}{N_f F_\pi^2} i\mathcal{F}.\mathcal{T}.\left\langle T\left(2N_f\frac{\alpha}{8\pi}G^{\mu\nu}\tilde{G}_{\mu\nu}(x)\cdot 2N_f\frac{\alpha}{8\pi}G^{\mu\nu}\tilde{G}_{\mu\nu}(0)\right)\right\rangle\bigg|_{q_\mu\to 0} \\ &\sim \frac{N_f}{F_\pi^2}\Lambda_{\text{IR}}^4\left[(\text{gluonloop}) + \frac{N_f}{N_c}(\text{fermionloop})\right] \\ &\sim \frac{N_f}{N_c}\Lambda_{\text{IR}}^2\left[(\text{gluonloop}) + \frac{N_f}{N_c}(\text{fermionloop})\right]. \end{aligned} \tag{2.19}$$

Here, "gluon loop" and "fermion loop" refer to the contributions from the diagrams in the left and right panels of Fig. 1, respectively [12].

In the Veneziano limit $n_f \equiv N_f/N_c \ll 1$, the theory is in the broken phase, and the gluonic loop contribution in Eq. (2.19) dominates over the fermionic one. In this case, the anomalous mass of the η' becomes

$$\frac{(M_{\eta'}^2)^{(\text{anomalous})}}{\Lambda_{\text{IR}}^2} \sim n_f \ll 1. \tag{2.20}$$

This matches the expectations that in this limit, the η' meson is a pseudo-NG boson with parametrically vanishing mass.[7]

In the anti-Veneziano limit as defined in Eq. (2.1), however, the fermion loop contribution in Eq. (2.19) dominates over the gluon one. This then gives

[7]In $N_f = N_c = 3$ QCD, as observed in experiments, we see a large value of $M_{\eta'}$ comparable with M_ρ, which does not align with this prediction of a parametrically vanishing mass. This is because $N_f = N_c = 3$ is far from the idealized Veneziano limit of $N_f \ll N_c$.

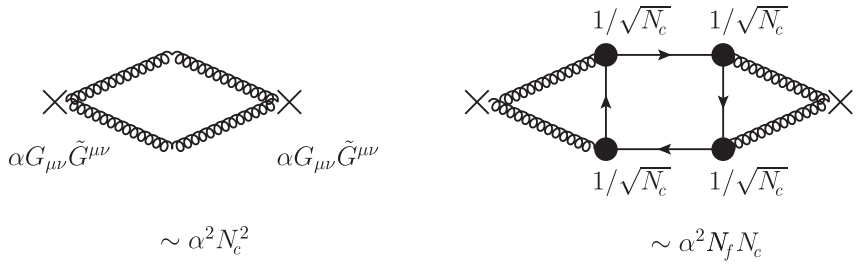

FIG. 1. The loop diagrams contributing to the correlation function of $\alpha G_{\mu\nu}\tilde{G}^{\mu\nu}$ coming from the gluon loop (left panel) and fermion loop (right panel). The large-N_c and -N_f scalings have also been specified.

$$(M_{\eta'}^2)^{(\text{anomalous})} \sim \frac{N_f\alpha^2}{F_\pi^2}(N_c^3 N_f \alpha^2 \Lambda_{\text{IR}}^4) \sim n_f^2 \cdot \Lambda_{\text{IR}}^2. \tag{2.21}$$

The nonanomalous contribution proportional to the pion mass is negligible in this limit, giving

$$\frac{M_{\eta'}^2}{\Lambda_{\text{IR}}^2} \simeq \frac{M_{\eta'}^{2\,(\text{anomalous})}}{\Lambda_{\text{IR}}^2}. \tag{2.22}$$

We therefore expect to observe the normalized η' mass to be approximately independent of m_f in the broken phase. Meanwhile, in the conformal phase, the only scale is provided by the explicit deforming fermion mass, meaning $M_{\eta'}^{2\,(\text{anomalous})}$ obeys the same hyperscaling relations as M_π^2 and $\Lambda_{\text{IR}}^2 = 1/(8t_0)$, and so the normalized η' mass should be fully independent of m_f.

We may now define the ratio

$$R_{N_f}^2 \equiv 8t_0 \cdot (M_{\eta'}^{(\text{anomalous})})_{N_f}^2 = \left(\frac{M_{\eta'}^{(\text{anomalous})}}{\Lambda_{\text{IR}}}\right)_{N_f}^2 = \left(\frac{M_{\eta'}^2 - M_\pi^2}{\Lambda_{\text{IR}}^2}\right)_{N_f} \sim n_f^2 \tag{2.23}$$

in the anti-Veneziano limit. Thus, for the values of N_f we consider, we expect

$$R_{12}^2 :\ R_8^2 : R_4^2 \simeq 9:4:1. \tag{2.24}$$

These will be shown to be consistent with our lattice data in Sec. V.

C. σ mass in the conformal and broken phases

The flavor-singlet scalar σ has a mass obeying the WT identity for the scale symmetry, such that

$$\theta_\mu^\mu = \partial_\mu D^\mu = \frac{\beta^{(\text{NP})}(\alpha)}{4\alpha} G_{\mu\nu}^2 + (1+\gamma_m) m_f \sum_{i=1}^{N_f} \bar{\psi}^i \psi^i, \tag{2.25}$$

where $\frac{\beta^{(\text{NP})}(\alpha)}{4\alpha} G_{\mu\nu}^2$ is the nonperturbative component of the trace anomaly, in which $G_{\mu\nu}$ is the gluon field strength, and $\beta^{(\text{NP})}(\alpha)$ is the nonperturbative beta function for the nonperturbative running (or walking) of the coupling. The mass anomalous dimension γ_m here is the nonperturbative infrared value $\gamma_m = \gamma_m(\alpha(\mu))|_{\mu=\Lambda_{\text{IR}}}$.

In the broken phase, both the nonperturbative beta function and the nonperturbative infrared mass anomalous dimension may be estimated via the ladder SD equation (which conceptually aligns with the anti-Veneziano limit), giving

$$\begin{aligned} m_f &\equiv m_f^{(R)} \cdot Z_m \sim m_f^{(R)} \cdot \frac{m_D}{\Lambda}, \\ \beta^{(\text{NP})}(\alpha) &= \left.\frac{\partial\alpha(\Lambda)}{\partial \ln\Lambda}\right|_{m_D=\text{fixed}} \\ &= -\frac{2\pi^2\alpha_{\text{cr}}}{\ln^3\left(\frac{4\Lambda}{m_D}\right)} = -\frac{2\alpha_{\text{cr}}}{\pi}\left(\frac{\alpha}{\alpha_{\text{cr}}} - 1\right)^{3/2}, \\ \gamma_m(\alpha) &= \left.\frac{\partial \ln Z_m^{-1}}{\partial \ln\Lambda}\right|_{m_D=\text{fixed}} = 1, \end{aligned} \tag{2.26}$$

and

$$m_D = 4\Lambda \exp\left(-\frac{\pi}{\sqrt{\alpha/\alpha_{\text{cr}} - 1}}\right); \tag{2.27}$$

then $m_D/\Lambda = m_D/\Lambda_{\text{UV}} \to 0$ near the conformal edge in an essential singularity and cannot be power expanded. (Fuller details are presented in Ref. [12] and references therein.)

We then expect bound state masses to have a hierarchy of order $\mathcal{O}(\Lambda_{\text{IR}}) = \mathcal{O}(2m_D) \ll \Lambda_{\text{UV}}$ as $\alpha \to \alpha_{\text{cr}}$. Noting that $n_f = n_f^{\text{cr}}$ at $\alpha = \alpha_* = \alpha_{\text{cr}}$, we have

$$\begin{aligned} \frac{\Lambda_{\text{IR}}}{\Lambda_{\text{UV}}} &\sim \frac{2m_D}{\Lambda_{\text{UV}}} \\ &\sim \exp\left(-\frac{\pi}{\sqrt{\alpha/\alpha_{\text{cr}} - 1}}\right) \sim \exp\left(-\frac{A}{\sqrt{n_f^{\text{cr}} - n_f}}\right) \\ &\to 0 \quad \text{as } \mathrm{n_f} \equiv \frac{\mathrm{N_f}}{\mathrm{N_c}} \to \mathrm{n_f^{cr}} \equiv \left(\frac{\mathrm{N_f}}{\mathrm{N_c}}\right)^{\mathrm{cr}}. \end{aligned} \tag{2.28}$$

At this point, at the two-loop level,

$$\alpha(\mu^2 = \Lambda_{\rm UV}^2) = \frac{\alpha_*}{1 + W(e^{-1})} \simeq 0.78\alpha_*, \tag{2.29}$$

where the IR fixed point is at

$$\alpha_* \simeq \frac{4\pi}{N_c} \cdot \frac{11 - 2n_f}{13n_f - 34}, \tag{2.30}$$

and the ladder critical coupling is

$$\alpha_{\rm cr} = \frac{\pi}{3} \cdot \frac{1}{C_2} = \frac{\pi}{3} \frac{2N_c}{N_c^2 - 1} \gtrsim \frac{2\pi}{3N_c}. \tag{2.31}$$

The two-loop values are then

$$A \simeq \frac{3\sqrt{2}\pi}{5} \simeq 2.7, \qquad n_f^{\rm cr} \lesssim 4. \tag{2.32}$$

This suggests that $N_f = 12$ is barely inside the conformal window, although the two-loop value for α_* is not expected to be precise, and hence neither is the value of $n_f^{\rm cr}$. Further details may be found in Ref. [12].

Turning our attention back to the conformal phase, we may at first sight expect that since we introduce a nonzero fermion mass, both the scale symmetry and chiral symmetry are broken explicitly but not spontaneously. In this case, all fermionic bound states, including the π and σ, would be Coulombic bound states as discussed in Eq. (2.3) above. This is what is observed in heavy quarkonia, for similar reasoning.

However, a key difference of the conformal phase from the heavy quarkonia is that the degenerate massive fermions giving rise to confinement decouple, with the induced confinement scale—the gluon condensate—totally governed by the fermion mass $m_f^{(R)}$ as described by Eq. (2.5). The gluon condensate breaks the scale symmetry not only explicitly, but also spontaneously. Specifically, the σ is a pseudo-NG boson of the scale symmetry (although the explicit breaking scale $m_f^{(R)}$ is much larger than the spontaneous breaking scale $\Lambda_{\rm YM} \simeq m_f^{(R)}/2$ in the $N_f = 12$ case). The gluon condensate does not however break chiral symmetry, which as such is only explicitly broken; the π therefore remains a non-NG boson.

Given this, we may try to estimate the σ mass not only in the broken phase, but also in the conformal phase, where the scale symmetry is broken both explicitly and spontaneously by the same infrared mass scale of the fermion mass $m_f^{(R)}$. (It is of course also explicitly broken in the UV by the regularization; this makes no difference to the formation of bound states.) Following the argument of Ref. [29], we may start with the dilatation current given in Eq. (2.25), whose WT identity [with single-pole dominance as in the case for η' in Eq. (2.16)] is

$$M_\sigma^2 F_\sigma^2 = i\mathcal{F}.\mathcal{T}.\langle T(\partial_\mu D^\mu(x) \cdot \partial_\mu D^\mu(0))\rangle\big|_{q_\mu \to 0}$$
$$= \langle [-iQ_D, \partial_\mu D^\mu(0)]\rangle \tag{2.33}$$

$$= -4 \cdot \frac{\beta^{\rm (NP)}(\alpha)}{4\alpha} \langle G_{\mu\nu}^2 \rangle - (3 - \gamma_m) \cdot (1 + \gamma_m) m_f \sum_{i=1}^{N_f} \langle \bar\psi^i \psi^i \rangle. \tag{2.34}$$

Similarly, the single-pole-dominated WT identity for the nonsinglet axial-vector current A_μ^α ($\alpha = 1, 2, 3$) for each doublet ψ^i ($i = 1, 2$) gives the Gell-Mann–Oakes–Renner (GMOR) relation:

$$\left(\frac{F_\pi}{\sqrt{2}}\right)^2 M_\pi^2 \cdot \delta^{\alpha\beta} = \langle [-iQ_5^\alpha, \partial^\mu A_\mu^\beta(0)]\rangle$$
$$= -m_f \sum_{i=1}^{2} \langle \bar\psi^i \psi^i \rangle \cdot \delta^{\alpha\beta}. \tag{2.35}$$

While Eqs. (2.33) and (2.35) are usually derived using the soft pion theorem, they are in fact based simply on the pole dominance and hence are valid in both the broken and conformal phases. This then gives [29]

$$M_\sigma^2 = \left(M_\sigma^{\rm (anomalous)}\right)^2 + \frac{(3 - \gamma_m) \cdot (1 + \gamma_m) \frac{N_f}{2} \left(\frac{F_\pi}{\sqrt{2}}\right)^2}{F_\sigma^2} \cdot M_\pi^2$$
$$= d_0 + d_1 \cdot M_\pi^2. \tag{2.36}$$

This may then be used as a fit form for lattice data.

When combined with an estimate of the anomalous dimension γ_m, the results of the fit for d_1 may be used to estimate the ratio $F_\sigma/(F_\pi/\sqrt{2}) = \sqrt{N_D} F_\sigma / v_{\rm EW}$ (where N_D is the number of electroweak doublets). From Eq. (2.36),

$$d_1 = \left(\sqrt{(3 - \gamma_m)(1 + \gamma_m)\frac{N_f}{2}} \cdot \frac{F_\pi/\sqrt{2}}{F_\sigma}\right)^2$$
$$\equiv \left(C_{\gamma_m} \cdot \frac{F_\pi/\sqrt{2}}{F_\sigma}\right)^2. \tag{2.37}$$

Linear sigma model and holographic QCD calculations in the near-conformal broken and conformal phases suggest that (via footnote 18 of Ref. [12] and references therein)

$$F_\sigma^2 = d_\sigma^2 \cdot \frac{N_f}{2} \left(\frac{F_\pi}{\sqrt{2}}\right)^2 = (3 - \gamma_m)^2 \cdot \frac{N_f}{2} \left(\frac{F_\pi}{\sqrt{2}}\right)^2, \tag{2.38}$$

with $d_\sigma = 3 - \gamma_m$ the scale dimension of $\sigma \sim \bar{\psi}\psi$.[8] If this is the case throughout the near-conformal and conformal phases, then from Eq. (2.37) we have

$$d_1 = \frac{1+\gamma_m}{3-\gamma_m}. \tag{2.39}$$

We may also use this result to make predictions informing potential lattice studies of $12 < N_f < 16.5$: In this case, the SD equation gives

$$\gamma_m \simeq 1 - \sqrt{1-\alpha_*/\alpha_{\rm cr}}, \tag{2.40}$$

$$\searrow 0 \quad \text{as } \alpha_* \searrow 0 (\mathrm{N_f} \nearrow 16.5). \tag{2.41}$$

This in turn would predict

$$d_1 \searrow 1/3 \quad \text{as } \mathrm{M}_\sigma \searrow \mathrm{M}_\pi/\sqrt{3} \quad \text{and} \tag{2.42}$$

$$\frac{F_\sigma}{F_\pi/\sqrt{2}} \nearrow 8.6 \quad \text{as } \mathrm{M}_\sigma^{\mathrm{w}} \simeq \mathrm{d}_1 \mathrm{M}_\pi^2 (\gg \mathrm{d}_0). \tag{2.43}$$

On the other hand,

$$d_0 = M_\sigma^{2\,(\text{anomalous})} = -\frac{4\cdot\langle\theta_\mu^\mu\rangle}{F_\sigma^2} = -\frac{\beta^{(\mathrm{NP})}(\alpha)}{\alpha}\frac{\langle G_{\mu\nu}^2\rangle}{F_\sigma^2} \tag{2.44}$$

comes from the nonperturbative trace anomaly. In the broken phase, it is nonzero even in the chiral limit, as m_D violates the scale symmetry, both spontaneously and explicitly. Thus, the chiral limit σ mass d_0 is a key observable to understand whether a theory is a suitable candidate for a walking technicolor model with a composite Higgs boson of appropriate mass.

In the anti-Veneziano limit, the fermion loop dominates over the gluon loop in the computation of the anomaly. Similar to the η' in Fig. 1, this then gives from Eq. (2.33)

$$M_\sigma^{2\,(\text{anomalous})} \cdot F_\sigma^2 = i\mathcal{F}.\mathcal{T}.\left\langle T\left(\frac{\beta^{(\mathrm{NP})}(\alpha)}{4\alpha}G_{\mu\nu}^2(x)\cdot\frac{\beta^{(\mathrm{NP})}(\alpha)}{4\alpha}G_{\mu\nu}^2(0)\right)\right\rangle\Big|_{q_\mu\to 0} \tag{2.45}$$

$$\sim N_f N_c m_D^4, \tag{2.46}$$

with

$$F_\sigma^2 \sim (3-\gamma_m)^2 N_f N_c m_D^2 \tag{2.47}$$

up to a numerical factor roughly independent of N_f and N_c. An implicit N_f dependence comes from $F_\sigma^2 \sim (3-\gamma_m)^2$ via the details of the dynamics as in the linear sigma model/holography discussed above.

This then implies

$$M_\sigma^2|_{m_f=0} = d_0 = \mathcal{O}\left(\left(\frac{m_D}{3-\gamma_m}\right)^2\right), \quad \forall\ N_f,. \tag{2.48}$$

As the conformal window is approached from below, we expect the anomalous dimension $\gamma_m \to 1$, and so this vanishes:

$$M_\sigma^2|_{m_f=0} = \mathcal{O}\left(\left(\frac{m_D}{2}\right)^2\right) \to 0 \qquad (n_f \nearrow n_f^{\rm cr}). \tag{2.49}$$

This is similar to other states in the spectrum, which obey

$$M_{\rm H}^2|_{m_f=0} = \mathcal{O}((2m_D)^2) \to 0 \qquad (n_f \nearrow n_f^{\rm cr}) \tag{2.50}$$

with no additional suppression, contrary to the popular assumption [5,30,55,56] that the vanishing beta function suppresses M_σ^2 relative to other states.[9] Thus, in the near-conformal region, σ as a pseudo-NG boson has a small but nonzero ratio:

$$\left.\frac{M_\sigma^2}{M_{\rm H}^2}\right|_{m_f=0} \to \text{const.}(\ll 1) \qquad (n_f \nearrow n_f^{\rm cr}). \tag{2.51}$$

Note that $M_\sigma^2|_{m_f=0} = d_0 \sim {m_D}^2$ has no additional dependence on N_f when expressed in units of $\Lambda_{\rm IR} = 1/\sqrt{8t_0}$ (aside from the abovementioned implicit N_f dependence of F_σ^2 through γ_m). Similarly, d_1 also has

[8]For $N_f = 2$, this becomes the standard linear sigma model relation $F_\sigma = F_\pi/\sqrt{2} = \langle\sigma\rangle$ for $d_\sigma = 1$, or equivalently, the Nambu–Jona-Lasinio (NJL) model with $\gamma_m = 2$. Note also that the kinetic term (the scale-invariant part) of the $N_f = 2$ linear sigma model (or the Standard Model Higgs Lagrangian) is rewritten into the dilaton chiral perturbation theory (dChPT) Lagrangian, Eq. (2) of Ref. [29], through polar decomposition, with its mass from the explicit scale-symmetry breaking potential $M^2 = 2\lambda\langle\sigma\rangle^2$ as a pseudodilaton for $\lambda \ll 1$. The interested reader is referred to Ref. [54] and references cited therein.

[9]An explicit ladder computation [12,57] shows that the vanishing beta function in Eq. (2.26) is precisely canceled by the diverging $\langle G_{\mu\nu}^2\rangle \sim N_f N_c m_D^4 \cdot \ln^3(\Lambda/m_D) \to \infty$, such that $-\beta^{(\mathrm{NP})}(\alpha)/\alpha \cdot \langle G_{\mu\nu}^2\rangle \sim N_f N_c m_D^4$ is independent of Λ, with the result precisely the same as an independent computation of $\langle\theta_\mu^\mu\rangle$ through the effective potential. Such a complete cancellation might be avoided only by including nonladder effects, such as in the holographic model [58].

no explicit dependence on N_f in the anti-Veneziano limit (but again has an implicit N_f dependence from γ_m). This contrasts the result in Eq. (2.23) that $M_{\eta'}^2 \cdot 8t_0 = M_{\eta'}^2/\Lambda_{\rm IR}^2 \sim N_f^2$.

Equation (2.36), here based on the WT identity for the scale symmetry, was originally derived in the broken phase via dChPT [29] at tree level. It has further been shown explicitly [29] that there exists a possible deviation from Eq. (2.36) due to the chiral log of the pion loop effects (as in the standard ChPT) near the chiral limit. For the loop expansion parameter

$$\chi = M_\pi^2/\Lambda_\chi^2 \ll 1, \tag{2.52}$$

where

$$\Lambda_\chi^2 = (4\pi \cdot (F/\sqrt{2}))^2/N_f, \qquad F \equiv F_\pi|_{m_f=0}, \tag{2.53}$$

as well as $M_\pi^2 \ll M_\sigma^2$. Then, from Eq. (10) of Ref. [29]

$$\frac{M_\sigma^2}{\Lambda_\chi^2} \simeq \frac{d_0}{\Lambda_\chi^2}\left(1+\frac{d_1}{2}\chi\ln\chi\right) + d_1\left(1+\frac{9}{4}\chi\ln\chi\right)\cdot\chi (N_f \gg 1). \tag{2.54}$$

While this expansion is relatively flat for $0 < \chi < 1$, as χ increases past this region, the chiral log present in dChPT no longer makes sense, and Eq. (2.36) should be used instead. This is the region where our numerical results lie, with $\chi \gg 1$ and (for $N_f = 8$) $M_\sigma^2 \lesssim M_\pi^2$. Further, since $\Lambda_\chi^2 \simeq (N_c/N_f)\cdot(2m_D)^2$, simulations at much smaller values of m_f would be needed in order to observe the loop effects.

This implies that the value obtained for d_0 by fitting using Eq. (2.36) is effectively shifted to a smaller value than the true chiral limit value of $d_0 = M_\sigma^2|_{m_f=0} = M_\sigma^{2\,(\rm anomalous)}$, as illustrated in Fig. 2 of Ref. [29]. On the other hand, the fit value of d_1 is the same as d_1 in the chiral limit $\chi \to 0$ where chiral log effects disappear, and so is the value $\frac{F_\sigma}{F_\pi/\sqrt{2}}$ in Eq. (2.59). We shall return to this point in Sec. IV where we discuss the new data of this paper on the mass of the σ as a candidate for the Higgs boson.

While dChPT is valid in the near-conformal broken phase, the alternative derivation [29] presented here shows that Eq. (2.36) is also valid not only deep in the broken phase (again with the d_0 fit value up to the chiral log) in the absence of any remnant of scale symmetry (and where we do not expect to observe hyperscaling), but also inside the conformal window where dChPT is irrelevant. Inside the conformal window, both d_0 and $\beta^{(\rm NP)}(\alpha)$ are identically zero in the chiral limit, where no bound states exist. As such, there is a "conformal phase transition" where the order parameter m_D continuously changes going from the broken to the conformal phase in the essential singularity form, while bound states do not [22].

When we introduce an explicit fermion mass m_f, the scale symmetry is broken explicitly and spontaneously as described in Sec. II A. We expect that similar to Eq. (2.5), the anomalous component of the σ mass is of the order of the confining scale of pure Yang-Mills theory $\Lambda_{\rm YM} \simeq m_f^{(R)}/2 = 1/(2\sqrt{8t_0})$ instead of $\Lambda_{\rm IR} = 1/\sqrt{8t_0}$, in contrast to that of η' [Eq. (2.23)], which is irrelevant to the spontaneous scale-symmetry breaking. Specifically,

$$d_0 = (M_\sigma^{(\rm anomalous)})^2 \simeq \frac{\Lambda_{\rm YM}^2}{(3-\gamma_m)^2} \simeq \frac{(m_f^{(R)})^2}{4(3-\gamma_m)^2} \simeq \frac{M_\pi^2}{16(3-\gamma_m)^2}, \tag{2.55}$$

where we have again relied on relation Eq. (2.38). Putting this back into Eq. (2.36) gives

$$M_\sigma^2 = \left(\frac{1}{16(3-\gamma_m)^2} + d_1\right) M_\pi^2. \tag{2.56}$$

Let us now briefly explore the compatibility of the predictions above with our previous work. Considering Eq. (2.36), for $N_f = 8$ we found in our previous work [17][10]:

$$d_0 = -0.0028(98)\binom{36}{354}, \qquad d_1 = 0.89(26)\binom{75}{11}. \tag{2.57}$$

Here, $d_0 \lesssim 0$ would suggest that

$$M_\sigma^2 \lesssim d_1 M_\pi^2 \simeq M_\pi^2, \tag{2.58}$$

suggesting that if the $N_f = 8$ theory is in the broken phase, then our data are far from the chiral limit, where we expect $M_\sigma^2 > M_\pi^2 = 0$.

Our previous observations for γ_* from hyperscaling would then indicate that for $N_f = 8$, $\gamma_m \simeq 1$. Considering Eq. (2.37), this then implies $\Rightarrow C_{\gamma_m} \simeq 4$, and so[11]

$$\frac{\sqrt{N_D}F_\sigma}{v_{\rm EW}} = \frac{F_\sigma}{F_\pi/\sqrt{2}} = C_{\gamma_m}\cdot\frac{1}{\sqrt{d_1}} \simeq 4. \tag{2.59}$$

This is consistent with the linear sigma model prediction in Eq. (8), and gives $d_1 \simeq 1$. For $N_f = 12$, $\gamma_m \simeq 0.4 - 0.5$ would give

[10]A consistent set of coefficients was obtained in the first lattice result for M_σ in $N_f = 8$ QCD [16].

[11]A consistent result was also obtained through the measurement of the scalar density decay constant F_S which is independent of the d_1 measurement; see Fig. 50 in Ref. [17].

$$d_1^{(N_f=12)} \simeq 0.54 - 0.6. \tag{2.60}$$

Equation (2.56) implies that M_σ is less than M_π for $N_f = 12$, since $d_1^{(N_f=12)} < 1$ [see Eq. (2.60)]; i.e., the smallness of the σ mass is related to that of its slope. Since there is no chiral log correction in the conformal phase, we expect $M_\sigma^2/M_\pi^2 < 1$ all the way down to near the chiral limit (although not, as previously discussed, at $m_f \equiv 0$, where no bound states exist).

By directly comparing the three theories, we will later demonstrate in Sec. IV how our updated lattice results for M_σ and M_π align with these formulas. Meanwhile, the relation $M_\sigma < M_\pi$ for $N_f = 12$ has been numerically confirmed in our previous lattice result [15], independently of these formulas.

III. SETUP OF LATTICE SIMULATIONS AND HADRON SPECTRUM

The LatKMI Collaboration has been systematically investigating $N_f = 4, 8, 12$, and 16 QCD using a common setup for the lattice action, exploring different fermion masses and volume sizes, and employing a single value for $N_f = 8$ and two values of the gauge coupling for $N_f = 4$ and $N_f = 12$ [13–17].

The fermionic action discretization used is the highly improved staggered quark (HISQ) action [59], while the gauge action is the tree-level improved Symanzik action [60]. It suppresses the effects of taste breaking that spoil flavor symmetry [14,17]. Moreover, for theories with a number of degenerate quarks that is a multiple of 4, staggered quarks are very efficient compared to other numbers of flavors, as taking a fourth root of the fermionic determinant is not required.

The spectrum of the low-lying flavor-non-singlet states is extracted using standard techniques involving the analysis of two-point correlation functions of interpolating operators with the correct quantum numbers. The benchmark states are the vector and the pseudoscalar, which are called the ρ and π meson, respectively, by analogy with the corresponding QCD states. Their masses, denoted by M_ρ and M_π, respectively, are easy to compute, and their mass ratio is a good qualitative indicator for spontaneous chiral-symmetry breaking or for conformality. In the first case, the π mass would be expected to go to zero and M_ρ/M_π to go to infinity in the massless fermion limit. On the other hand, an infrared conformal spectrum in the presence of an explicit fermion mass would show a constant finite M_ρ/M_π toward the masslesss limit, with possible corrections to this behavior at large quark masses.

Our previous studies have shown that the SU(3) gauge theory with $N_f = 4$ and 8 is in a hadronic, chirally broken phase where the lattice simulations show a decisive increase of the ratio M_ρ/M_π toward the massless quark limit. On the contrary, the $N_f = 12$ theory displays a constant ratio in our simulations. We repeat this computation using an updated set of lattice simulations (discussed in more detail in the specific subsection below), and confirm that we continue to observe this effect, as can be seen in Fig. 2. Note that, while the fermion mass range for the three theories is similar (in lattice units), the hadron mass ratio M_ρ/M_π has a different scale, highlighting a large deviation from a constant in the $N_f = 4$ and 8 cases. The staggered fermion taste-symmetry breaking, which is the relevant lattice discretization effect in this investigation, is briefly discussed in Appendix C; this includes, for example, $N_f = 4$ simulations performed at different lattice spacings. For $N_f = 8$, we have already shown that these effects are small [17].

In the following subsections, we will first define the means by which we set the scale using the gradient flow, as well as how this scale can be used to extract the anomalous dimension via finite-size hyperscaling, and then revisit the spectrum computations of our previous work. After

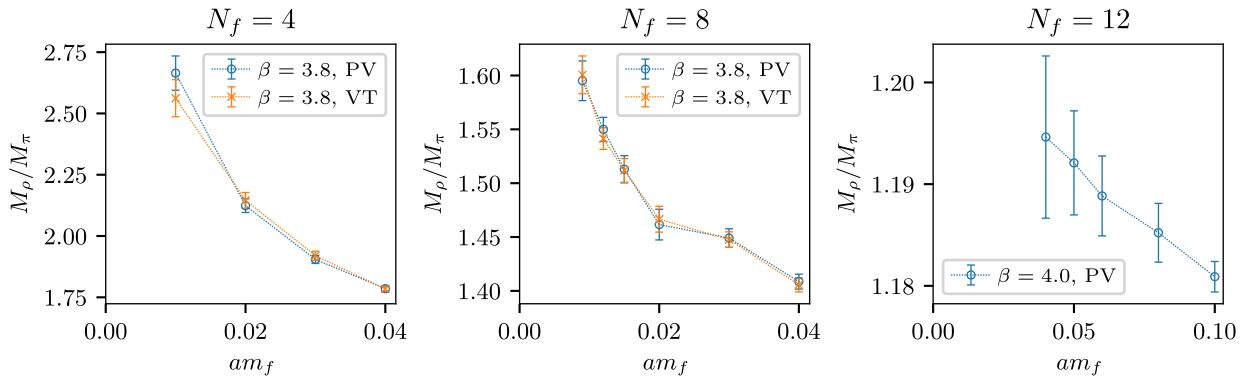

FIG. 2. The ratio M_ρ/M_π shows indications of spontaneous chiral-symmetry breaking in the massless fermion limit for $N_f = 4$ and 8 QCD different from $N_f = 12$ QCD. For $N_f = 8$, the results using different taste operators for the ρ meson are shown. The range of fermion mass considered in the three theories is similar. Lines connecting the data points are meant to guide the eye, and points are horizontally shifted for clarity.

establishing that the conclusions of our previous work still hold for $N_f = 8$ with the updated simulations at smaller quark masses, we will not repeat a full chiral or conformal analysis; subsequent sections will focus on the flavor-singlet spectrum.

A. Gradient flow scale and hyperscaling

In addition to the mass scales of the hadronic spectrum, we measure the gradient flow scale t_0 [53]. We use the Symanzik flow kernel to smooth the clover definition of the one-point energy operator $\langle E \rangle$. From this, we define the scale $t_{\mathcal{E}}$ as the value of flow time t such that $t^2\langle E(t)\rangle \equiv \mathcal{E}$, and in particular, the scale t_0 as the value of $t_{\mathcal{E}}$ where $\mathcal{E} = 0.3 \equiv \mathcal{E}_0$. This is the same setup we used in our previous publications [17,61]. We calculate t_0 for $N_f = 4$ at two β values and four quark masses m_f, for $N_f = 8$ at one β and six quark masses, and for $N_f = 12$ at one β and five quark masses, while we have simulated at two β values for $N_f = 12$ (see Ref. [17] for details of the mass spectra analysis). The results are summarized in Table I. While t_0 is in units of a^2, it is convenient to define a length scale (associated with the smearing radius of the diffusion process to which the gradient flow is equivalent) as $r = \sqrt{8t_0}$, which can be intuitively associated with the Sommer radius r_0 in QCD [62]. We plot the energy scale

TABLE I. The gradient flow scale t_0 in lattice spacing units for the ensembles used in the spectrum analysis.

N_f	β	L	m_f	t_0
4	3.7	20	0.01	1.13807(89)
4	3.7	20	0.02	1.09109(73)
4	3.7	20	0.03	1.05237(86)
4	3.7	20	0.04	1.01459(73)
4	3.8	20	0.01	1.4535(19)
4	3.8	20	0.02	1.3841(20)
4	3.8	20	0.03	1.3262(17)
4	3.8	20	0.04	1.2752(15)
8	3.8	48	0.009	5.0762(72)
8	3.8	42	0.012	4.7543(56)
8	3.8	36	0.015	4.4556(64)
8	3.8	36	0.02	4.0304(49)
8	3.8	30	0.03	3.3842(35)
8	3.8	30	0.04	2.9563(39)
8	3.8	24	0.05	2.6599(70)
8	3.8	24	0.06	2.39320(77)
8	3.8	24	0.07	2.1885(32)
12	4.0	36	0.04	11.206(57)
12	4.0	36	0.05	8.292(26)
12	4.0	30	0.05	8.338(26)
12	4.0	30	0.06	6.603(19)
12	4.0	36	0.08	4.632(17)
12	4.0	24	0.08	4.627(12)
12	4.0	24	0.1	3.6133(70)

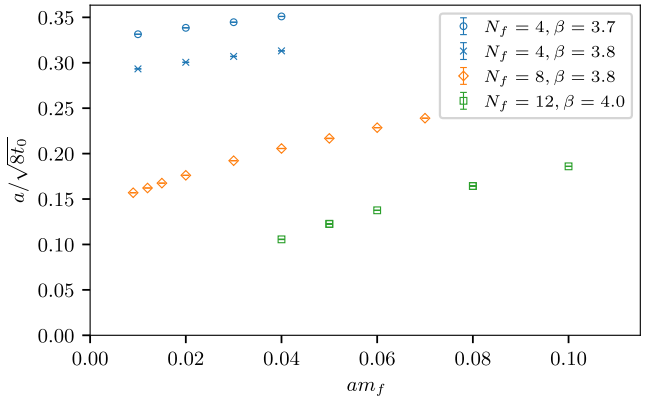

FIG. 3. The hadronic energy scale $1/\sqrt{8t_0}$ in lattice units as a function of the bare quark mass is plotted for all values of N_f.

corresponding to $1/\sqrt{8t_0}$ for all values of N_f as a function of the bare quark mass in lattice units in Fig. 3. We observe smaller $a/\sqrt{8t_0}$ as N_f/N_c increases, which indicates that the chiral limit values would decrease toward the conformal window.

To understand the scaling behavior of $a/\sqrt{8t_{\mathcal{E}}}$, we fit these data with a finite-size hyperscaling (FSHS) ansatz of the form

$$\frac{L}{\sqrt{8t_{\mathcal{E}}}} = f(Lm_f^{\frac{1}{1+\gamma_m}}), \tag{3.1}$$

where γ_m is the mass anomalous dimension, as enters into Eq. (2.3) in the conformal phase. This fit was performed using the piecewise-interpolating curve-collapse method proposed by Bhattacharjee and Seno [63] and previously deployed by DeGrand [64]. The value found for γ_m shows significant dependence on $\mathcal{E}$, as shown in Fig. 4. As the gradient flow has a smoothing effect removing ultraviolet effects, the fit result at larger values of t—and since t^2E increases monotonically with t, larger values of $\mathcal{E}$—is closer to the infrared value than that at smaller values. Furthermore, since the residual $P(\gamma_m)$ (analogous to a χ^2 measure for this type of fit) decreases as $1/\mathcal{E}$ approaches zero for $N_f = 12$, this suggests that $a/\sqrt{8t_{\mathcal{E}}}$ can be well described by the FSHS ansatz at larger flow times t.

This result, together with the observation in Fig. 3, supports our identification of a hadronic energy scale $\Lambda_{\mathrm{IR}}/\Lambda_{\mathrm{UV}} = a/\sqrt{8t_0}$, as indicated in Eq. (2.9), though Eq. (2.9) strictly applies only in the infinite volume limit. Among various possible definitions, for comparisons across different theories, it is convenient to use a gluonic definition $a/\sqrt{8t_0}$ as the reference scale $\Lambda_{\mathrm{IR}}/\Lambda_{\mathrm{UV}}$, since it exhibits only mild fermion mass dependence, as discussed later in Secs. IV and V. As a result, in the following we will often use the length scale $r = \sqrt{8t_0}$ (and its reciprocal) as a reference scale across theories with different number of flavors.

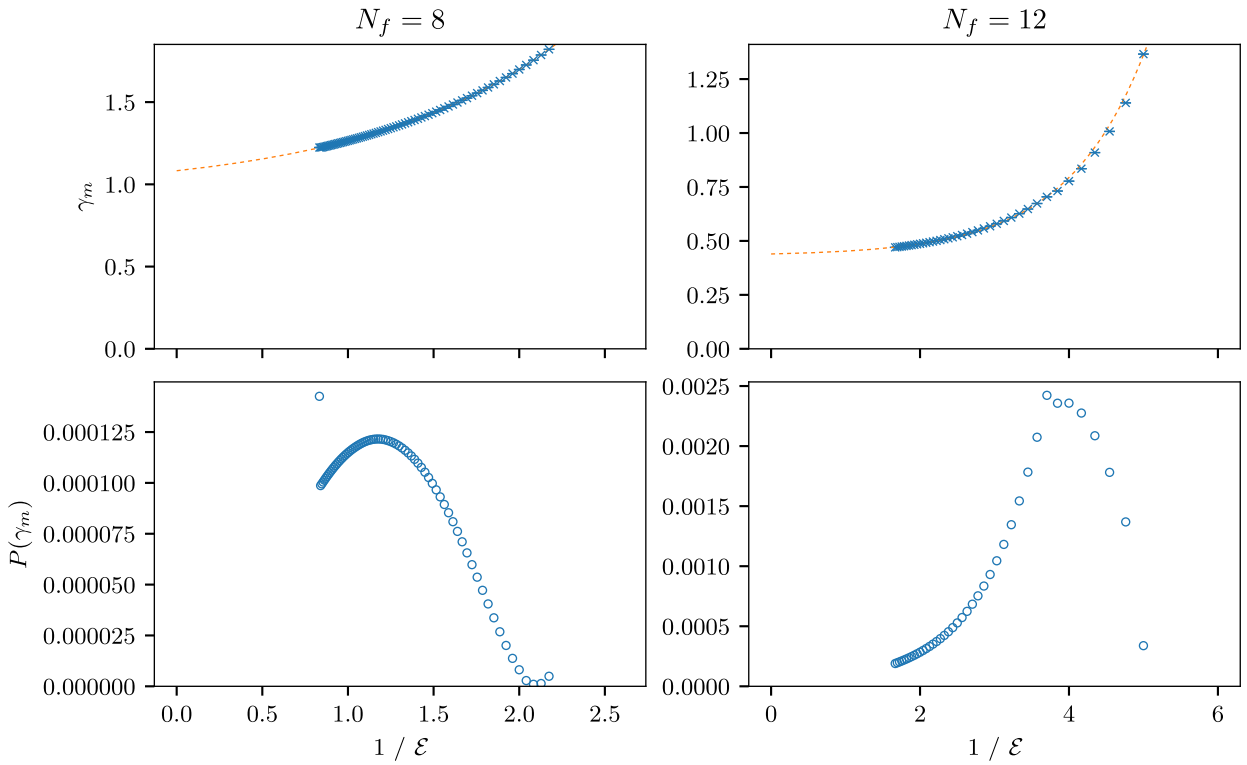

FIG. 4. The result of the finite-size hyperscaling analysis for $N_f = 8$ (left) and $N_f = 12$ (right). In each case, the upper panel shows the value of the anomalous dimension γ_m obtained via a fit of the energy scale t as a function of the reference scale $\mathcal{E}$ (points), and the lower panel the residual $P(\gamma_m)$ [defined in Eq. (19) of [65]] of the fits for the points in the upper plot. The dashed line shows the exponential fit used to find the final quoted values for γ_*.

In Fig. 4, we show the result for γ_m as a function of $1/\mathcal{E}$, for both values of $N_f = 8, 12$. We note that the region of $\mathcal{E}$ in which a stable fit is obtained differs between the two cases. This is due to differences in the fermion masses and lattice volumes considered in the two cases, since there must be sufficient overlap between the data at different L to allow all data to contribute to the fit; we would anticipate that dedicated studies controlling these parameters could allow overlapping regions of $\mathcal{E}$ to be explored.

In both cases, the data visibly begin to level off at larger values of $\mathcal{E}$, which we interpret as $\gamma_* = \lim_{\mathcal{E}\to\infty} \gamma_m$. This is most pronounced in the $N_f = 12$ case, which appears to almost reach its plateau value; in the $N_f = 8$ case, extrapolation to the $\mathcal{E} \to \infty$ limit is needed. Imposing *ad hoc* an exponential form for this behavior gives a limiting value of $\gamma_* = 1.0830(11)$ for $N_f = 8$ and $\gamma_* = 0.4395(20)$ for $N_f = 12$, both of which agree closely with results previously obtained from (basic and finite-size) hyperscaling of the mass spectrum [17] (specifically that obtained for states other than the π in the $N_f = 8$ case).

B. Updates of hadron spectra in $N_f = 8$ QCD

Before discussing the scalar spectrum, we will give an update of the hadron spectra and their chiral extrapolations, which include a newly added lightest mass point in $N_f = 8$ QCD at $m_f = 0.009$. These new data were generated with volume $L^3 \times T = 48^3 \times 64$ at $\beta = 3.8$, using the same algorithm as in our previous works [14,16,17] where the lightest point was $m_f = 0.012$ on $L^3 \times T = 48^3 \times 64$ lattices.

We report details of the simulation parameters and a finite volume study in Appendix A.

In the analyses that follow, physical quantities are extrapolated to the chiral limit by a polynomial function of m_f, as in the previous work [17], whereas effects from chiral

TABLE II. Fit results for F and M_π^2/m_f in the chiral limit of $N_f = 8$ using a fit form $C_0 + C_1 m_f + C_2 m_f^2$. "Linear" and "Quadratic" denote the fit forms with $C_2 = 0$ and $C_2 \neq 0$, respectively. The value of χ^2/d.o.f., the number of d.o.f. in the fits, and the fit range are also tabulated.

	C_0	χ^2/d.o.f.	d.o.f.	Fit form	m_f fit range
F	0.02105(61)	0.17	2	Quadratic	[0.009, 0.03]
F	0.0212(13)	0.33	1	Quadratic	[0.009, 0.02]
F	0.02371(52)	1.22	1	Linear	[0.009, 0.015]
M_π^2/m_f	1.892(41)	0.24	2	Quadratic	[0.009, 0.03]
M_π^2/m_f	1.945(92)	0.06	1	Quadratic	[0.009, 0.02]
M_π^2/m_f	1.938(39)	0.07	1	Linear	[0.009, 0.015]

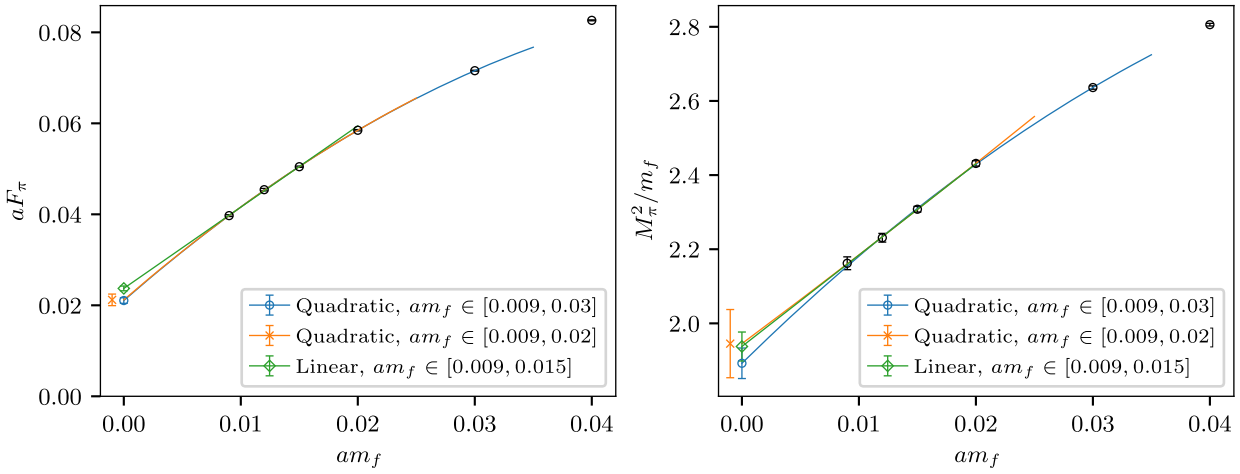

FIG. 5. Left: chiral extrapolations of F_π in $N_f = 8$. The range of m_f considered for each fit curve is noted in the legend. Right: same as the left panel but for M_π^2/m_f.

logarithm are taken into account to estimate the systematic error of chiral extrapolation for some limited cases.

1. F_π and M_π

The decay constant F_π is fitted by a quadratic fit with the fitting range $am_f \in [0.009, 0.03]$, because including larger masses results in large fit residuals (χ^2/degree of freedom). Having a new lightest mass point at $m_f = 0.009$ allows us to shift our fitting ranges toward the chiral limit while keeping the same number of fit degrees of freedom.

The chiral limit extrapolations of these fits (F) are shown in Table II. The result of F with a quadratic form using the fit range $m_f \in [0.009, 0.03]$ agrees reasonably well with other fit results, which are from quadratic and linear fit forms using the data in the intervals $m_f \in [0.009, 0.02]$ and $m_f \in [0.009, 0.015]$, respectively. These results are presented in Fig. 5, and a comparison of these results with those from the LSD Collaboration [42] is provided in Appendix C.

The data for M_π^2/m_f are also fitted by the same fit forms as F_π and shown in Fig. 5. The results are presented in Table II, and are in good agreement with those in the previous paper [17]: $F = 0.0212(12)(^{+49}_{-71})$ and $M_\pi^2/m_f = 1.866(57)$, including the possible chiral log effects for F.

Although the updated and previous results are consistent, our data are far from the chiral limit. At $m_f = 0.009$ the expansion parameter of ChPT for $N_f = 8$ QCD [66–68] is still large,

$$\chi = M_\pi^2/\Lambda_\chi^2 = 2N_f(M_\pi/4\pi F)^2 = 4.388(528)(^{43}_{737}) \gg 1. \tag{3.2}$$

In order to obtain a more reliable value of F, we would need several data points at yet smaller values of m_f. The systematic error of F is estimated with the same procedure we used in our previous paper [17], and we obtain

$$F = 0.0210(6)(^{+27}_{-70}), \tag{3.3}$$

where the quoted uncertainties are statistical and systematic, respectively. The central value and statistical error are determined from the quadratic fit with $m_f \in [0.009, 0.03]$. The lower systematic error is estimated from the effect of the chiral log term in next-to-leading-order ChPT, and the upper from the difference between the quadratic and linear fit results tabulated in Table II.

2. Chiral condensate

We estimate the chiral condensate in the chiral limit with two analyses. The first is a direct measurement of the chiral condensate

$$\langle\bar{\psi}\psi\rangle = \frac{\mathrm{Tr}[D_{\mathrm{HISQ}}^{-1}]}{4}. \tag{3.4}$$

The chiral extrapolation of $\langle\bar{\psi}\psi\rangle$ using a quadratic fit in the range $m_f \in [0.009, 0.03]$ is presented in Appendix B.

The second analysis is based on the GMOR relation,

$$\langle\bar{\psi}\psi\rangle|_{m_f\to 0} = \frac{F^2 B}{2}, \tag{3.5}$$

where $2B = M_\pi^2/m_f$ in the chiral limit. We calculate Σ given by

$$\Sigma = \frac{F_\pi^2 M_\pi^2}{4m_f} \tag{3.6}$$

at each m_f. The data in the interval $m_f \in [0.009, 0.02]$ are extrapolated to the chiral limit with a quadratic function of

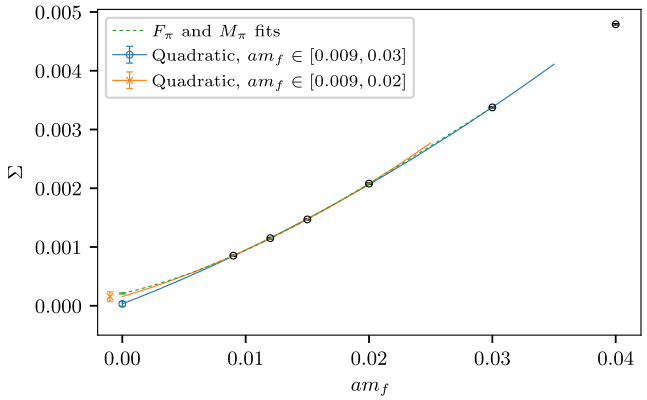

FIG. 6. Chiral extrapolations of $\Sigma = F_\pi^2 M_\pi^2/4m_f$ in $N_f = 8$ using a quadratic fit form. The dashed line represents the estimated m_f dependence of Σ using the fit results for F_π and M_π.

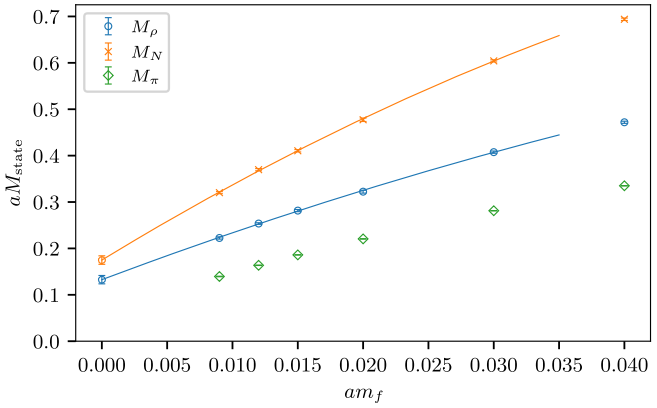

FIG. 7. Chiral extrapolations of M_ρ and M_N in $N_f = 8$ using a quadratic fit form. There is a noticeable curvature at the lightest fermion masses.

m_f, as shown in Fig. 6. Comparing the fit curve with one estimated using the fit results of F_π and M_π^2/m_f shows a reasonably good agreement. However, we observe a large fit range dependence of the chiral limit value, similar to our previous study [17]. A fit with a wider fit range gives a smaller value in the chiral limit, as presented in Table III.

The fit results in the chiral limit are summarized in Table III. We also tabulate the estimated value from the GMOR relation in Eq. (3.5), using the fit results for F_π and M_π^2/m_f presented in Table II. The fit result of the direct measurement agrees with the GMOR relation, and also with the result in the previous paper [17], which was $\langle\bar\psi\psi\rangle|_{m_f\to 0} = 0.00022(4)$. The new result $\langle\bar\psi\psi\rangle|_{m_f\to 0} = 0.000200(20)$ has a smaller error thanks to the wider mass range for the fit given by the addition of a precise value at a lighter fermion mass.

The result of Σ with the shorter fit range $m_f \in [0.009, 0.02]$ is consistent with the direct measurement, although the error is large. It is in tension with the fit results with Σ in our previous work [17], where all the extrapolated values are negative. It is expected that the chiral extrapolation of Σ will become more stable as we add several smaller m_f data points.

TABLE III. Fit results for the chiral condensate $\langle\bar\psi\psi\rangle$ and $\Sigma = F_\pi^2 M_\pi^2/4m_f$ in the chiral limit of $N_f = 8$ using a quadratic fit form $C_0 + C_1 m_f + C_2 m_f^2$ together with the result from the GMOR relation $F^2B/2$. The value of χ^2/d.o.f., the number of d.o.f., and the fit range in the fits are also tabulated.

	C_0	χ^2/d.o.f.	d.o.f.	m_f fit range
$\langle\bar\psi\psi\rangle$	0.000200(20)	0.41	2	[0.009, 0.03]
$\langle\bar\psi\psi\rangle$	0.000198(42)	0.82	1	[0.009, 0.02]
Σ	0.000031(39)	1.69	2	[0.009, 0.03]
Σ	0.000156(79)	0.09	1	[0.009, 0.02]
$F^2B/2$	0.000210(13)	…	…	…

3. Masses of mesons and baryons

We extrapolate the masses of the ρ, a_0, a_1, b_1, N, and N_1^* states to the chiral limit using a linear fit of the data for $m_f \in [0.009, 0.03]$. The ρ and N states show a curvature in this range, and so they are also extrapolated using a quadratic fitting form, for the same fit range, as shown in Fig. 7. The results of these fits are tabulated in Table IV; plots of the individual fits for the different mesons are included in Appendix B. As the χ^2/degree of freedom (d.o.f.) of the linear fit of N is large, we consider only the quadratic fit result for the following discussion. While the linear fit of ρ is acceptable, we choose the quadratic fit result as the central value, and the linear fit result is used to estimate a systematic error. The results in the chiral limit are consistent with the ones in the previous paper [17], except for M_N: This is about 20% smaller than the previous result due to the curvature at light m_f.

Note that M_ρ agrees with the value in the previous paper within the systematic error coming from the difference of the quadratic and linear fits. Using the results in Table IV, we obtain $M_{a_1}/M_\rho = 1.59(14)\binom{0}{19}$, where the first and second errors are statistical and systematic ones, respectively. Here we have used the quadratic fit for M_ρ and the linear fit for M_{a_1} to determine the central values. This agrees with the result in the previous paper within uncertainties.[12] Moreover, it is also compatible with the Particle Data Group value [69] of $M_{a_1}/M_\rho = 1260/770 \approx 1.64$ corresponding to ordinary QCD. A more detailed discussion of this ratio will be presented in a forthcoming publication [70]. To obtain more stable results in the chiral limit, calculations with several lighter fermion will be necessary. We also note that our extrapolations are not based on a rigorous effective description, but rather are

[12]In Ref. [17], we extrapolated linearly the ratio M_{a_1}/M_ρ; repeating the same analysis with our new data reproduces the same results within uncertainties.

TABLE IV. Fit results for hadron masses in the chiral limit of $N_f = 8$ with a polynomial fit form $C_0 + C_1 m_f + C_2 m_f^2$ in the range $m_f \in [0.009, 0.03]$. "Linear" and "Quadratic" denote the fit forms with $C_2 = 0$ and $C_2 \neq 0$, respectively. The value of χ^2/d.o.f. and the number of d.o.f. in the fits are also tabulated.

	C_0	χ^2/d.o.f.	d.o.f.	Fit form
M_ρ	0.1485(25)	1.68	3	Linear
M_ρ	0.1326(90)	0.83	2	Quadratic
M_{a_0}	0.1450(99)	0.85	3	Linear
M_{a_1}	0.210(12)	1.28	3	Linear
M_{b_1}	0.206(18)	0.39	3	Linear
M_N	0.2058(26)	4.84	3	Linear
M_N	0.1749(92)	1.10	2	Quadratic
$M_{N_1^*}$	0.273(11)	0.00	3	Linear

meant to provide guidance for interpreting our results in the context of strongly coupled theories near the edge of the conformal window, and as a comparison with previous results.

The ratios for the hadron masses (shown in Table IV) to F [in Eq. (3.3)] are presented in Table V and are our chiral limit predictions for the spectrum of the $N_f = 8$ QCD theory. These ratios are suggesting that this theory is in the hadronic, chirally broken phase, but these results alone cannot establish how close the theory is to the conformal window.

Note that the central values for ρ and N are determined from the quadratic fit results, and the systematic error quoted for $\sqrt{2}M_\rho/F$ includes the difference between the quadratic and linear fit results for M_ρ shown in Table IV. Our result in Table V

$$\frac{\sqrt{2}M_\rho}{F} = 8.91(66)\left(^{+4.44}_{-1.00}\right) \tag{3.7}$$

obtained from a quadratic fit for both M_ρ and F is consistent with the values included in our previous works: $\sqrt{2}M_\rho/F = 7.7(1.5)\left(^{+3.8}_{-0.4}\right)$ in [14] and $\sqrt{2}M_\rho/F = 10.1(0.6)\left(^{+5.0}_{-1.9}\right)$ in [17], where the latter was obtained from a linear extrapolation for M_ρ and a quadratic one for F.

TABLE V. Ratios of $\sqrt{2}M_H/F$ in the chiral limit. The first and second errors are statistical and systematic errors. ρ and N are evaluated from the quadratic fit results, and others from the linear results shown in Table IV.

H	$\sqrt{2}M_H/F$
M_ρ	$8.91(66)\left(^{4.44}_{1.00}\right)$
M_{a_0}	$9.74(72)\left(^{4.85}_{1.09}\right)$
M_{a_1}	$14.13(88)\left(^{7.04}_{1.59}\right)$
M_{b_1}	$13.9(1.3)\left(^{6.9}_{1.6}\right)$
M_N	$11.75(70)\left(^{5.86}_{1.32}\right)$
$M_{N_1^*}$	$18.34(92)\left(^{9.14}_{2.06}\right)$

Finally, we should discuss the discretization effects and their implications for our study of the phase structure. In the $N_f = 8$ theory, the suppression of taste breaking indicates that lattice artifacts are at least reduced in the fermion sector. However, the overall magnitude of the discretization error is difficult to estimate, and with the present data we cannot definitively exclude the conformal scenario. At the same time, our spectrum analysis provides strong evidence for chiral-symmetry breaking. Unlike other bound states, the pion mass does not exhibit universal hyperscaling. Instead, the effective anomalous dimension γ_m extracted from M_π decreases as m_f increases. This behavior is naturally explained by the GMOR relation

$$M_\pi^2 = 4\frac{\Sigma}{F_\pi^2} m_f = \frac{4\langle\bar{\psi}\psi\rangle|_{m_f\to 0}}{F^2} m_f + \mathcal{O}(m_f^2), \tag{3.8}$$

in which the linear term dominates near the chiral limit ($\gamma_m \simeq 1$), while the quadratic term controls the large-mass regime ($\gamma_m \simeq 0$). Our $N_f = 8$ results are fully consistent with this tendency, which is characteristic of NG bosons, in sharp contrast to conformal dynamics. For $N_f = 12$, by contrast, the effective γ_m never decreases with m_f and shows a universal value at small fermion masses, as confirmed for two different β values (Fig. 33 of our previous paper [17]). For the $N_f = 8$ theory, it remains possible that all γ_m values could converge near 1 at much smaller fermion masses than we have simulated, making it exceedingly difficult to distinguish a chirally broken phase from a conformal one based solely on spectrum analysis (cf. Ref. [46]). Furthermore, the theory could undergo a phase transition at stronger coupling, as recently suggested in Refs. [27,28]. Since our $N_f = 8$ study is limited to a single β and masses far from the chiral limit, exploring a wider range of β values and smaller fermion masses will be essential for a more definitive conclusion, though such an analysis lies beyond the scope of this work.

IV. THE FLAVOR-SINGLET SCALAR STATE

In this section, we report our results for the lightest flavor-singlet scalar state in the $N_f = 8$ and $N_f = 4$ theories. While the former is an update of our previous results by adding a new lightest fermion mass, the latter is new to this work. We also summarize these data, comparing both with theoretical predictions and with the nonsinglet spectrum together with the data for $N_f = 12$ previously reported in [13,17].

A. Update for $N_f = 8$ QCD

The mass of the flavor-singlet scalar in $N_f = 8$ QCD at $\beta = 3.8$, $m_f = 0.009$ is calculated in the same way as the

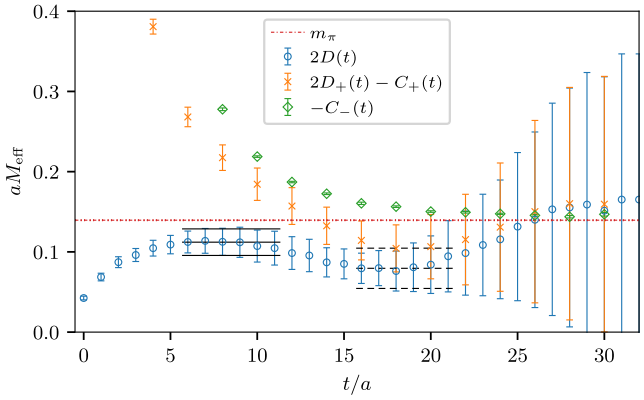

FIG. 8. The effective σ mass at $m_f = 0.009$ in $N_f = 8$. The circle and diamond symbols represent effective masses from positive parity projected and disconnected correlators, respectively. The effective mass of the connected correlator with negative parity projection is also plotted for comparison. Solid and dashed horizontal lines express the fit results with 1 standard deviation error bands. The dot-dashed line is M_π.

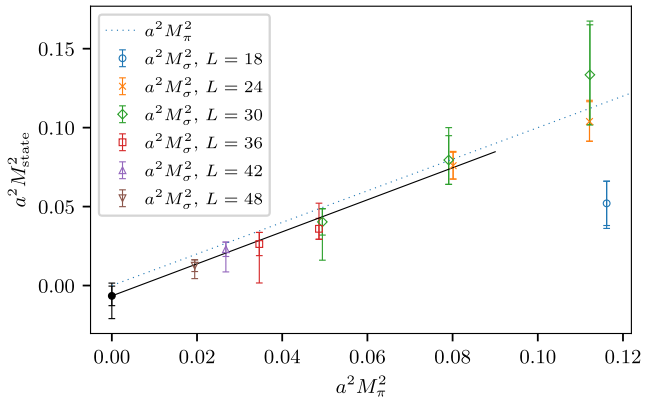

FIG. 9. The chiral extrapolation of M_σ in $N_f = 8$, fitted with $M_\sigma^2 = d_0 + d_1 M_\pi^2$. The inner error is statistical, while the outer error represents the combined error, where statistical and systematic errors are added in quadrature. The dotted line shows the case where $M_\sigma^2 = M_\pi^2$.

results at larger m_f presented in our previous work [15–17]. The simulation parameters, including the number of configurations and the bin size for the jackknife analysis, are summarized in Table X.

Figure 8 shows the effective mass of the σ state at $m_f = 0.009$ evaluated from the vacuum subtracted disconnected correlator $2D(t)$. The effective masses from the positive parity projected full correlator $2D_+(t) - C_+(t)$ and the negative parity projected connected correlator $-C_-(t)$ are also plotted, where $C_\pm(t) = 2C(t) \pm C(t+1) \pm C(t-1)$ at even t. We estimate M_σ separately from two fit ranges, $t \in [6, 11]$ and $t \in [16, 21]$. Both results are statistically consistent with each other and also with the effective σ mass of the full correlator. We obtain $M_\sigma = 0.112(17)\binom{0}{33}$ as shown in Table XI. The central value is determined from the result with the fit range at smaller t. The result from the larger-t fit range is used to estimate the systematic error, as in our previous work [15–17]. At this m_f, finite volume effects are expected to be small, because the value of $LM_\sigma = 5.38(79)\binom{0}{1.56}$ statistically satisfies the criterion for negligible finite volume effects $LM_\sigma \geq 6$ [17].

We have updated the chiral extrapolations of the σ mass with this new data point. The data are fitted using the form from the WT identity/dChPT discussed in Sec. II, Eq. (2.36), represented here for convenience,

$$M_\sigma^2 = d_0 + d_1 M_\pi^2, \tag{4.1}$$

and with an empirical linear fit form,

$$M_\sigma = c_0 + c_1 m_f. \tag{4.2}$$

The results of these fits are tabulated in Table VI and plotted in Figs. 9 and 10. As emphasized in Sec. II, any possible deviations of the dChPT from the WT identity Eq. (2.36) that may arise near the chiral limit (due to the π loop [29]) are not relevant to our lattice data, lying as they do far from the chiral limit.

TABLE VI. Results of the chiral extrapolation of M_σ in $N_f = 8$ with the fit form from the anomalous WT identity/dChPT, Eq. (4.1), and the linear fit form. The fit range in both cases is $m_f \in [0.009, 0.03]$. The first and second errors are statistical and systematic errors, respectively. The value of χ^2/d.o.f. and the number of d.o.f. in the fits are also tabulated.

Fit form	$M_\sigma^2 = d_0 + d_1 M_\pi^2$	$M_\sigma = c_0 + c_1 m_f$
	$d_0 = -0.0066(62)\binom{81}{144}$	$c_0 = 0.0526(184)\binom{26}{787}$
	$d_1 = 1.01(20)\binom{32}{49}$	$c_1 = 7.35(96)\binom{2.95}{39}$
χ^2/d.o.f.	0.21	0.34
d.o.f.	3	3

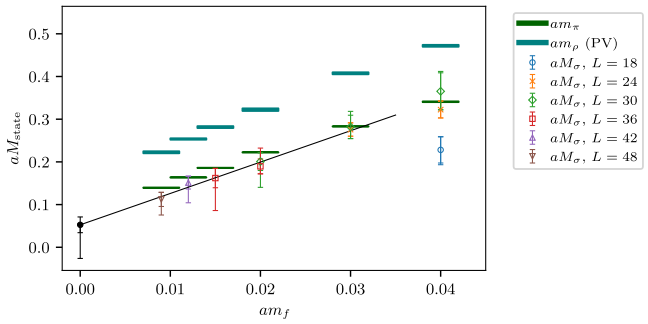

FIG. 10. The chiral extrapolation of M_σ in $N_f = 8$ fitted with $M_\sigma = c_0 + c_1 m_f$. The inner error is statistical, while the outer error represents the combined error, where statistical and systematic errors are added in quadrature. M_π and M_ρ are plotted for comparison.

These results are consistent with the those presented previously [16,17] with a good overlap, while the lower systematic errors are improved by more than a factor of 2.

The linear fit result $c_0 = 0.0526(184)(^{26}_{787})$ combined with our chiral fit value of $F = F_\pi|_{m_f=0} = 0.02120\times(127)(^{252}_{15})$, Eq. (3.3), gives $M_\sigma/(F/\sqrt{2}) = 3.51\times(1.25)(^{17}_{5.27})$. This is slightly smaller than, but consistent within uncertainties, with our previous result omitting the new lightest point [17] $M_\sigma/(F/\sqrt{2}) = 4.2(2.0)(^{1.4}_{9.5})$. The new value would give $M_\sigma/v_{\rm EW} = (M_\sigma/F)\times\sqrt{2/N_D} \sim 1.75$ for $N_D = 4$ (the one-family model), which remains consistent (within uncertainties, which remain large) with the possibility to identify σ with the Higgs boson, with $M_\sigma/v_{\rm EW} \simeq \frac{1}{2}$.

The fit results for d_0 and d_1 from the WT identity and dChPt presented in Table VI also remain consistent with the previous ones [16,17] discussed in Eq. (2.57). As such, the logic of Eqs. (2.58) and (2.59) holds:

$$M_\sigma^2 \lesssim d_1 M_\pi^2 \simeq M_\pi^2,$$
$$\frac{F_\sigma}{F_\pi/\sqrt{2}} = C_{\gamma_m}\cdot\frac{1}{\sqrt{d_1}} = 3.97(40)(^{96}_{63}) \quad \text{for } C_{\gamma_m} = 4. \tag{4.3}$$

d_0 is consistent (up to a large uncertainty, and the possible chiral log effects discussed in Sec. II) with the value

$$d_0 = M_\sigma^2|_{m_f=0} \simeq \frac{v_{\rm EW}^2}{4} = \frac{N_D}{4}\cdot\frac{F^2}{2} \simeq \frac{N_D}{4}\cdot 0.0002247(270)(^{377}_{22}) \tag{4.4}$$

that would be required for σ to be identified with the Higgs boson in the TC model with N_D electroweak doublets.

Our data for M_σ^2 vs M_π^2 (and $\gamma_m \simeq 1$) are also consistent with those of the LSD Collaboration [42]; we provide details of the comparison in Appendix C. As such, the result Eq. (4.3) is also consistent with $F_\sigma/(F_\pi/\sqrt{2}) \simeq 3.4$ in Ref. [33],[13] fit from the LSD Collaboration's data (see also similar estimates in Refs. [34,48]).

B. Results for $N_f = 4$ QCD

The σ mass in $N_f = 4$ at $\beta = 3.8$ on $L^3\times T = 20^3\times 30$ is calculated using the same action as in $N_f = 8$. Fermion masses are chosen to be $m_f = 0.01$, 0.02, and 0.03 in lattice units.

In contrast to $N_f = 8$, the effective σ mass of $D(t)$ in $N_f = 4$ has a strong oscillating behavior. (A typical example is the data at $m_f = 0.01$, as plotted in Fig. 11.)

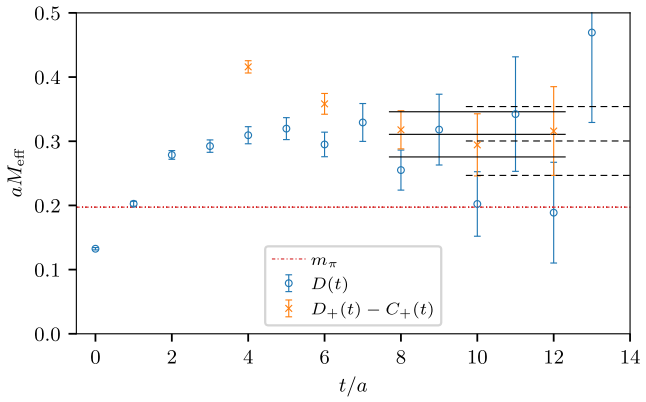

FIG. 11. Effective masses for the $D_+(t) - C_+(t)$ and $D(t)$ correlators at $m_f = 0.01$ and $\beta = 3.8$ for $N_f = 4$. The dot-dashed line represents M_π. The solid lines express the fit result of $D_+(t) - C_+(t)$ with the 1 standard deviation band.

This is because, despite using the HISQ action, the taste-symmetry breaking of the pseudoscalar masses is larger in $N_f = 4$ QCD (cf. Fig. 27) [17].

Because of this oscillating behavior, we do not determine M_σ from $D(t)$; instead, we calculate M_σ from the positive parity projected correlator $D_+(t) - C_+(t)$, whose effective mass and fit result are plotted in Fig. 11.[14] Since the signal of the effective σ mass is limited in the $N_f = 4$ case compared to the one in $N_f = 8$, we do not estimate the systematic error coming from the choice of the fit range. In contrast to $N_f = 8$, the figure shows that $M_\sigma > M_\pi$ in $N_f = 4$, which is similar to the usual QCD [71–74] and to the $N_f = 4$ QCD result reported by the LSD Collaboration [42] with a different choice of lattice regularization.

We also obtain M_σ in $m_f = 0.02$ and 0.03 using the same method. The results are tabulated in Table VII together with the masses for π and ρ. The extraction of M_σ becomes harder as m_f increases, as the correlator of σ rapidly degrades as m_f increases, as can be seen in Fig. 12 where we plot the data in lattice units. Similar to the $N_f = 8$ case, we extrapolate the σ mass to the chiral limit using Eq. (4.1).

C. Comparison of theories

Here we present summary plots of M_σ^2 vs M_π^2 for the three theories considered. Figure 13 shows the results in lattice units, including the fits for d_0, d_1, while Fig. 14 shows the results in units of $1/\sqrt{8t_0}$.

Our new data summarized in Table VIII indicate that M_σ^2 is dominated by the term $d_1 M_\pi^2 \gg d_0$, such that $M_\sigma^2 \simeq d_1 M_\pi^2$ not only for $N_f = 12$ but also for $N_f = 4$ and 8 (with the caveat that our data are still some distance from the

[13]Their fit formula, Eq. (14) combined with Eq. (15) in [33], is the same as our Eq. (2.59), with the parameters corresponding to $C_{\gamma_m} = \sqrt{(N_f/2)y(4-y)} = 4.00$ [from $y(=3-\gamma_m) = 2.06\pm 0.05$ in their Eq. (16)], and $\sqrt{d_1} = M_\sigma/M_\pi \gtrsim 1$ from their Fig. 1, thus with $F_\sigma/(F_\pi/\sqrt{2})$ slightly smaller than ours.

[14]We have confirmed that the same M_σ is obtained from the positive parity projected correlator after subtracting the contribution of the parity partner of σ.

TABLE VII. Results for M_σ, M_π, F_π, and M_ρ at each m_f in $N_f = 4$ at $\beta = 3.8$. The number of configurations in the ensemble analyzed ($N_{\rm conf}$) and the bin size ($N_{\rm bin}$) for the flavor-singlet scalar calculation are also tabulated.

am_f	aM_σ	$N_{\rm conf}$	$N_{\rm bin}$	aM_π	aF_π	aM_ρ
0.01	0.311(35)	3750	150	0.19731(26)	0.09039(17)	0.526(14)
0.02	0.498(49)	6250	250	0.27927(26)	0.10487(13)	0.5931(78)
0.03	0.58(10)	6250	250	0.34384(24)	0.11555(12)	0.6549(56)
0.04	⋯	⋯	⋯	0.40030(20)	0.124636(96)	0.7146(46)

chiral limit). As suggested in Sec. II, this implies that whether $M_\sigma^2 > M_\pi^2$ is determined by whether $d_1 > 1$, which may in turn be linked to whether $\gamma_m > 1$. The approximate equality of the power-law behavior of m_f for σ as well as π (i.e., the nonuniversal "γ_m" value [16,17]) may be the cause of the comparable values of the M_σ and M_π in the $N_f = 8$ theory.

The fit result $d_0 \simeq 0$ within (large) uncertainties, both for $N_f = 4$ and $N_f = 8$, arises from Eq. (4.1), which is obtained from the WT identity, and it so is valid for the present lattice data with $\chi \gg 1$. However, in the region of the chiral limit we would expect chiral log effects to become more significant. As discussed in Eq. (2.54) of Sec. II, this will increase the chiral limit value of d_0, relative to that obtained from these relatively heavy-mass data, as $d_0 = M_\sigma^2|_{m_f=0} > 0$ [29]. In contrast, the fit result $d_0 \simeq 0$ in $N_f = 12$ in the conformal phase has no such chiral log corrections.

Meanwhile, the fit value of d_1 has no such chiral log effects, neither in the broken nor the conformal phase, and hence the obtained result for $F_\sigma/(F_\pi/\sqrt{2})$ may be identified with that in the chiral limit, which is of direct relevance to the comparison with the anticipated properties of a composite Higgs boson.

In addition to the result of a hyperscaling fit for $N_f = 8$ and 12, we also present in Table VIII the value of γ_m obtained by solving Eq. (2.39) (the prediction of d_1 from holographic and linear sigma models) for the fitted value of d_1. For $N_f = 8$ and 12, this is consistent with the hyperscaling result. The larger value $\gamma_m = 2.11(21)$ in the $N_f = 4$ case cannot be verified, as that theory does not exhibit hyperscaling. However, it may be suggestive of an alternative description of infrared QCD with $N_f \lesssim 4$, with $\Lambda_{\rm IR} \sim \Lambda_{\rm UV}$: the gauged NJL model with induced strong four-fermion interaction and effectively reduced gauge coupling $\alpha_{\rm eff} \ll 1$. The model in the broken phase has $\gamma_m \simeq 1 + \sqrt{1 - \alpha_{\rm eff}/\alpha_{\rm cr}} \simeq 2$ for $\alpha_{\rm eff} \ll \alpha_{\rm cr}$, with the four-fermion operator becoming relevant [75]. By contrast, in the $N_f = 8$ case, $\Lambda_{\rm IR} \ll \Lambda_{\rm UV}$ is realized by the essential singularity scaling, with

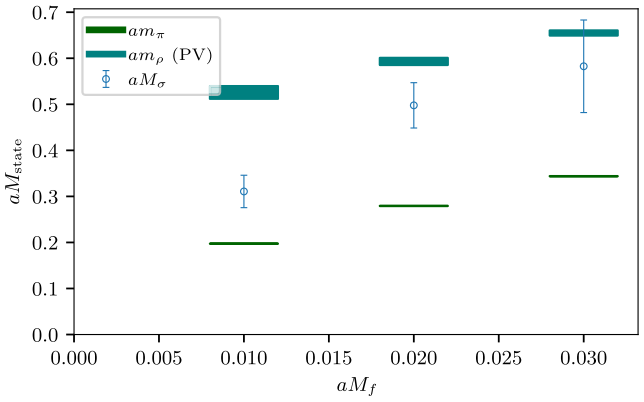

FIG. 12. The fermion mass dependence of M_σ in $N_f = 4$ at $\beta = 3.8$ compared with M_π and M_ρ.

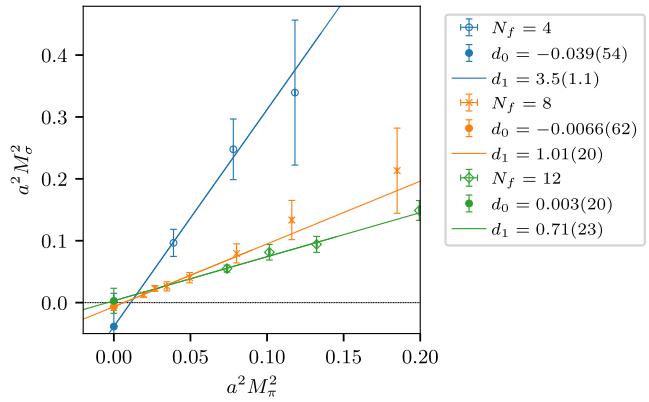

FIG. 13. Results for M_σ^2 for $N_f = 4, 8, 12$, showing in each case the fit to Eq. (4.1).

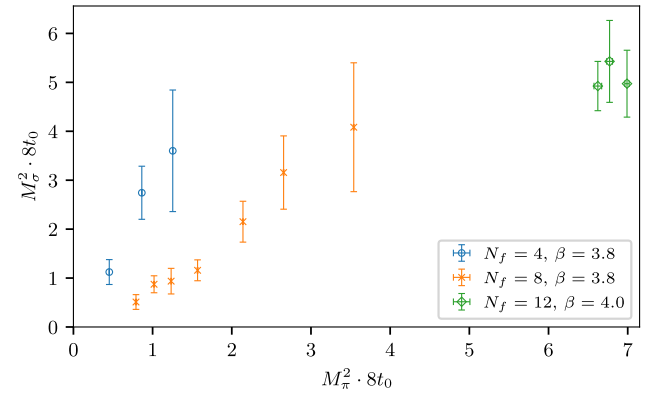

FIG. 14. Results for M_σ^2 for $N_f = 4, 8, 12$ in units of $1/\sqrt{8t_0}$.

TABLE VIII. Summary of the fits of the data for M_σ to Eq. (4.1) in lattice units, including also the approximate value of γ_m estimated by comparing the fit value for d_1 with Eq. (2.39) and that from hyperscaling, both consistent with each other for $N_f = 8$ and 12. (We do not observe hyperscaling in the $N_f = 4$ case.).

N_f	$d_0 a^2$	d_1	γ_m	$\gamma_m\|_{\text{hyperscaling}}$
4	−0.039(54)	3.5(1.1)	2.11(21)	
8	$-0.0066(62)\binom{81}{144}$	$1.01(20)\binom{32}{49}$	1.01(20)	≃1 [14,17,23]
12	$0.0030(202)\binom{41}{27}$	$0.712(229)\binom{36}{40}$	0.66(31)	0.4–0.5 [13,17]

the gauge coupling staying strong $\alpha_{\text{eff}} \simeq \alpha_{\text{cr}}$ even at induced four-fermion coupling, such that $\gamma_m \simeq 1$. If it is the case, from Eq. (2.37) we may have $F_\sigma/(F_\pi/\sqrt{2}) \simeq \sqrt{3N_f/2}/\sqrt{d_1} \simeq \sqrt{2}$ for $N_f = 4$.[15]

Further, we may also observe from Fig. 14, though with large uncertainty, that

$$M_\sigma^{(\text{anomalous})}\sqrt{8t_0} \simeq \frac{1}{2(3-\gamma_m)}, \quad \forall\ N_f, \tag{4.5}$$

consistent with the arguments in Sec. II, Eqs. (2.9), (2.48), and (2.56).

Considering now each N_f in more detail, in the $N_f = 4$ case, M_σ lies between ρ and π in the observed range of m_f, similar to the behavior observed in $N_f = 2 + 1$ QCD. M_σ^2 decreases rapidly, with slope $d_1 \simeq 3.5(1.1)$, toward the chiral limit. d_0 appears very small, comparable with the value in the $N_f = 8$ case, up to a factor of $1/(3-\gamma_m)^2$ in units of $\Lambda_{\text{IR}} = 1/\sqrt{8t_0}$.[16] However, the relatively large uncertainties on these data mean that this statement cannot yet be made definitively.

For $N_f = 8$, the σ mass is comparable with (with hints of being slightly smaller than) that of the pseudo-NG boson π in the observed range of m_f. The values found for d_0 and d_1 obtained Eq. (4.3) are consistent with those previously found [16,17], with $F_\sigma/(F_\pi/\sqrt{2})$ also observed to be consistent with the holographic and linear sigma models described in Eq. (2.38).

We may regard σ in the $N_f = 8$ theory as the technidilaton in the walking technicolor model [4,5] with N_D electroweak doublets, which would correspond to the physical Higgs boson with mass $M_{\text{Higgs}} \simeq 125\ \text{GeV} \simeq v_{\text{EW}}/2$. Then we would expect $d_0 = M_{\text{Higgs}}^2 \simeq N_D \cdot (F/\sqrt{2})^2/4$, which reads $d_0 \simeq N_D/4 \times 0.0002247 \times (270)\binom{377}{22}$, with our result $F \simeq 0.02120(127)\binom{252}{15}$ in Eq. (3.3). This is in rough consistency with our direct measurement of d_0 in Table VIII [up to chiral log effects, Eq. (2.54), and large uncertainties]. Taken together with Eq. (2.10), which reads $d_0 \sim (2 \cdot F/\sqrt{2})^2$ (with $M_\rho/(F/\sqrt{2}) \sim 8$, from Table V), Eq. (4.5) would imply $d_0 \sim (1/4 \times 1/\sqrt{8t_0})^2 \simeq (M_\rho/4)^2$; that is, the implied Higgs mass would be roughly consistent with reality, up to a factor of 2, for $N_D = 4$. The result in Eq. (4.3) implies that $v_{\text{EW}}/F_\sigma \simeq \sqrt{N_D}/4$, which may be compared directly with ≃0.27 from the LHC experiments for the signal strength of the 125 GeV Higgs boson [12].

For $N_f = 12$, d_0 is also very small, consistent with zero as suggested by Eq. (2.56). Setting $d_0 = 0$ for simplicity in Eq. (4.1) and adopting the scale $\Lambda_{\text{IR}} = 1/\sqrt{8t_0}$ gives

$$M_\sigma^2 \cdot 8t_0 = d_1 M_\pi^2 \cdot 8t_0; \tag{4.6}$$

hyperscaling implies that both sides of this equation should be constant in a conformal theory, independent of the deforming mass m_f. This is indeed what we see in Fig. 14. In this case, the reason that $M_\sigma < M_\pi$ is that $d_1 < 1$ [in turn, via Eq. (2.39), because $\gamma_m < 1$] because σ in the conformal phase is a pseudo-NG boson, while π is not, as discussed in Sec. II C. Using the measured values of d_1 and γ_m, we then find

$$\begin{aligned} &M_\sigma \simeq \sqrt{d_1} M_\pi \simeq 0.844(136)\binom{21}{24} M_\pi, \\ &\frac{F_\sigma}{F_\pi/\sqrt{2}} \simeq 5.6 - 5.7 \quad (\text{for } \gamma_m = 0.4 - 0.5). \end{aligned} \tag{4.7}$$

We also present summary plots of σ mass together with nonsinglet spectra in units of $\sqrt{2}F_\pi$ in Fig. 15 and in units of $1/\sqrt{8t_0}$ in Figs. 14 and 16. The former are consistent with the picture that for $N_f = 8$ the nonsinglet masses behave in the same hyperscaling as F_π, while σ and π do not, and for $N_f = 12$ all the spectra behave in the universal hyperscaling. In the latter case, the m_f dependence is approximately consistent with Eq. (2.10).

It is interesting to note that the ratio $\sqrt{2}M_\rho/F_\pi \simeq 8$ is almost independent of m_f for all $N_f = 4, 8, 12$, consistent with our previous results [14,17]. Its value is also close to

[15]Indeed, we may expect this to extend to $N_f = 2$, where $\gamma_m \simeq 2 \Rightarrow d_1 \simeq 3$, and hence, $F_\sigma/(F_\pi/\sqrt{2}) \simeq 1$; this would also be expected from linear sigma model predictions, as discussed in footnote 8.

[16]Equation (4.5) also implies that for $N_f = 2$, with $\gamma_m = 2$ similar to $N_f = 4$, $M_\sigma^2 \sim (M_\rho/2)^2 + 3M_\pi^2 \simeq (450\ \text{MeV})^2$ for the physical point $M_\pi \simeq 140$ MeV, in rough agreement with the reality for $f_0(500)$.

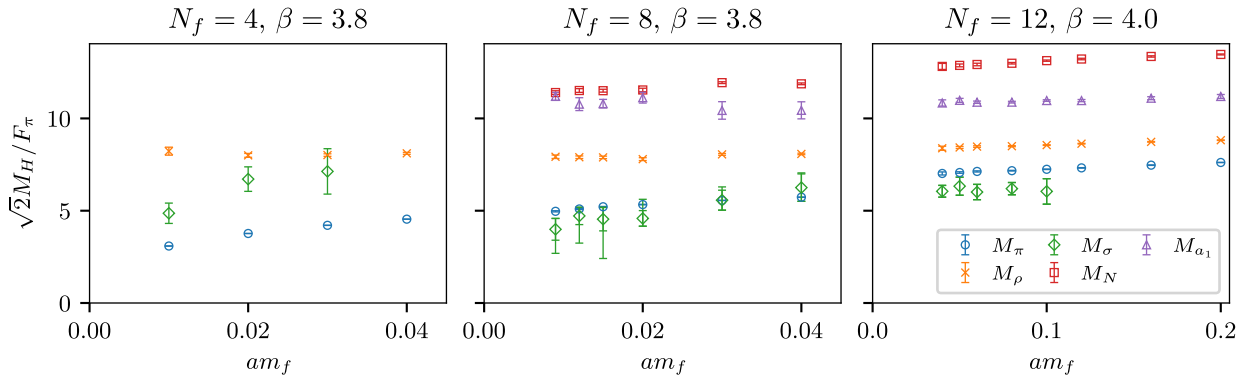

FIG. 15. The ratio $\sqrt{2}M_H/F_\pi$ for $H = \pi, \sigma, \rho, a_1$, and N as a function of m_f for $N_f = 4, 8$, and 12 QCD using the $N_f = 12$ data from Appendix G of Ref. [17] and the $N_f = 4$ data from Table VII.

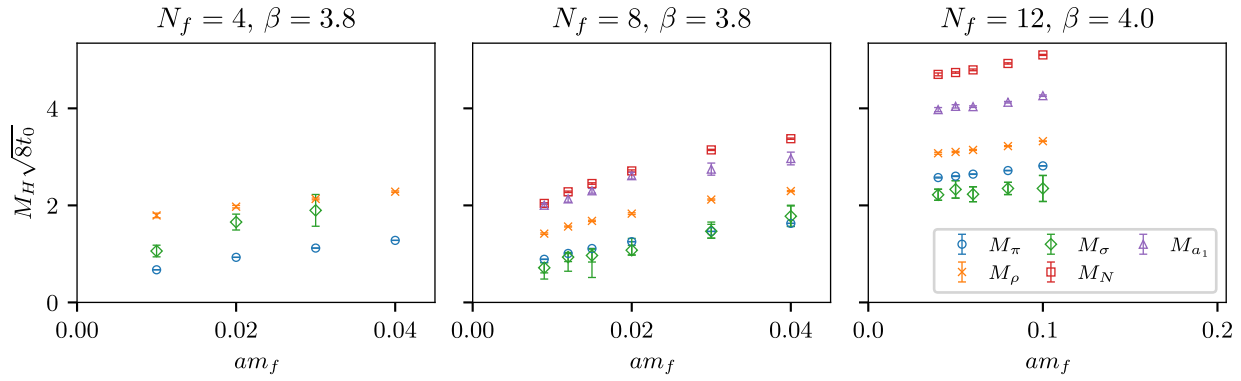

FIG. 16. The ratio $M_H\sqrt{8t_0}$ for $H = \pi, \sigma, \rho, a_1$, and N as a function of m_f for $N_f = 4, 8$, and 12 QCD.

that of $N_f = 2 + 1$ QCD (experimental value ≈8.3).[17] The chiral extrapolation of this ratio for $N_f = 8$ given in Eq. (3.7) is also consistent. The Kawarabayashi-Suzuki-Ryazuddin-Fayyazuddin relation [76,77] suggests that this ratio should be equal to the ρ–$\pi\pi$ coupling (up to a factor of $\sqrt{2}$) in the broken phase, which would then also be universal—independent of both m_f and $n_f(< n_f^{\rm cr})$. A similar observation has already been reported in [42,78,79], where lattice numerical results confirm that the ratio M_ρ/F_π remains insensitive to N_f up to $N_f \leq 10$. We will further explore this ratio in a companion publication to this work focusing on the S parameter [70].

From a phenomenological perspective, in the $N_f = 8$ walking technicolor scenario, such nonsinglet spectra could appear as resonances detectable in experiments, while new particles predicted by many other extensions of the Standard Model have yet to be observed. Notably, the ρ meson in the $N_f = 8$ theory could lie at the order of a TeV within uncertainties, as indicated in Eq. (3.7). This opens the possibility that the 2 TeV diboson excess reported by ATLAS and CMS could be interpreted as a contribution from technivector mesons [80,81]. To confirm or exclude this scenario, further progress is needed on two fronts: lattice simulations with lighter fermion masses near the chiral limit, and more precise experimental studies of TeV-scale resonances in ongoing and future LHC runs.

V. THE FLAVOR-SINGLET PSEUDOSCALAR STATE

In this section, we present lattice results for the flavor-singlet pseudoscalar state for a different number of flavors: $N_f = 4, 8$, and 12. Preliminary results have been reported before in conference proceedings [49,50].

The flavor-singlet pseudoscalar state has quantum numbers $J^{PC} = 0^{-+}$. In $N_f = 2 + 1$ QCD, this state is known as the η' particle, with mass $M_{\eta'} = 958$ MeV. In the following, for convenience we refer to the flavor-singlet pseudoscalar state in theories with many flavors using the same name as in QCD. Witten [51] and Veneziano [82]

[17]This is roughly consistent with the Pagels-Stokar formula $(F_\pi/\sqrt{2})^2 = \frac{N_c}{4\pi^2}\int_0^{\Lambda_{\rm UV}^2} dx x \frac{\Sigma(x)^2 - \frac{x}{4}d(\Sigma(x)^2)/dx}{(x+\Sigma(x)^2)^2} \simeq (3/4\pi^2)\cdot M_F^2 \simeq (M_F/4)^2$ $(M_F = m_f^{(\rm constituent)})$ with the integral dominated by $x < M_F^2$, roughly independently of N_f, under the simplest ansatz for the mass function $\Sigma(x) \simeq M_F (x < M_F^2)$. This is to be compared with $M_\rho \simeq 2M_F$ $(= 2m_f^{(R)} \simeq M_\pi$ for $N_f = 12)$ roughly independently of N_f.

showed that the η' mass is directly related to the contribution of the axial anomaly as

$$M_{\eta'}^2 = (M_{\eta'}^2)^{(\text{anomalous})} + M_\pi^2. \tag{5.1}$$

As discussed in Sec. II, in the Veneziano limit, where $N_c \to \infty$ with $N_c\alpha =$ fixed and $n_f \equiv N_f/N_c =$ fixed $\ll 1$, where $\Lambda_{\text{IR}} \sim \Lambda_{\text{UV}}$ and gluon loops dominate, we have

$$(M_{\eta'}^2)^{(\text{anomalous})}/\Lambda_{\text{IR}}^2 \sim (M_{\eta'}^2)^{(\text{anomalous})}/\Lambda_{\text{UV}}^2 \sim n_f \ll 1. \tag{5.2}$$

Hence, the η' has a parametrically small mass in the chiral limit $M_\pi^2 = 0$ and behaves as a pseudo-NG boson. In the realistic $N_f = 2+1$, $N_c = 3$ QCD with $m_s \gg m_d \gg m_u$, however, we have

$$(M_{\eta'}^2)^{(\text{anomalous})} \simeq M_{\eta'}^2 + M_\eta^2 - 2M_K^2 \simeq (0.726\ \text{GeV})^2, \tag{5.3}$$

and hence [52],

$$(M_{\eta'}^2)^{(\text{anomalous})}/\Lambda_{\text{IR}}^2 \sim (M_{\eta'}^2)^{(\text{anomalous})}/M_\rho^2 \simeq 1 (\sim n_f). \tag{5.4}$$

Thus, the η' behaves as a pseudo-NG boson only in the idealized case of the Veneziano limit where $n_f \ll 1$, even in the chiral limit.

Conversely, as we described in Sec. II, large $N_f = 4, 8, 12$ QCD is close to the anti-Veneziano limit, where $n_f \equiv N_f/N_c =$ fixed $\gg 1$ for $N_c \to \infty$ with $N_c\alpha =$ fixed, in which case $\Lambda_{\text{IR}} \ll \Lambda_{\text{UV}}$, and fermion loops dominate over gluon loops in the computation of the chiral anomaly, and we have [12]

$$(M_{\eta'}^2)^{(\text{anomalous})}/\Lambda_{\text{IR}}^2 \sim n_f^2 \gg 1. \tag{5.5}$$

Then we have as in Eq. (2.23):

$$M_{\eta'}^2/\Lambda_{\text{IR}}^2 \simeq (M_{\eta'}{}^{(\text{anomalous})}/\Lambda_{\text{IR}})^2 \propto n_f^2 \gg 1. \tag{5.6}$$

It is notoriously difficult to compute the mass of the flavor-singlet pseudoscalar, because the pion contribution to the two-point function on the lattice is statistically challenging to remove. In our calculations, we design a gluonic operator (without fermion fields) to construct the correlation function. This bypasses the challenge, because a gluonic operator does not couple directly to π states. The same method has been adopted in $N_f = 2+1$ QCD and has led to results in agreement with experiment [83].

In practice, the gluonic interpolating operator used in our calculations is the topological charge density. On the lattice, the topological charge density operator is defined through the clover-plaquette field strength tensor $G^{\mu\nu}(x)$:

$$q(x) = \frac{1}{32\pi}\epsilon_{\mu\nu\rho\sigma}\text{Tr}G^{\mu\nu}(x)G^{\rho\sigma}(x). \tag{5.7}$$

The two-point function $\langle q(x)q(y)\rangle$ is computed for all pairs of points (x, y) in the four-dimensional volume $L^3 \times T$. Using a fast Fourier transform allows this to be done efficiently, obtaining a full-volume object in a single calculation step. Moreover, because of translation invariance, the two-point correlator only depends on the distance $r = |x - y|$, and we average all contributions at fixed distance to increase statistics and reduce discretization effects due to the breaking of rotational symmetry. For a particle freely propagating in four dimensions [84], the correlator takes the form

$$C(r) = \frac{A}{r^{1.5}}\left(1 + \frac{3}{8r}\right)e^{-M_{\eta'}r} \tag{5.8}$$

at large distances $r \to \infty$. We fit the lattice data of $C(r)$ to the form in Eq. (5.8), and we choose a specific fitting window of distances $r \in [r_{\text{min}}, r_{\text{max}}]$ to extract the two parameters A and $M_{\eta'}$ corresponding to the propagating single-particle ground state. *A posteriori*, we check that the fitting window is at large enough r that the form in Eq. (5.8) is valid. For the fitting procedure we use the LSQFIT Python package [85], and we assign large (uninformative) Bayesian priors on the parameters based on the analysis of effective masses at large r.

Additionally, it is well known that ultraviolet fluctuations strongly affect the operator in Eq. (5.7). We utilize the gradient flow [53] of the Symanzik action as a smearing technique to remove the UV components and smooth the operator before constructing the two-point function. In other words, the interpolating operator in Eq. (5.7) is used to construct the correlator, but $G^{\mu\nu}(x)$ is computed for several values of the flow time t_w. We choose t_w values in units of the lattice spacing a^2 lying in the interval [0, 3] and in steps of 0.15. This is a large range and we expect that the operator $q(x)$ at some smearing t_w will have an approximate physical size with good overlap to the ground state. This physical size can be identified with a smearing scale $s_w = \sqrt{8t_w}$. As a consequence, we obtain a large number of correlators $C_{t_w}(r) = -\langle q_{t_w}(x)q_{t_w}(y)\rangle$. The statistical fluctuations are dramatically reduced by the gradient flow smearing, such that correlators at larger t_w can be easily fitted to the exponential form in Eq. (5.8). Moreover, the autocorrelation effects on $C_{t_w}(r)$ are negligible. However, the smearing scale s_w introduces systematic corrections that have to be addressed [86]. In fact, it turns out that the dominant source of uncertainty in extracting $M_{\eta'}$ comes from systematic effects of the fitting procedure. There are mainly two competing effects:

(1) Equation (5.8) can only be assumed to be valid in a specific region of large r, where the ground state dominates: In other words, we should make sure that the extracted mass does not depend on the value of r_{min}.
(2) The correlator at large distances suffers from larger statistical fluctuations and can be extracted only at large values of the smearing scale s_w, where smearing artifacts [86] are larger: In other words, we should check that the extracted mass does not depend on r_{max}.

We estimate the systematic uncertainty on $M_{\eta'}$ by looking for a plateau in the fitting range $[r_{\mathrm{min}}, r_{\mathrm{max}}]$ and for a plateau in the smearing range $s_w = \sqrt{8t_w}$. Representative examples of such plateaux for one ensemble of $N_f = 12$ QCD are shown in Fig. 17. Note that s_w is always smaller than the fit range boundary $r_{\mathrm{min}} \geq 7$ we typically choose, and that r_{max} is always less than half the lattice spatial extent L. When the smearing range s_w is considered in units of the characteristic radius given by the gradient flow scale $\sqrt{8t_0}$, we seem to find a common region of $\sqrt{t_w/t_0}$ values for all the ensembles at fixed N_f where the fitted mass does not change within the statistical uncertainty. This region does not appear to depend on the fermion mass or on the volume: It corresponds to the interval [0.69, 0.81] for $N_f = 4$, [0.39, 0.51] for $N_f = 8$, and [0.35, 0.41] for $N_f = 12$. The difference in these intervals might be related with the nature of the flavor-singlet pseudoscalar state as N_f is increased because such a smearing scale s_w corresponds to some physical scale for the operator with the best coupling to the ground state. In the identified region, we take the difference between the largest and the smallest fitted mass as an estimate of the systematic error. The statistical errors of the individual points are typically smaller than or of the same order as this systematic uncertainty. Additional plots for the rest of the ensembles are collated in Appendix D.

We can now compare the flavor-singlet pseudoscalar state with the rest of the low-lying spectrum as we change the number of flavors. The results obtained for $N_f = 4, 8$, and 12 QCD are summarized in Fig. 18 in units of $1/a$. We identify a notable increase in the gap between the flavor-singlet pseudoscalar and the vector meson visible in Fig. 19. In $N_f = 4$ QCD the mass ratio $M_{\eta'}/M_\rho$ is close to 1 and gradually increases toward the chiral limit, while it grows rapidly from near 2 to ∼3–4 for $N_f = 8$, and it stays around 2.5 for $N_f = 12$. We shall return to this point later.

In Sec. II, we discussed the expectation that

$$\frac{M_{\eta'}^{2\,(\mathrm{anomalous})}}{\Lambda_{\mathrm{IR}}^2} \sim n_f^2. \tag{5.9}$$

As anticipated in that discussion, we do not see this proportionality when we choose M_ρ as the IR scale, as is shown in Fig. 19. None of the values of N_f gives flat behavior, and the $N_f = 12$ data are not higher than $N_f = 8$ as would be predicted.

However, when $\Lambda_{\mathrm{IR}} = 1/\sqrt{8t_0}$ is chosen instead, we obtain the result shown in Fig. 20. In this case, the resulting behavior for each N_f is significantly flatter, and the values

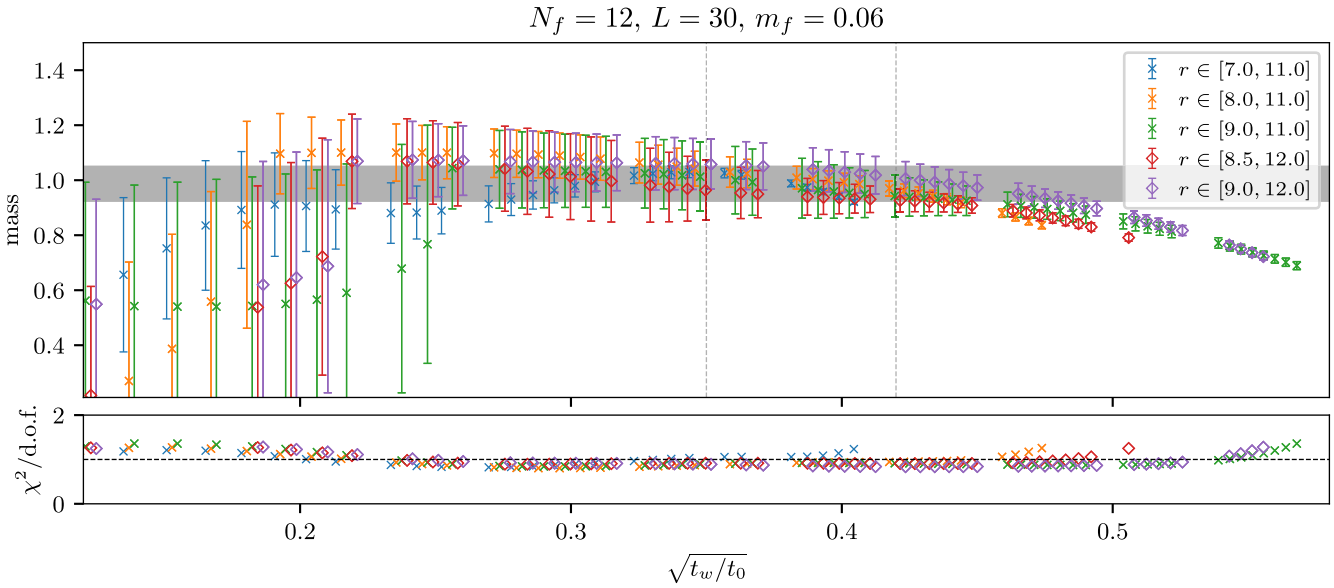

FIG. 17. The η' mass fitted for different distance regions and smearings, for a specific ensemble of $N_f = 12$ QCD. The error bars on the horizontal axis are much smaller than the symbols, and points for different fitting ranges are shifted for clarity. $\sqrt{8t_0} = 7.2680(99)$ for this ensemble. The gray band shows the estimate of the systematic error computed as described in the text.

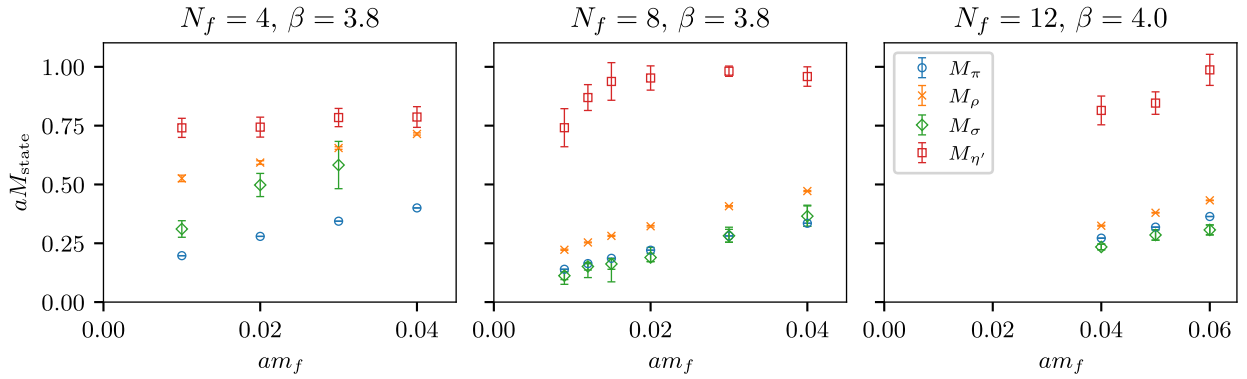

FIG. 18. The flavor-singlet scalar and pseudoscalar spectrum compared to flavor-non-singlet pseudoscalar and vector spectrum for $N_f = 4, 8$, and 12. The η' mass has error bars that reflect a large systematic uncertainty. For the other states, only statistical errors are reported.

obtained in the three cases display the predicted scaling. Specifically, we observe that

$$M_{\eta'}^2 \cdot 8t_0 \simeq M_{\eta'}^{2\,(\text{anomalous})} \cdot 8t_0 \simeq \begin{cases} (2.5)^2 & N_f = 4, \\ (5.0)^2 & N_f = 8, \\ (7.5)^2 & N_f = 12, \end{cases} \tag{5.10}$$

independent of m_f, in close agreement with the expectation Eq. (2.23) in the anti-Veneziano limit as shown in Fig. 21.

In view of this result, we may now gain some further understanding of the gross features of $M_{\eta'}/M_\rho$ shown in Fig. 19. From Eq. (2.10), we expect that in the broken phase, $M_\rho\sqrt{8t_0} \to 1$ toward the chiral limit, and $\to 2$ toward the heavy-fermion limit, while we have observed that $M_{\eta'}$ is roughly constant. For $N_f = 4$ and 8, moving to larger M_π/M_ρ in Fig. 19 corresponds to dividing the constant $M_{\eta'}\sqrt{8t_0}$ by $M_\rho\sqrt{8t_0} \to 2$, and so giving $M_{\eta'}/M_\rho \simeq 1.25$ and 2.5 respectively, which is approximately what we observe. Moving to smaller M_π/M_ρ meanwhile takes the opposite limit, and in Fig. 19 we do indeed see the data move in this direction, although the limit is not reached. Meanwhile, the data for $N_f = 12$ are constant within uncertainties, as we would expect.

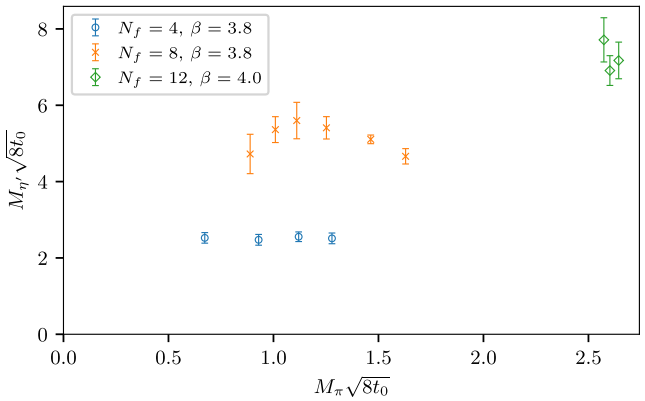

FIG. 20. Comparison of the flavor-singlet pseudoscalar mass for $N_f = 4, 8$, and 12 as a function of the pion mass. The hadronic masses are in units of the gradient flow scale $1/\sqrt{8t_0}$ for the various N_f theories. Different quark mass regions are explored for different N_f values, in particular for $N_f = 12$.

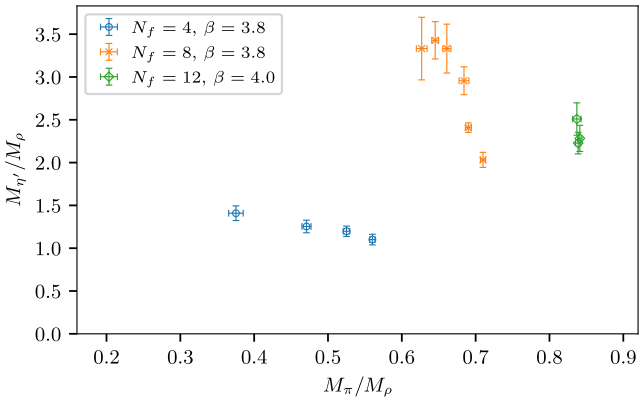

FIG. 19. Comparison of the results for $M_{\eta'}$ between the theories with $N_f = 4, 8, 12$ when normalized by M_ρ.

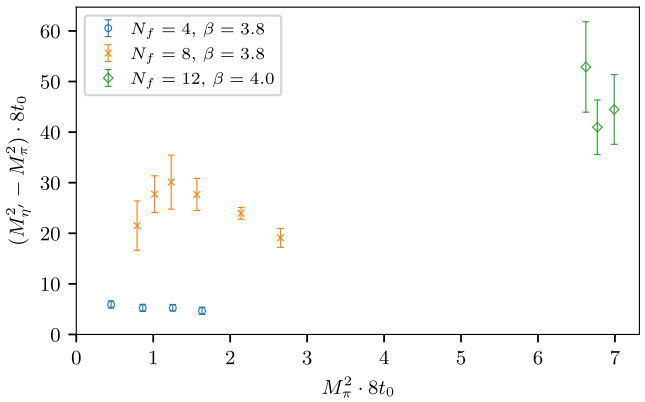

FIG. 21. Comparison of the difference $M_{\eta'}^2 - M_\pi^2$ normalized by the gradient flow scale $\sqrt{8t_0}$.

VI. SUMMARY

We have investigated the mass spectra of the SU(3) gauge theory with $N_f = 4$, 8, and 12 fundamental flavors (4-, 8-, and 12-flavor QCD), using a first-principles lattice gauge theory analysis. This analysis used the tree-level improved Symanzik gauge action and the HISQ fermion action.

In the case of $N_f = 8$ QCD, we observe approximate conformality, which we interpret as indicating the theory is in the hadronic phase just below the conformal window; i.e., the chiral limit shows walking dynamics with a light flavor-singlet scalar "σ" as a pseudo-NG boson (pseudo-dilaton) of the scale symmetry, broken spontaneously and explicitly by the same origin of the spontaneous mass generation, a candidate for the composite Higgs boson [16,17]. This property and the $N_f = 8$ flavor structure match the simplest version of the WTC model, which is advocated as a viable candidate for a theory of physics beyond the Standard Model (BSM). Regarding the walking dynamics, the mass spectra at small fermion mass m_f are of particular interest. These have been investigated in this paper by updating our previous results [16,17] with a new lightest fermion mass: $m_f = 0.009$ (in lattice units). We have compared the $N_f = 8$ spectra with those in $N_f = 4$ QCD the latter is close to real-world QCD, showing spontaneous chiral-symmetry breaking, but without the walking dynamics. For $N_f = 4$, we have updated our data to include a finer lattice spacing. This has allowed us to extract the flavor-singlet scalar spectrum in $N_f = 4$.

We also compared the spectrum for $N_f = 4$, 8 on the same footing as the previous results of $N_f = 12$ [13,17], which was shown to be the conformal phase without spontaneous chiral-symmetry breaking in contrast to $N_f = 4, 8$.

Moreover, we have examined the flavor-singlet pseudoscalar spectra "η'" for all $N_f = 4, 8$, and 12 QCD, and discussed the N_f dependence of the spectra in terms of the scaling law emerging in the anti-Veneziano limit described in Sec. II.

For $N_f = 8$, we have confirmed that two important properties remains intact in the updated data: First, the improvement in the HISQ action has continued to allow the taste violation to be suppressed to 5% or less of the Goldstone pion mass, and second, the ratio M_ρ/M_π increases with decreasing m_f, consistent with the spontaneous breaking of the chiral symmetry. We have also observed this ratio increasing similarly for $N_f = 4$ QCD.

In $N_f = 8$, we have evaluated the chiral limits of F_π, M_π/m_f, M_ρ, M_{a_0}, M_{a_1}, M_{b_1}, M_N, and $M_{N_1^*}$ with a polynomial ansatz in m_f. All of their chiral limit values have been positive finite with good fit qualities and are consistent with our previous studies [17]. For the chiral condensate, we have investigated three different observables: $\langle\bar{\psi}\psi\rangle$, Σ, and $F^2B/2$, as defined in Eqs. (3.5) and (3.6). With the inclusion of the new data at the lightest value of m_f, the chiral limit values for these three observables are now consistent when a linear fit ansatz is used, as is expected theoretically. While previously, the central value of the Σ extrapolation was negative [17], the inclusion of the updated spectral data gives a positive result for the central value. Thus, the update has provided further evidence of the broken chiral symmetry for $N_f = 8$.

We have observed that the flavor-singlet scalar mass M_σ in the new ensemble for $N_f = 8$ at $m_f = 0.009$, similar to previous observations at heavier m_f [16,17], is significantly smaller than the other hadron masses except the pion. At this new mass in particular, M_σ is still even smaller than the pion mass M_π, similar to the previous result, and in contrast to the expectation in the chiral limit that $M_\sigma > M_\pi = 0$. Conversely, M_σ in $N_f = 4$ tends to remain larger than M_π, though getting closer, with decreasing m_f. The light M_σ in $N_f = 8$ indicates a dilatonic feature and a stable sigma meson, which contrasts sharply with real-world QCD. We have performed chiral extrapolations of the light M_σ data both with a simple linear ansatz $M_\sigma = c_0 + c_1 m_f$ and with the WT identity for the scale symmetry $M_\sigma^2 = d_0 + d_1 M_\pi^2$, Eq. (2.36). The results are given together with those for $N_f = 4, 12$ in Table VIII. Both extrapolations for $N_f = 8$ resulted in masses consistent with the discovered Higgs boson mass 125 GeV $\simeq v_{\rm EW}/2 = \sqrt{N_D/4}\cdot F/\sqrt{2}$. Owing to the updated data, the lower systematic errors are improved by more than a factor of 2.

Equation (2.36) may also be derived by the dChPT in the broken phase, up to chiral log effects that are irrelevant to our data points, lying as they do far from the chiral limit. However, chiral log effects will raise the value of M_σ near the chiral limit, and as such a value estimated from a fit form excluding them (and extrapolated from data in the region where they are not present) will by necessity underestimate the chiral limit value d_0. This is reflected in our data; the central value for the fit of d_0 is negative, although the large uncertainties still do allow for a positive value.

On the other hand, the fit value of d_1 is identified with that in the chiral limit where chiral log effects disappear, and so is the ratio $F_\sigma/(F_\pi/\sqrt{2})$ as in Eq. (2.37), which is most relevant to the Higgs phenomenology. It was obtained from the observed value of d_1 for $N_f = 8$ to give Eq. (4.3):

$$F_\sigma/(F_\pi/\sqrt{2}) = 3.97(40)\binom{96}{63} \quad \text{for } \gamma_m = 1, \tag{6.1}$$

which is consistent with the previous results $F_\sigma/(F_\pi/\sqrt{2}) \simeq 4$ [16,17]. This implies $v_{\rm EW}/(F_\sigma|_{m_f=0}) \simeq \sqrt{N_D}/4$ to be compared with $v_{\rm EW}/F_\sigma|_{m_f=0} \simeq 0.27$, the value from the LHC data when σ identified with the Higgs boson [12], where $v_{\rm EW} = 250$ GeV and N_D is the number of weak doublets of the WTC model.

More importantly, the WT identity formula Eq. (2.36) is valid in both the broken (at least for our data points, which lie away from the chiral limit) and the conformal phase, thus is our basic framework to compare $N_f = 4, 8, 12$ on the same footing. The measured values of d_1 for $N_f = 8$ and $N_f = 12$, when combined with the measured γ_m through hyperscaling, give values of $F_\sigma/F_\pi/\sqrt{2}$ consistent with those from linear sigma and holographic models, Eq. (2.38); this in turn gives the relation between $d_1 = (1+\gamma_m)/(3-\gamma_m)$, Eq. (2.39), consistent with the fit values, as summarized in Table VIII. It is remarkable that for $N_f = 12$, σ with $M_\sigma^2 \simeq 0.7 M_\pi^2$ is definitely lighter than π in spite of the P-wave bound state compared with the S-wave π; this is consistent with the picture discussed in Sec. II that σ is a pseudo-NG boson while π is not. If this relation is also valid for $N_f = 4$ without a fit value of γ_m due to the lack of hyperscaling, then the large value of d_1 would imply $\gamma_m \simeq 2.11(21)$, suggesting the system to be effectively described by the gauged NJL model with reduced effective gauge coupling in the infrared. If this relation is valid also in the whole conformal phase where the SD equation gives $\gamma_m = 1 - \sqrt{1-\alpha_*/\alpha_{\rm cr}}$, then we may predict $M_\sigma^2 \simeq d_1 M_\pi^2 = M_\pi^2(n_f = n_f^{\rm cr})$ further down to $M_\sigma^2 \simeq d_1 M_\pi^2 = 1/3 \cdot M_\pi^2(n_f = 16.5/3)$.

Our focus in this work has been on the flavor-singlet pseudoscalar meson η'. We have extracted the η' correlator from the two-point function of the topological charge density $\langle q(x)q(y)\rangle$, where pion contaminations are absent. To increase the statistics, the correlator has been expressed as a function of the distance $r = |x-y|$, and all contributions at a fixed r have been averaged. We have utilized the gradient flow smearing technique to remove UV noise and achieve enhanced overlap with the ground state.

We have estimated $M_{\eta'}$ from a plateau region $[r_{\rm min}, r_{\rm max}]$ in the correlator. To avoid lattice spacing, smearing, and finite-size artifacts, the plateau region was restricted to values of r much larger than the smearing scale (which in turn was much larger than the lattice spacing), and much smaller than the spatial lattice extent, in all cases. Within these constraints, $M_{\eta'}$ was observed to be independent of the exact choice of the plateau region and the smearing scale. We have found such a parameter region for all our ensembles. In particular, a suitable range of smearing scale was found that was independent of m_f for each N_f.

There are theoretical expectations [12] that the mass $M_{\eta'}$ scales with N_f, as a consequence of an anti-Veneziano limit where $n_f \equiv N_f/N_c \gg 1$ is fixed as $N_c \to \infty$ with $N_c\alpha$ fixed, based on the WT identity for the flavor-singlet axial-vector current Eq. (2.16) with Eqs. (2.18) and (2.19). For each $N_f = 4, 8, 12$, $M_{\eta'}$ was found to be heavier than the other hadrons, and less dependent on m_f. We have adopted the gradient flow scale $\sqrt{8t_0}$ as a common measure to compare the theories with different N_f. The normalized mass $M_{\eta'} \cdot \sqrt{8t_0} \sim n_f$ was observed to increase as a function of n_f [see Fig. 20 and Eq. (5.10)]

$$M_{\eta'}^2 \cdot 8t_0 \simeq \begin{cases} (2.5)^2 & N_f = 4, \\ (5.0)^2 & N_f = 8, \\ (7.5)^2 & N_f = 12, \end{cases} \tag{6.2}$$

independent of m_f, which is suggestive of anti-Veneziano scaling in Eq. (2.23). This is the core result of this paper.

Several subjects remain to be studied in future work. For $N_f = 8$ QCD, there are number of reasons to study a region of m_f even smaller than the $m_f = 0.009$ to which this study was extended: to achieve a stable chiral limit value of the chiral condensate Σ, to obtain a more precise value for the chiral limit value of the dilatonic σ mass in the chiral limit in order to confirm (or otherwise) the consistency with the discovered Higgs mass, and to verify whether the pion becomes lighter than the Higgs-identified dilaton, which for a walking theory is expected to happen in the vicinity of the chiral limit. Another important topic is to explore the mass spectra in the continuum limit. To this end, the simulations presented here need to be extended to multiple smaller lattice spacings. Infrared dominance and the suppression of taste violations by the HISQ action means that the majority of the spectra of $N_f = 8$ QCD are not expected to be very sensitive to the lattice spacing; in particular, we anticipate this being the case for the η' mass. To study the anti-Veneziano scaling discussed above in detail, continuum and chiral extrapolations of $M_{\eta'}$ are needed for all of $N_f = 4, 8,$ and 12.

We believe that our first-principles results indicating the walking dynamics in $N_f = 8$ QCD will provide a very important guide for BSM model building with the composite Higgs perspective.

ACKNOWLEDGMENTS

We thank the LSD Collaboration for sharing their plots and their preliminary unpublished results for the flavor-singlet scalar mass on their ensembles. We gratefully acknowledge Dr. Masafumi Kurachi and Dr. Kei-ichi Nagai for their collaboration during the early stages of this work. Numerical calculations have been carried out on the high-performance computing systems at KMI (φ), at the Information Technology Center in Nagoya University (CX400), and at the Research Institute for Information Technology in Kyushu University (CX400 and HA8000) both through the High Performance Computing Infrastructure System Research Projects (Projects ID No. hp140152, No. hp150157, and No. hp160153) and

through general use. This work is supported by the JSPS Grants-in-Aid for Scientific Research (S) Grants No. 22224003, (C) No. 16K05320 (Y. A.) for Young Scientists (A) No. 16H06002 (T. Y.), (B) No. 25800138 (T. Y.), (B) No. 25800139 (H. O.), and (B) No. 15K17644 (K. M.). E. B. acknowledges the support of the UKRI Science and Technology Facilities Council Research Software Engineering Fellowship No. EP/V052489/1, the EPSRC ExCALIBUR program ExaTEPP (Project No. EP/X017168/1), the STFC Consolidated Grant No. ST/T000813/1, and the Supercomputing Wales program, which is partially funded by the European Regional Development Fund via the Welsh Government. K. M. is supported by the OCEVU Labex (Grant No. ANR-11-LABX-0060) and the A*MIDEX project (Grant No. ANR-11-IDEX-0001-02) funded by the "Investissements d'Avenir" French government program and managed by the ANR. H. O. is supported in part by the JSPS KAKENHI (Grants No. 21K03554 and No. 22H00138). T. Y. is supported in part by Grants-in-Aid for Scientific Research (Grants No. 19H01892, No. 23H01195, and No, 23K25891) and MEXT as "Program for Promoting Researches on the Supercomputer Fugaku" Grant No. JPMXP1020230409. This work is supported by the Japan Lattice Data Grid constructed over the Science Information NETwork 6 of NII. This work was in part based on the MILC Collaboration's public lattice gauge theory code, version 7 [87].

DATA AVAILABILITY

The data that support the findings of this article, and the workflow used to analyse them and transform them into the format presented herein, are openly available [88].

APPENDIX A: DETAILS OF LATTICE SIMULATIONS AT $m_f = 0.009$

The simulation parameters of the new ensemble are summarized in Table IX. The measurements of the hadron spectra are carried out with the parameters shown in Table X. The statistical error is estimated by the jackknife analysis.

The hadron masses for π, ρ, N, and their parity partners a_0, a_1, b_1, $N_{\mathbf{1}}^*$ at $m_f = 0.009$ are tabulated in Table XI. The table also shows the results for the decay constant F_π and the chiral condensate $\langle\bar{\psi}\psi\rangle$. The notations and calculation methods for the hadron spectra are described in our previous paper [17]. As in the paper, we observe a small taste-symmetry breaking in the pion mass as shown in Table XII.

In the previous study [17], we found that the finite volume effects for M_π and F_π are negligible when $LM_\pi \gtrsim 7$ at smaller m_f by using

$$\delta M_\pi(L) = \frac{M_\pi(L) - M_\pi(L_{\max})}{M_\pi(L_{\max})} \quad \text{and} \quad \delta F_\pi(L) = \frac{F_\pi(L) - F_\pi(L_{\max})}{F_\pi(L_{\max})}, \tag{A1}$$

with $L_{\max}$ being the largest lattice volume at each m_f. Figure 22 is the updated figure from the previous study [17]. The figure shows that the value of LM_π at $m_f = 0.009$, which is the vertical solid line, is similar to the one at $m_f = 0.012$. From this observation, we expect that the finite volume effects in the new data are similarly suppressed as at higher m_f values.

TABLE IX. Parameters of the new ensemble in $N_f = 8$. L and T for the spatial and temporal size for $L^3 \times T$ lattice, staggered fermion mass m_f, molecular dynamics time step $\Delta\tau$, number of masses for the Hasenbusch preconditioning $N_{m_{\mathrm{H}}}$, values of Hasenbusch masses m_{H}^i, and maximum number of thermalized trajectories $\bar{N}_{\mathrm{Traj}}^{\max}$ in $\tau = 0.5$ unit are shown for each "stream." $N_{\mathrm{Traj}}^{\max}$ denotes the maximum number of thermalized trajectories in $\tau = 1$ unit as in other ensembles [17].

L	T	m_f	τ	$\Delta\tau$	$N_{m_{\mathrm{H}}}$	m_{H}^1	m_{H}^2	m_{H}^3	m_{H}^4	$\bar{N}_{\mathrm{Traj}}^{\max}(N_{\mathrm{Traj}}^{\max})$	Stream
48	64	0.009	0.5	0.0025	4	0.2	0.4	0.6	0.8	864(432)	1
										10240(5120)	2

TABLE X. Numbers for trajectories (N_{Traj}) in $\tau = 1$ unit, stream (N_{str}), configuration (N_{conf}), for the spectrum and singlet scalar (σ) measurements in the $N_f = 8$ new ensemble. The bin size of the jackknife analysis (N_{bin}) and number of measurements per configuration (N_{meas}) are also summarized.

Meas	L	T	m_f	N_{Traj}	N_{str}	N_{conf}	N_{bin}	N_{meas}
Spectrum	48	64	0.009	5440	2	680	68	8
σ	48	64	0.009	5120	1	2560	160	64

TABLE XI. Results of hadron spectra and M_σ at $m_f = 0.009$ on $L = 48$ in $N_f = 8$.

M_π	0.13950(56)
F_π	0.03971(20)
$\langle\bar{\psi}\psi\rangle$	0.0055516(54)
M_ρ	0.2225(24)
M_{a_0}	0.2355(71)
M_{a_1}	0.3144(59)
M_{b_1}	0.3196(86)
M_N	0.3202(22)
$M_{N_1^*}$	0.4156(65)
M_σ	$0.112(17)\binom{0}{33}$

TABLE XII. Mass of the NG pion and the taste partners M_{π_ξ} at $m_f = 0.009$ on $L = 48$ in $N_f = 8$.

ξ_5	$\xi_4\xi_5$	$\xi_i\xi_5$	$\xi_i\xi_4$	$\xi_i\xi_j$	ξ_4	ξ_i	ξ_I
0.13950(56)	0.14062(56)	0.14042(54)	0.14112(59)	0.14131(58)	0.14181(60)	0.14198(57)	0.14263(54)

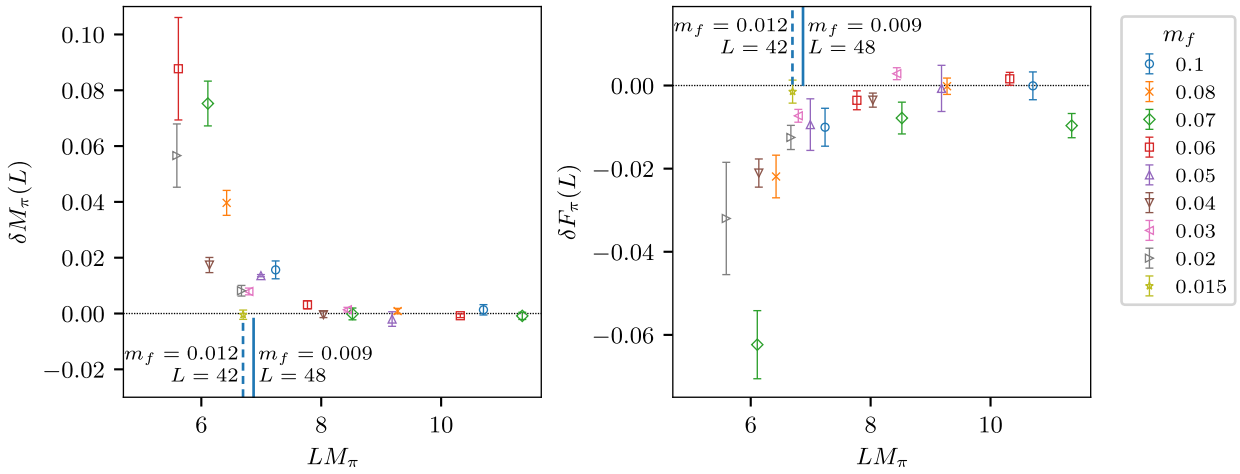

FIG. 22. Updated figures for $\delta M_\pi(L)$ and $\delta F_\pi(L)$ defined in Eq. (A1) from the one in the previous paper [17]. In this paper, we do not use fermion masses heavier than $m_f = 0.04$, and they are reported here only for comparison with our previous results. Points with error bars show the difference between the specified quantity at the given lattice size L and at the largest volume considered for that value of the bare mass. Different symbols and colors represent different bare masses as indicated in the legend. The two vertical lines in blue represent the two values of mass at which only a single volume was considered: The solid line is $m_f = 0.009$, $L = 48$, and the dashed line $m_f = 0.012$, $L = 42$.

APPENDIX B: DETAILS OF THE NEW CHIRAL EXTRAPOLATIONS WITH $m_f = 0.009$

In Fig. 23, we show the chiral extrapolations for $\langle\bar{\psi}\psi\rangle$, supplementing that of the GMOR relation presented in Sec. III B. In Figs. 24–26, we show the chiral extrapolations of the meson masses including the new $m_f = 0.009$ mass point.

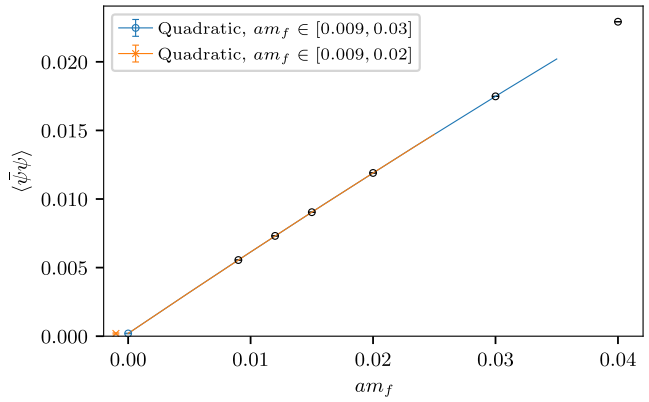

FIG. 23. Chiral extrapolations of the chiral condensate $\langle\bar{\psi}\psi\rangle$ in $N_f = 8$. The range of m_f considered for each fit curve is noted in the legend.

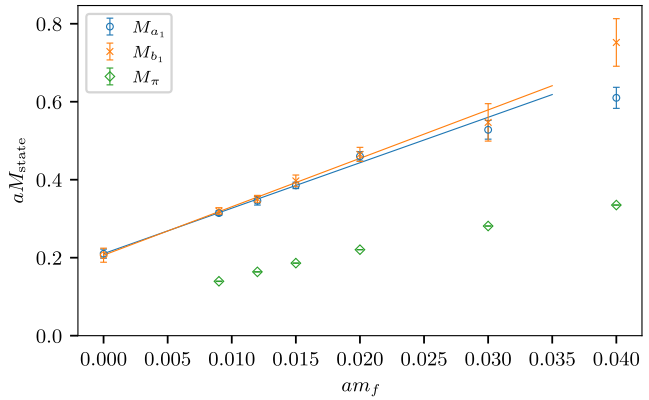

FIG. 25. Chiral extrapolations for M_{a_1} and M_{b_1} in $N_f = 8$. Data for M_π are also plotted for comparison.

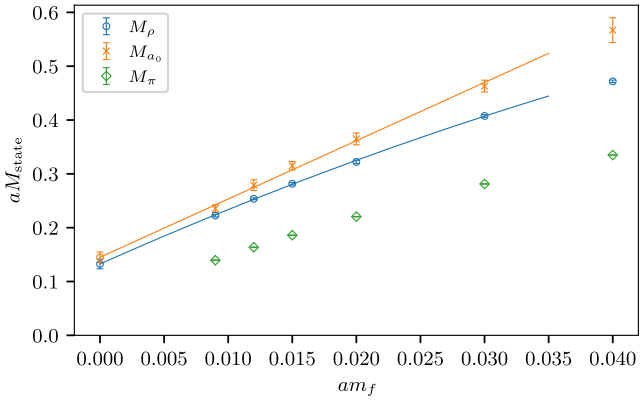

FIG. 24. Chiral extrapolations for M_ρ and M_{a_0} in $N_f = 8$. Data for M_π are also plotted for comparison.

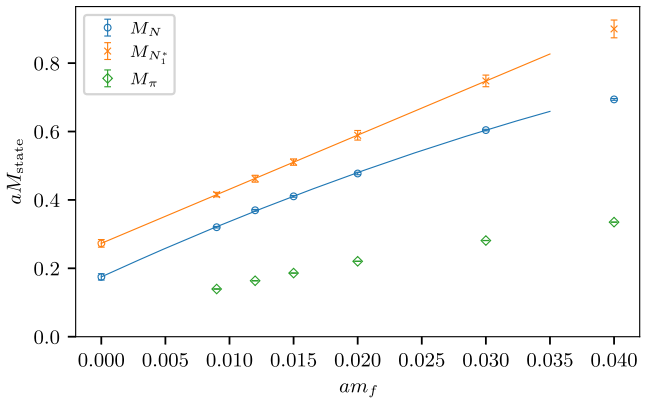

FIG. 26. Chiral extrapolations for M_N and $M_{N_1^*}$ in $N_f = 8$. Data for M_π are also plotted for comparison.

APPENDIX C: TASTE-SYMMETRY BREAKING EFFECTS

We report two different lattice spacings for $N_f = 4$ and show the ratio M_ρ/M_π using different states for the pseudoscalar meson: the lightest (Goldstone boson) state π_5 and the heaviest state π_{ij} (which comes from operators with tensor taste structure $\xi_i\xi_j$). Both states are going to be degenerate in the continuum limit, and we can see the reduction in taste-symmetry breaking effects when moving from a coarser ($\beta = 3.7$) to a finer ($\beta = 3.8$) lattice spacing. The results are shown in Fig. 27 as a function of the pion mass, $\pi = \pi_5$ or π_{ij}, in units of the gradient flow scale.

At the smallest mass considered, the results for $N_f = 8$ align more closely with those from the LSD Collaboration [42] when compared using a common scale given by the Nambu-Goldstone pion mass in units of the gradient flow scale $\sqrt{8t_0}$. This is illustrated in Fig. 28. However, the two collaborations use different lattice actions, which can introduce discretization effects, including variations in taste breaking. We noted in Sec. III that the taste splitting in our data remains small. We may observe this by

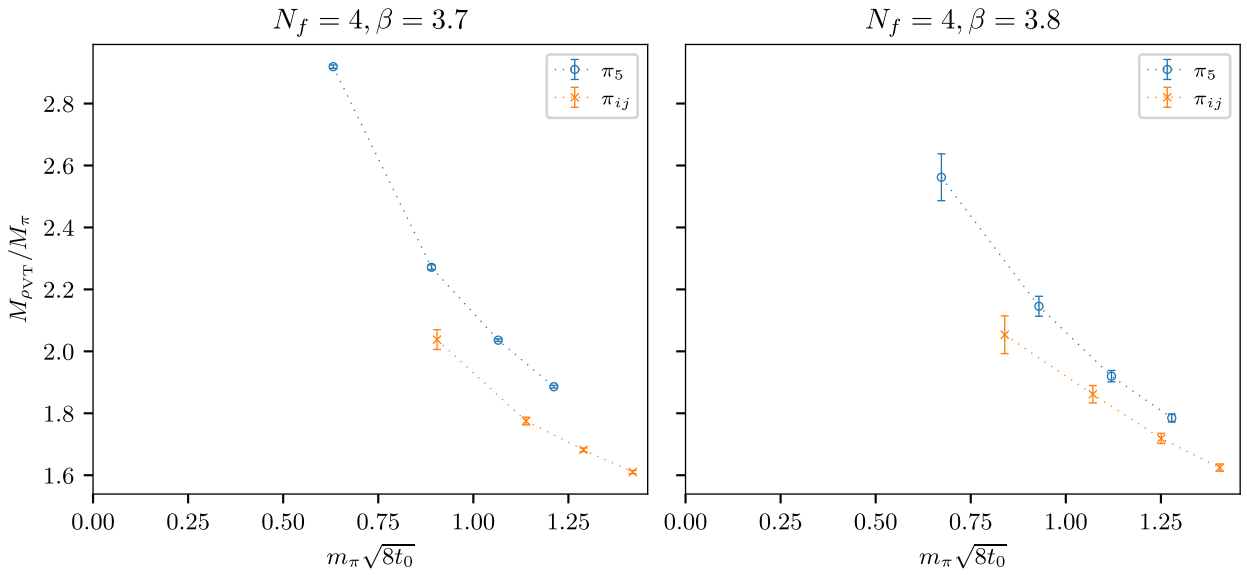

FIG. 27. The ratio M_ρ/M_π is shown for $N_f = 4$ QCD using different fermion taste combinations for the pseudoscalar meson. Results from two lattice spacings are shown in the two panels. The ratio of masses is shown using the Goldstone pion π_5 and the heaviest pseudoscalar meson π_{ij}. The horizontal axis uses the pion mass rescaled in units of the gradient flow scale $\sqrt{8t_0}$.

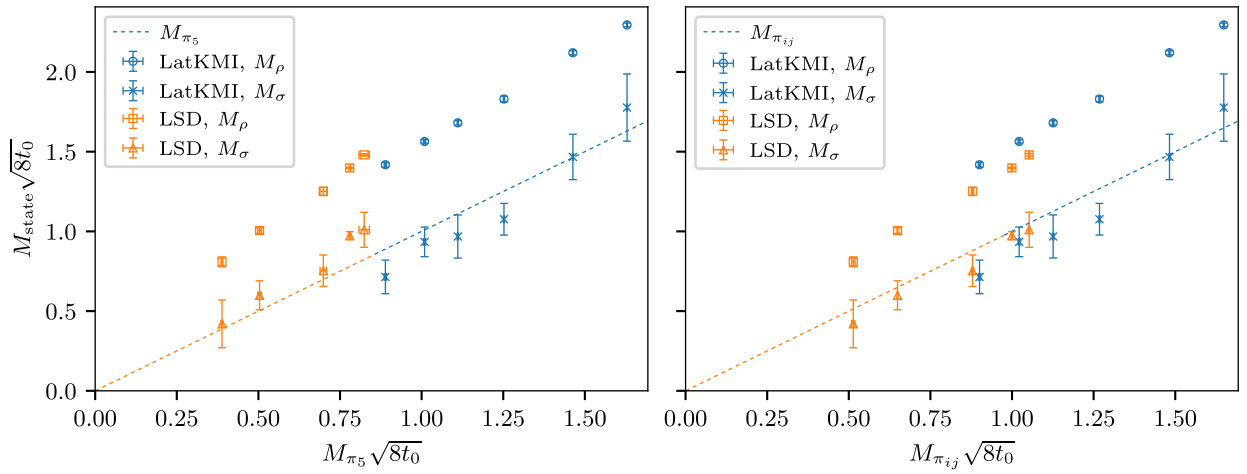

FIG. 28. Comparison of the flavor-singlet scalar mass and the vector meson mass between the LatKMI Collaboration and the LSD Collaboration for $N_f = 8$. The pion mass in units of the gradient flow scale is used on the x axis. The left panel uses the Goldstone pion π_5, while the right panel uses the tensor taste structure pion π_{ij}. The corresponding pion mass is used to draw the dashed line.

comparing the pion masses of different taste channels. For example, if we replace the Goldstone pion mass M_{π_5} with the heavier tensor taste pion mass $M_{\pi_{ij}}$, our data do not appreciably change. In contrast, the data from the LSD Collaboration shift significantly toward heavier masses, as shown in Figs. 28 and 29, making the compatibility between the two datasets even more striking. The results for $N_f = 4$ are also shown in Fig. 30. Based on the scale of t_0, it appears that the LSD results for $N_f = 4$ correspond to a finer lattice spacing, which likely reduces taste-breaking effects.

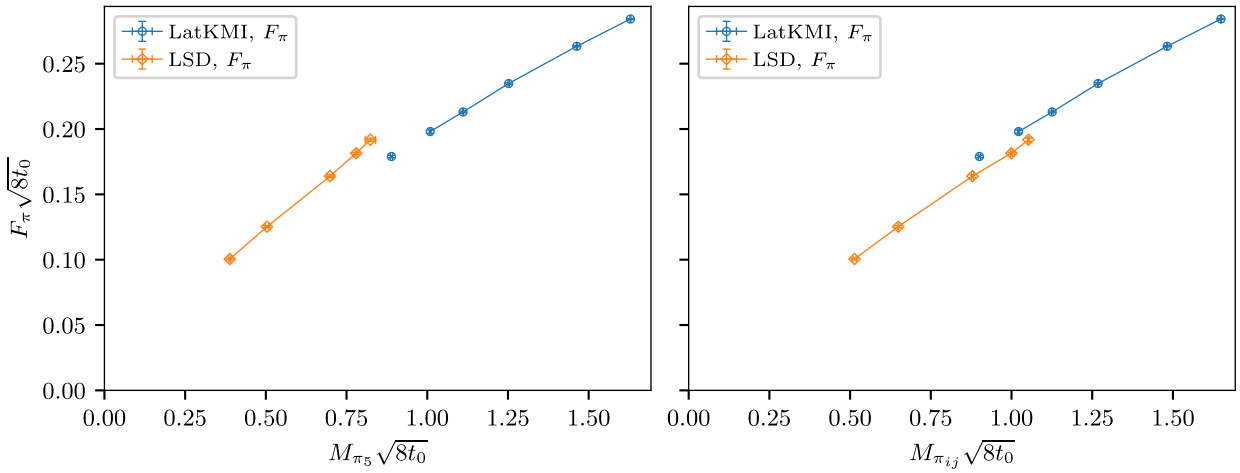

FIG. 29. Comparison of the pion decay constant between the LatKMI Collaboration and the LSD Collaboration for $N_f = 8$. The pion mass in units of the gradient flow scale is used on the x axis. The left panel uses the Goldstone pion π_5, while the right panel uses the tensor taste structure pion π_{ij}. The decay constant has been normalized to the 131 MeV convention in usual QCD [17].

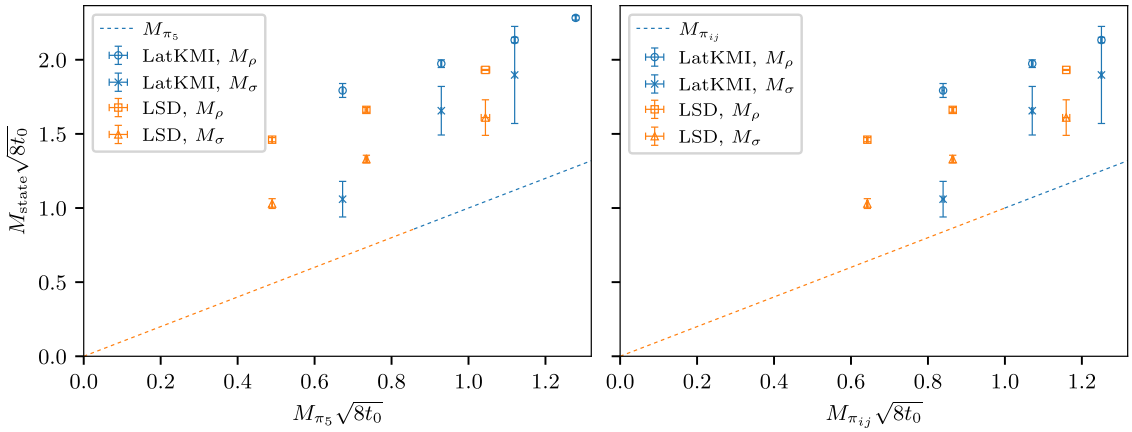

FIG. 30. Comparison of the flavor-singlet scalar mass and the vector meson mass between the LatKMI Collaboration and the LSD Collaboration for $N_f = 4$. The pion mass in units of the gradient flow scale is used on the x axis. The left panel uses the Goldstone pion π_5, while the right panel uses the tensor taste structure pion π_{ij}. The corresponding pion mass is used to draw the dashed line. The LSD data are only at $\beta = 6.6$.

APPENDIX D: FITS OF THE FLAVOR-SINGLET PSEUDOSCALAR

1. $N_f = 4$

The plateaux for the fits for each ensemble studied in the $N_f = 4$ theory are presented in Figs. 31, 32, 33, 34, and 35.

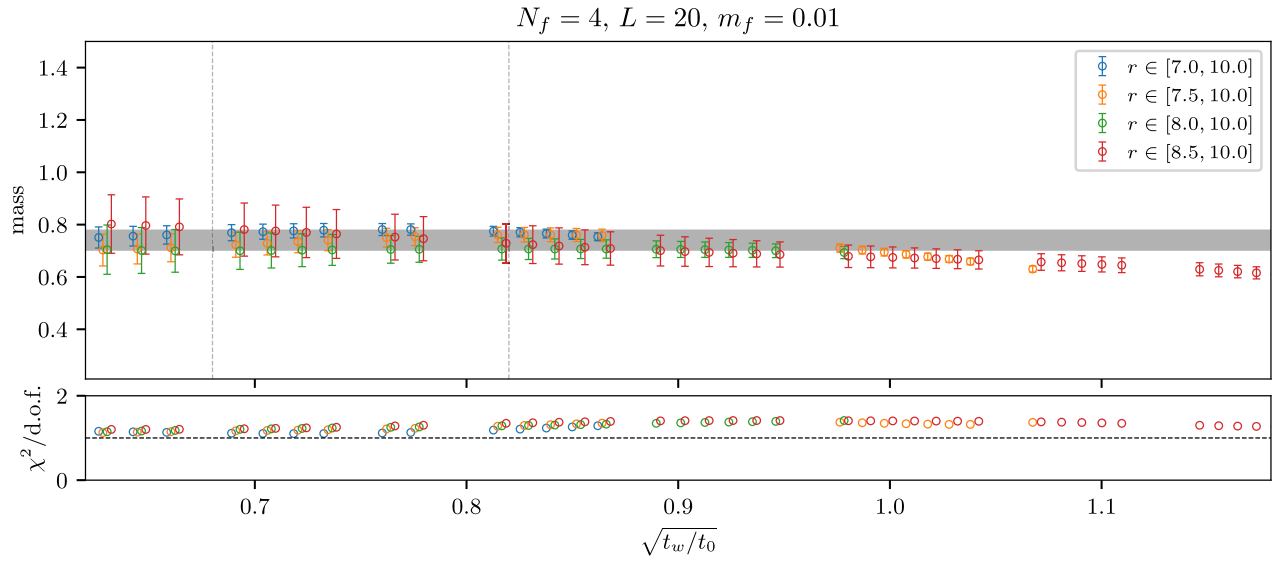

FIG. 31. The η' mass fitted for different distance regions and smearings for a specific ensemble of $N_f = 4$ QCD with $L = 20$ and $m_f = 0.01$.

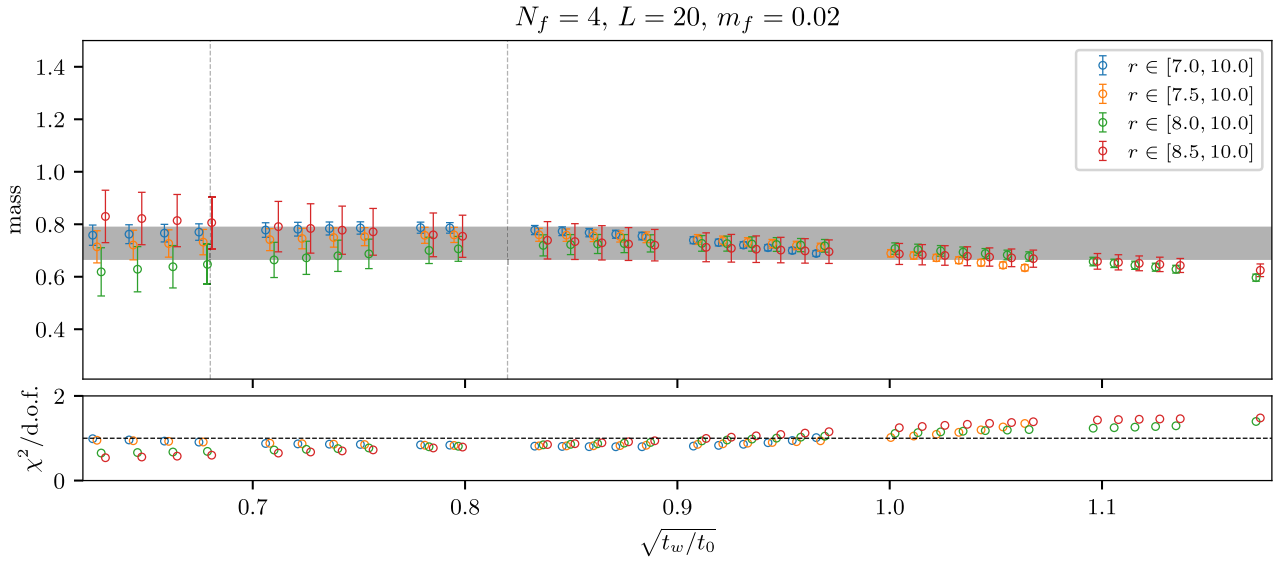

FIG. 32. The η' mass fitted for different distance regions and smearings for a specific ensemble of $N_f = 4$ QCD with $L = 20$ and $m_f = 0.02$.

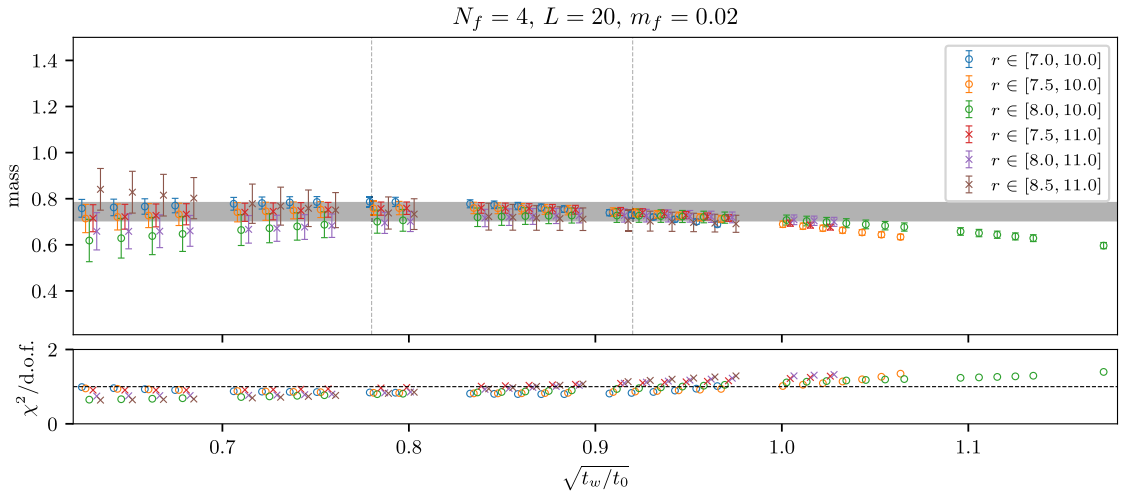

FIG. 33. The η' mass fitted for different distance regions and smearings for a specific ensemble of $N_f = 4$ QCD with $L = 20$ and $m_f = 0.02$. Different $r_{\max} = 11$.

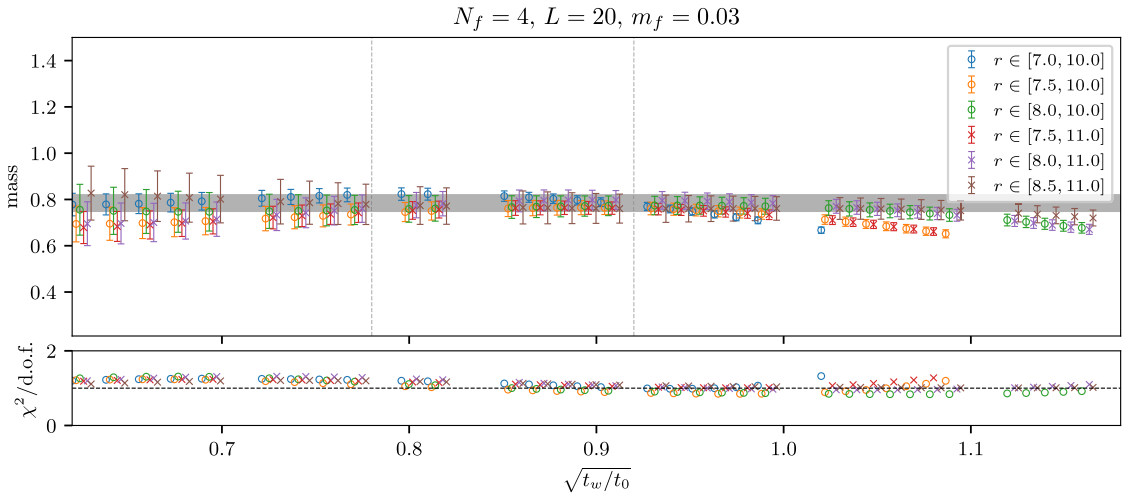

FIG. 34. The η' mass fitted for different distance regions and smearings for a specific ensemble of $N_f = 4$ QCD with $L = 20$ and $m_f = 0.03$.

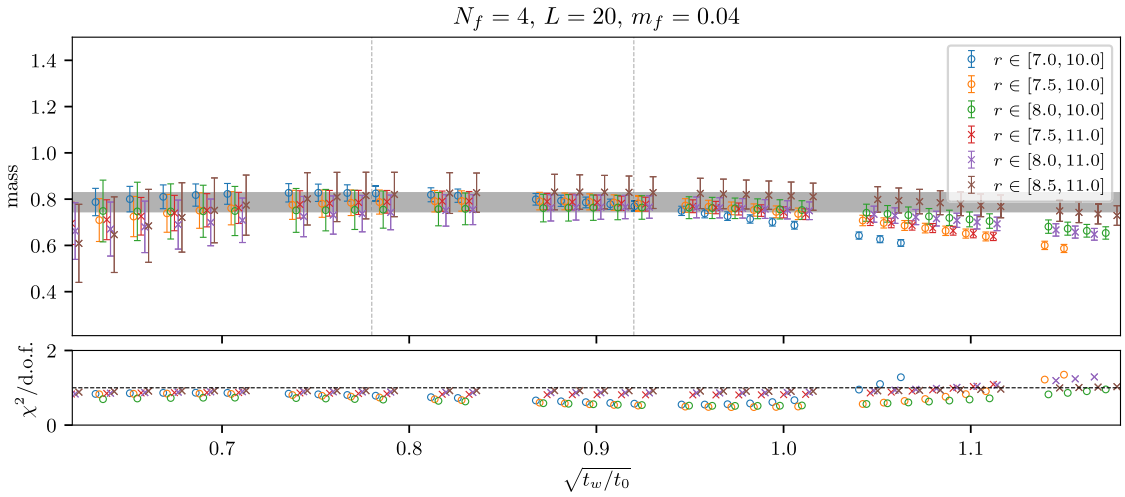

FIG. 35. The η' mass fitted for different distance regions and smearings for a specific ensemble of $N_f = 4$ QCD with $L = 20$ and $m_f = 0.04$.

2. $N_f = 8$

The plateaux for the fits for each ensemble studied in the $N_f = 8$ theory are presented in Figs. 36, 37, 38, 39, 40, and 41.

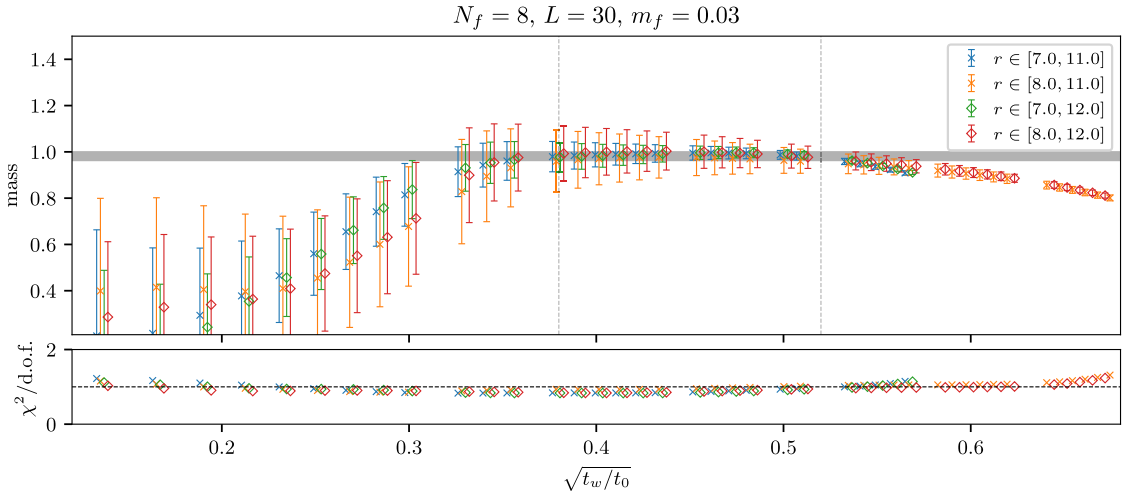

FIG. 36. The η' mass fitted for different distance regions and smearings for a specific ensemble of $N_f = 8$ QCD with $L = 30$ and $m_f = 0.03$.

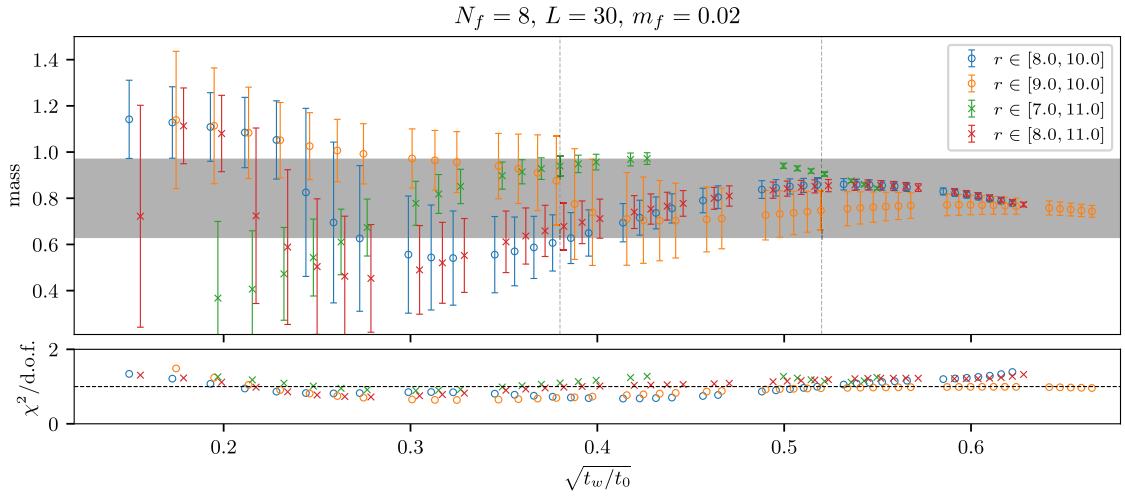

FIG. 37. The η' mass fitted for different distance regions and smearings for a specific ensemble of $N_f = 8$ QCD with $L = 30$ and $m_f = 0.02$.

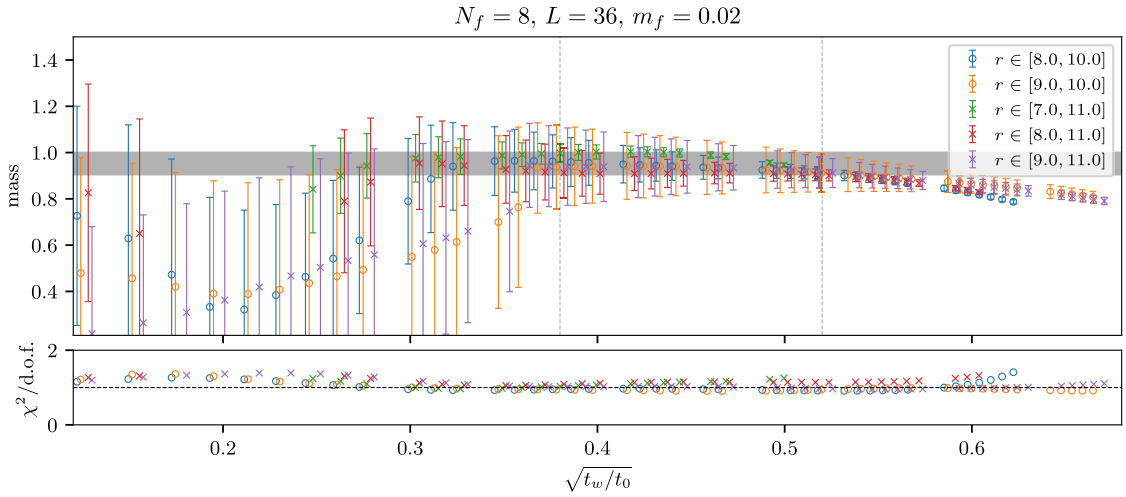

FIG. 38. The η' mass fitted for different distance regions and smearings for a specific ensemble of $N_f = 8$ QCD with $L = 36$ and $m_f = 0.02$.

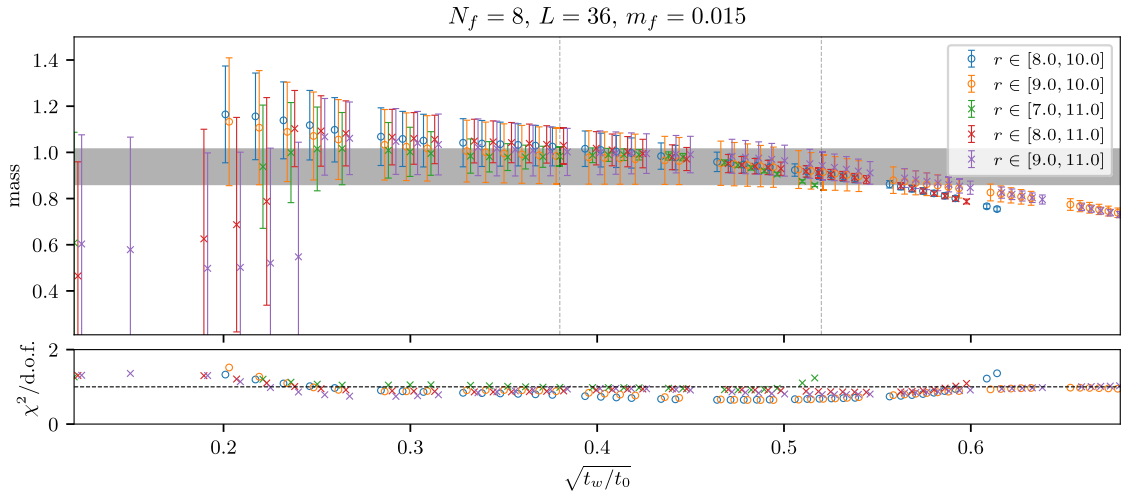

FIG. 39. The η' mass fitted for different distance regions and smearings for a specific ensemble of $N_f = 8$ QCD with $L = 36$ and $m_f = 0.015$.

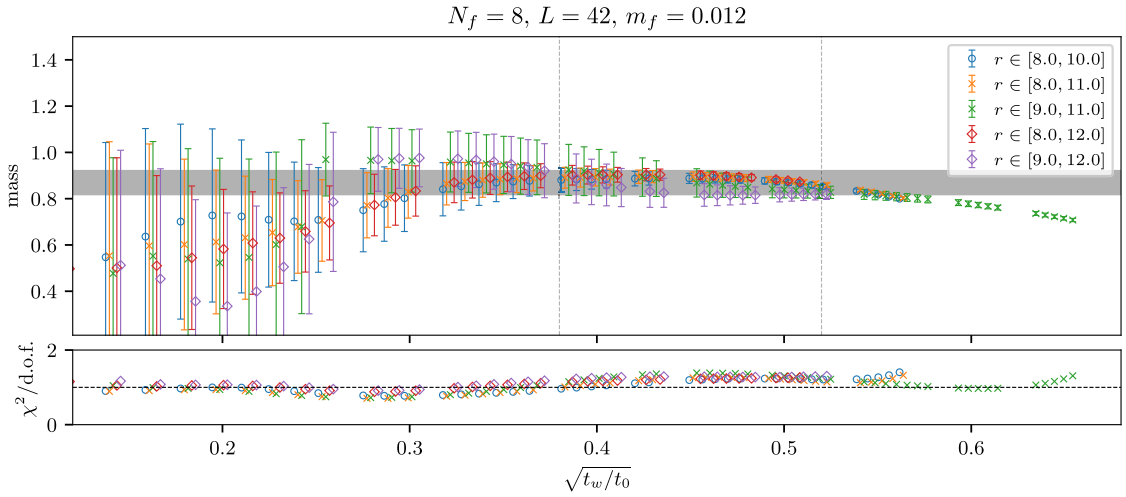

FIG. 40. The η' mass fitted for different distance regions and smearings for a specific ensemble of $N_f = 8$ QCD with $L = 42$ and $m_f = 0.012$.

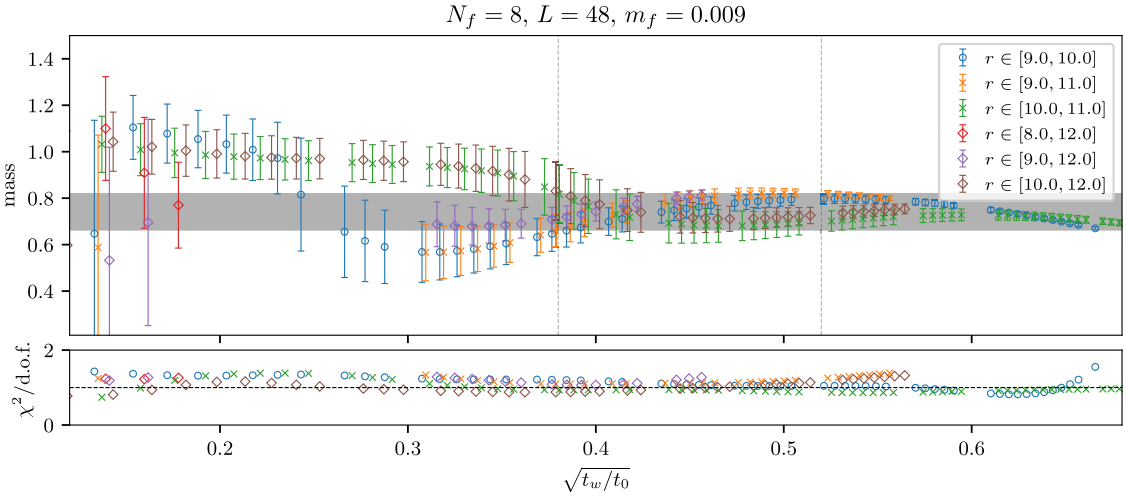

FIG. 41. The η' mass fitted for different distance regions and smearings for a specific ensemble of $N_f = 8$ QCD with $L = 48$ and $m_f = 0.009$.

3. $N_f = 12$

The plateaux for the fits for each ensemble studied in the $N_f = 12$ theory are presented in Figs. 42, 43, and 44.

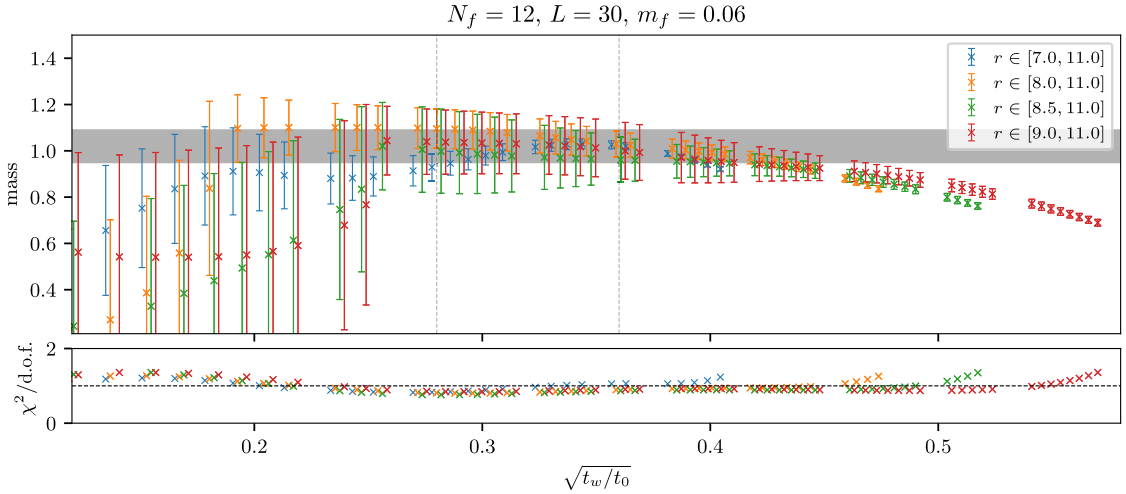

FIG. 42. The η' mass fitted for different distance regions and smearings for a specific ensemble of $N_f = 12$ QCD with $L = 30$ and $m_f = 0.06$.

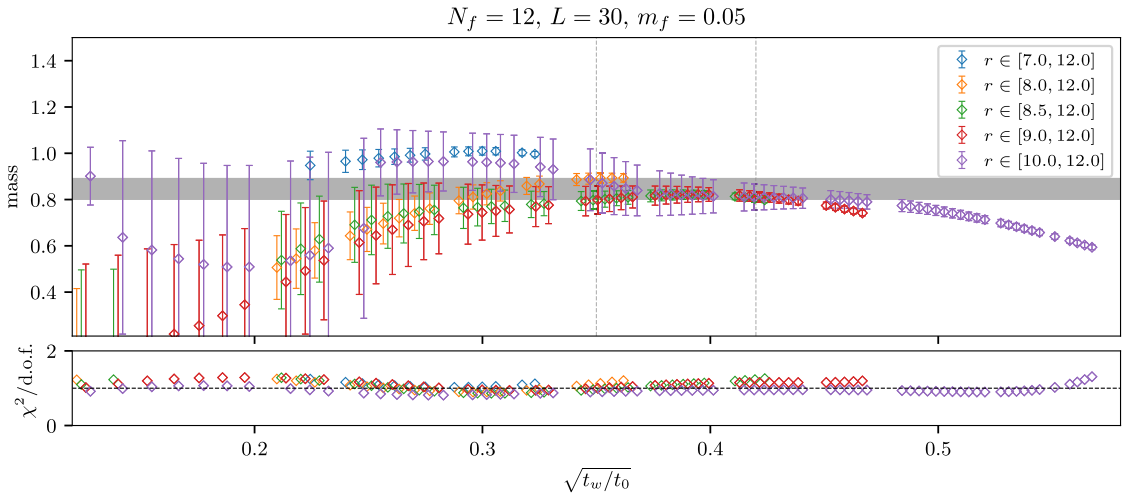

FIG. 43. The η' mass fitted for different distance regions and smearings for a specific ensemble of $N_f = 12$ QCD with $L = 30$ and $m_f = 0.05$.

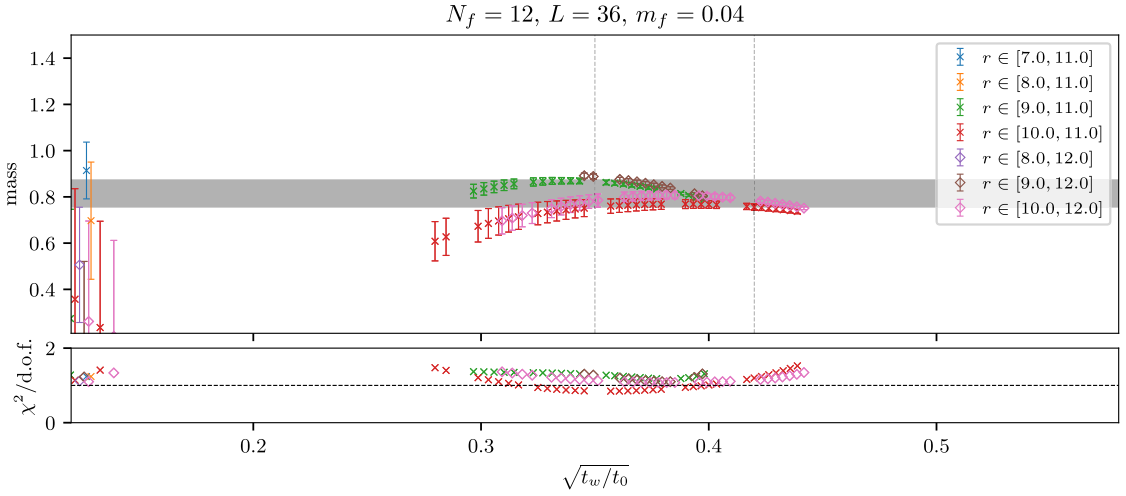

FIG. 44. The η' mass fitted for different distance regions and smearings for a specific ensemble of $N_f = 12$ QCD with $L = 36$ and $m_f = 0.04$.

[1] G. Aad *et al.* (ATLAS Collaboration), Observation of a new particle in the search for the standard model Higgs boson with the ATLAS detector at the LHC, Phys. Lett. B **716**, 1 (2012).

[2] S. Chatrchyan *et al.* (CMS Collaboration), Observation of a new boson at a mass of 125 GeV with the CMS experiment at the LHC, Phys. Lett. B **716**, 30 (2012).

[3] N. Craig, Naturalness: A snowmass white paper, Eur. Phys. J. C **83**, 825 (2023).

[4] K. Yamawaki, M. Bando, and K.-i. Matumoto, Scale invariant technicolor model and a technidilaton, Phys. Rev. Lett. **56**, 1335 (1986).

[5] M. Bando, K.-i. Matumoto, and K. Yamawaki, Technidilaton, Phys. Lett. B **178**, 308 (1986).

[6] B. Holdom, Techniodor, Phys. Lett. **150B**, 301 (1985).

[7] T. Akiba and T. Yanagida, Hierarchic chiral condensate, Phys. Lett. **169B**, 432 (1986).

[8] T. W. Appelquist, D. Karabali, and L. C. R. Wijewardhana, Chiral hierarchies and the flavor changing neutral current problem in technicolor, Phys. Rev. Lett. **57**, 957 (1986).

[9] T. Appelquist, J. Terning, and L. C. R. Wijewardhana, The zero temperature chiral phase transition in SU(N) gauge theories, Phys. Rev. Lett. **77**, 1214 (1996).

[10] W. E. Caswell, Asymptotic behavior of non-Abelian gauge theories to two loop order, Phys. Rev. Lett. **33**, 244 (1974).

[11] T. Banks and A. Zaks, On the phase structure of vector-like gauge theories with massless fermions, Nucl. Phys. **B196**, 189 (1982).

[12] S. Matsuzaki and K. Yamawaki, Walking on the ladder: 125 GeV technidilaton, or conformal Higgs, J. High Energy Phys. 12 (2015) 053; 11 (2016) 158(E).

[13] Y. Aoki, T. Aoyama, M. Kurachi, T. Maskawa, K.-i. Nagai, H. Ohki, A. Shibata, K. Yamawaki, and T. Yamazaki (LatKMI Collaboration), Lattice study of conformality in twelve-flavor QCD, Phys. Rev. D **86**, 054506 (2012).

[14] Y. Aoki, T. Aoyama, M. Kurachi, T. Maskawa, K.-i. Nagai, H. Ohki, A. Shibata, K. Yamawaki, and T. Yamazaki (LatKMI Collaboration), Walking signals in $N_f = 8$ QCD on the lattice, Phys. Rev. D **87**, 094511 (2013).

[15] Y. Aoki, T. Aoyama, M. Kurachi, T. Maskawa, K.-i. Nagai, H. Ohki, E. Rinaldi, A. Shibata, K. Yamawaki, and T. Yamazaki (LatKMI Collaboration), Light composite scalar in twelve-flavor QCD on the lattice, Phys. Rev. Lett. **111**, 162001 (2013).

[16] Y. Aoki, T. Aoyama, M. Kurachi, T. Maskawa, M. Kohtaroh, K.-i. Nagai, H. Ohki, E. Rinaldi, A. Shibata, K. Yamawaki, and T. Yamazaki (LatKMI Collaboration), Light composite scalar in eight-flavor QCD on the lattice, Phys. Rev. D **89**, 111502 (2014).

[17] Y. Aoki, T. Aoyama, E. Bennett, M. Kurachi, T. Maskawa, M. Kohtaroh, K.-i. Nagai, H. Ohki, E. Rinaldi, A. Shibata, K. Yamawaki, and T. Yamazaki (LatKMI Collaboration), Light flavor-singlet scalars and walking signals in $N_f = 8$ QCD on the lattice, Phys. Rev. D **96**, 014508 (2017).

[18] V. A. Miransky, Dynamics in the conformal window in QCD like theories, Phys. Rev. D **59**, 105003 (1999).

[19] L. Del Debbio and R. Zwicky, Hyperscaling relations in mass-deformed conformal gauge theories, Phys. Rev. D **82**, 014502 (2010).

[20] L. Del Debbio and R. Zwicky, Scaling relations for the entire spectrum in mass-deformed conformal gauge theories, Phys. Lett. B **700**, 217 (2011).

[21] Y. Aoki, T. Aoyama, M. Kurachi, T. Maskawa, K.-i. Nagai, H. Ohki, A. Shibata, K. Yamawaki, and T. Yamazaki, Study of the conformal hyperscaling relation through the Schwinger-Dyson equation, Phys. Rev. D **85**, 074502 (2012).

[22] V. A. Miransky and K. Yamawaki, Conformal phase transition in gauge theories, Phys. Rev. D **56**, 5051 (1997); **56**, 3768(E) (1997).

[23] Y. Aoki, T. Aoyama, M. Kurachi, T. Maskawa, K.-i. Nagai, H. Ohki, A. Shibata, K. Yamawaki, and T. Yamazaki, Exploring walking behavior in SU(3) gauge theory with 4 and 8 HISQ quarks, Proc. Sci. LATTICE2012 (**2012**) 035 [arXiv:1301.3367].

[24] A. Cheng, A. Hasenfratz, G. Petropoulos, and D. Schaich, Scale-dependent mass anomalous dimension from Dirac eigenmodes, J. High Energy Phys. 07 (2013) 061.

[25] T. Appelquist, R. C. Brower, G. T. Fleming, J. Kiskis, M. F. Lin, E. T. Neil, J. C. Osborn, C. Rebbi, E. Rinaldi, D. Schaich, C. Schroeder, S. Syritsyn, G. Voronov, P. Vranas, E. Weinberg, and O. Witzel (LSD Collaboration), Lattice simulations with eight flavors of domain wall fermions in SU(3) gauge theory, Phys. Rev. D **90**, 114502 (2014).

[26] T. Appelquist *et al.* (LSD Collaboration), Hidden conformal symmetry from the lattice, Phys. Rev. D **108**, L091505 (2023).

[27] A. Hasenfratz, Emergent strongly coupled ultraviolet fixed point in four dimensions with eight Kähler-Dirac fermions, Phys. Rev. D **106**, 014513 (2022).

[28] O. Witzel and A. Hasenfratz (Lattice Strong Dynamics Collaboration), Investigating SU(3) with $N_f = 8$ fundamental fermions at strong renormalized coupling, Proc. Sci. LATTICE2024 (**2025**) 146 [arXiv:2412.10322].

[29] S. Matsuzaki and K. Yamawaki, Dilaton chiral perturbation theory: Determining the mass and decay constant of the technidilaton on the lattice, Phys. Rev. Lett. **113**, 082002 (2014).

[30] M. Golterman and Y. Shamir, Low-energy effective action for pions and a dilatonic meson, Phys. Rev. D **94**, 054502 (2016).

[31] T. Appelquist, J. Ingoldby, and M. Piai, Dilaton EFT framework for lattice data, J. High Energy Phys. 07 (2017) 035.

[32] M. Golterman and Y. Shamir, Large-mass regime of the dilaton-pion low-energy effective theory, Phys. Rev. D **98**, 056025 (2018).

[33] T. Appelquist, J. Ingoldby, and M. Piai, Dilaton potential and lattice data, Phys. Rev. D **101**, 075025 (2020).

[34] Z. Fodor, K. Holland, J. Kuti, and C. H. Wong, Tantalizing dilaton tests from a near-conformal EFT, Proc. Sci. LATTICE2018 (**2019**) 196 [arXiv:1901.06324].

[35] Z. Fodor, K. Holland, J. Kuti, and C. H. Wong, Dilaton EFT from p-regime to RMT in the ϵ-regime, Proc. Sci. LATTICE2019 (**2020**) 246 [arXiv:2002.05163].

[36] M. Golterman and Y. Shamir, Explorations beyond dilaton chiral perturbation theory in the eight-flavor SU(3) gauge theory, Phys. Rev. D **102**, 114507 (2020).

[37] T. Appelquist, J. Ingoldby, and M. Piai, Dilaton effective field theory, Universe **9**, 10 (2023).

[38] A. Freeman, M. Golterman, and Y. Shamir, Dilaton chiral perturbation theory at next-to-leading order, Phys. Rev. D **108**, 074506 (2023).

[39] M. Golterman and Y. Shamir, Power counting of the pion-dilaton effective field theory, Phys. Rev. D **111**, 074505 (2025).

[40] Y. Aoki *et al.* (LatKMI Collaboration), Lattice study of the scalar and baryon spectra in many-flavor QCD, Int. J. Mod. Phys. A **32**, 1747010 (2017).

[41] T. Appelquist, R. C. Brower, G. T. Fleming, A. Hasenfratz, X. Y. Jin, J. Kiskis, E. T. Neil, J. C. Osborn, C. Rebbi, E. Rinaldi, D. Schaich, P. Vranas, E. Weinberg, and O. Witzel (LSD Collaboration), Strongly interacting dynamics and the search for new physics at the LHC, Phys. Rev. D **93**, 114514 (2016).

[42] T. Appelquist *et al.* (Lattice Strong Dynamics Collaboration), Nonperturbative investigations of SU(3) gauge theory with eight dynamical flavors, Phys. Rev. D **99**, 014509 (2019).

[43] O. Witzel, Review on composite Higgs models, Proc. Sci. LATTICE2018 (**2019**) 006 [arXiv:1901.08216].

[44] B. Svetitsky, Looking behind the Standard Model with lattice gauge theory, EPJ Web Conf. **175**, 01017 (2018).

[45] C. Pica, Beyond the standard model: Charting fundamental interactions via lattice simulations, Proc. Sci. LATTICE2016 (**2016**) 015 [arXiv:1701.07782].

[46] R. C. Brower *et al.* (Lattice Strong Dynamics Collaboration), Light scalar meson and decay constant in SU(3) gauge theory with eight dynamical flavors, Phys. Rev. D **110**, 054501 (2024).

[47] T. Appelquist, J. Ingoldby, and M. Piai, Analysis of a dilaton EFT for lattice data, J. High Energy Phys. 03 (2018) 039.

[48] M. Golterman, E. T. Neil, and Y. Shamir, Application of dilaton chiral perturbation theory to $N_f = 8$, SU(3) spectral data, Phys. Rev. D **102**, 034515 (2020).

[49] Y. Aoki, T. Aoyama, E. Bennett, M. Kurachi, T. Maskawa, M. Kohtaroh, K.-i. Nagai, H. Ohki, E. Rinaldi, A. Shibata, K. Yamawaki, and T. Yamazaki (LatKMI Collaboration), Walking and conformal dynamics in many-flavor QCD, Proc. Sci. LATTICE2015 (**2016**) 213 [arXiv:1601.02287].

[50] Y. Aoki, T. Aoyama, E. Bennett, M. Kurachi, T. Maskawa, M. Kohtaroh, K.-i. Nagai, H. Ohki, E. Rinaldi, A. Shibata, K. Yamawaki, and T. Yamazaki (LatKMI Collaboration), Flavor-singlet spectrum in multi-flavor QCD, EPJ Web Conf. **175**, 08023 (2018).

[51] E. Witten, Current algebra theorems for the U(1) goldstone boson, Nucl. Phys. **B156**, 269 (1979).

[52] G. Veneziano, U(1) without instantons, Nucl. Phys. **B159**, 213 (1979).

[53] M. Lüscher, Properties and uses of the Wilson flow in lattice QCD, J. High Energy Phys. 08 (2010) 071; 03 (2014) 092(E).

[54] K. Yamawaki, Dynamical gauge boson of hidden local symmetry within the standard model, arXiv:1803.07271.

[55] T. Appelquist and Y. Bai, A light dilaton in walking gauge theories, Phys. Rev. D **82**, 071701 (2010).

[56] L. Del Debbio and R. Zwicky, Dilaton and massive hadrons in a conformal phase, J. High Energy Phys. 08 (2022) 007.

[57] M. Hashimoto and K. Yamawaki, Techni-dilaton at conformal edge, Phys. Rev. D **83**, 015008 (2011).

[58] S. Matsuzaki and K. Yamawaki, Holographic techni-dilaton at 125 GeV, Phys. Rev. D **86**, 115004 (2012).

[59] E. Follana, Q. Mason, C. Davies, K. Hornbostel, G. P. Lepage, J. Shigemitsu, H. Trottier, and K. Wong (HPQCD and UKQCD Collaborations), Highly improved staggered quarks on the lattice, with applications to charm physics, Phys. Rev. D **75**, 054502 (2007).

[60] K. Symanzik, Continuum limit and improved action in lattice theories. 1. Principles and ϕ^4 theory, Nucl. Phys. **B226**, 187 (1983).

[61] Y. Aoki, T. Aoyama, E. Bennett, M. Kurachi, T. Maskawa, M. Kohtaroh, K.-i. Nagai, H. Ohki, E. Rinaldi, A. Shibata, K. Yamawaki, and T. Yamazaki (LatKMI Collaboration), Topological observables in many-flavour QCD, Proc. Sci. LATTICE2015 (**2016**) 214 [arXiv:1601.04687].

[62] R. Sommer, A new way to set the energy scale in lattice gauge theories and its applications to the static force and α_s in SU(2) Yang-Mills theory, Nucl. Phys. **B411**, 839 (1994).

[63] S. M. Bhattacharjee and F. Seno, A measure of data collapse for scaling, J. Phys. A **34**, 6375 (2001).

[64] T. DeGrand, Finite-size scaling tests for SU(3) lattice gauge theory with color sextet fermions, Phys. Rev. D **80**, 114507 (2009).

[65] A. Athenodorou, E. Bennett, G. Bergner, and B. Lucini, Investigating the conformal behavior of SU(2) with one adjoint Dirac flavor, Phys. Rev. D **104**, 074519 (2021).

[66] M. Soldate and R. Sundrum, Z couplings to pseudo-Goldstone bosons within extended technicolor, Nucl. Phys. **B340**, 1 (1990).

[67] R. S. Chivukula, M. J. Dugan, and M. Golden, Analyticity, crossing symmetry and the limits of chiral perturbation theory, Phys. Rev. D **47**, 2930 (1993).

[68] M. Harada and K. Yamawaki, Hidden local symmetry at loop: A new perspective of composite gauge boson and chiral phase transition, Phys. Rep. **381**, 1 (2003).

[69] P. A. Zyla *et al.* (Particle Data Group), Review of particle physics, Prog. Theor. Exp. Phys. **2020**, 083C01 (2020).

[70] Y. Aoki, T. Aoyama, E. Bennett, M. Kurachi, T. Maskawa, M. Kohtaroh, K.-i. Nagai, H. Ohki, E. Rinaldi, A. Shibata, K. Yamawaki, and T. Yamazaki (LatKMI Collaboration), The Peskin-Takeuchi S parameter and vector meson decay constants in $N_f = 8$ QCD (to be published).

[71] Z. Fu, Preliminary lattice study of σ meson decay width, J. High Energy Phys. 07 (2012) 142.

[72] T. Kunihiro, S. Muroya, A. Nakamura, C. Nonaka, M. Sekiguchi, and H. Wada (SCALAR Collaboration), Scalar mesons in lattice QCD, Phys. Rev. D **70**, 034504 (2004).

[73] R. A. Briceno, J. J. Dudek, R. G. Edwards, and D. J. Wilson, Isoscalar $\pi\pi$ scattering and the σ meson resonance from QCD, Phys. Rev. Lett. **118**, 022002 (2017).

[74] R. A. Briceno, J. J. Dudek, R. G. Edwards, and D. J. Wilson, Isoscalar $\pi\pi, K\bar{K}, \eta\eta$ scattering and the σ, f_0, f_2 mesons from QCD, Phys. Rev. D **97**, 054513 (2018).

[75] V. A. Miransky and K. Yamawaki, On gauge theories with additional four fermion interaction, Mod. Phys. Lett. A **04**, 129 (1989).

[76] K. Kawarabayashi and M. Suzuki, Partially conserved axial vector current and the decays of vector mesons, Phys. Rev. Lett. **16**, 255 (1966).

[77] Riazuddin and Fayyazuddin, Algebra of current components and decay widths of ρ and K^* mesons, Phys. Rev. **147**, 1071 (1966).
[78] D. Nogradi and L. Szikszai, The flavor dependence of m_ϱ/f_π, J. High Energy Phys. 05 (2019) 197; 06 (2022) 031(E).
[79] A. Y. Kotov, D. Nogradi, K. K. Szabo, and L. Szikszai, More on the flavor dependence of m_ρ/f_π, J. High Energy Phys. 07 (2021) 202; 06 (2022) 032(E).
[80] H. S. Fukano, S. Matsuzaki, K. Terashi, and K. Yamawaki, Conformal barrier and hidden local symmetry constraints: Walking technirhos in LHC diboson channels, Nucl. Phys. **B904**, 400 (2016).
[81] H. S. Fukano, M. Kurachi, S. Matsuzaki, K. Terashi, and K. Yamawaki, 2 TeV walking technirho at LHC?, Phys. Lett. B **750**, 259 (2015).
[82] G. Veneziano, Goldstone mechanism from gluon dynamics, Phys. Lett. **95B**, 90 (1980).
[83] H. Fukaya, S. Aoki, G. Cossu, S. Hashimoto, T. Kaneko, and J. Noaki (JLQCD Collaboration), η' meson mass from topological charge density correlator in QCD, Phys. Rev. D **92**, 111501 (2015).
[84] E. V. Shuryak and J. J. M. Verbaarschot, Screening of the topological charge in a correlated instanton vacuum, Phys. Rev. D **52**, 295 (1995).
[85] P. Lepage and C. Gohlke, GPLEPAGE/LSQFIT: LSQFIT version 11.8 (2021), 10.5281/zenodo.4568470.
[86] M. Bruno, S. Schaefer, and R. Sommer (ALPHA Collaboration), Topological susceptibility and the sampling of field space in $N_f = 2$ lattice QCD simulations, J. High Energy Phys. 08 (2014) 150.
[87] MILC Collaboration, The MILC code, https://github.com/milc-qcd/milc_qcd/.
[88] Y. Aoki, T. Aoyama, E. Bennett, M. Kurachi, T. Maskawa, M. Kohtaroh, K.-i. Nagai, H. Ohki, E. Rinaldi, A. Shibata, K. Yamawaki, and T. Yamazaki, A novel view of the flavor-singlet spectrum from multi-flavor QCD on the lattice—data and workflow release (2025), 10.5281/zenodo.17037868.